DE-FG-22-93PC93226-99

Investigation of Mineral Transformations and Ash Deposition During Staged Combustion

Final Report
October 1, 1993 - September 30, 1997

By
John N. Harb

Work Performed Under Contract No.: DE-FG22-93PC93226

For
U.S. Department of Energy
Office of Fossil Energy
Federal Energy Technology Center
P.O. Box 880
Morgantown, West Virginia 26507-0880

By
Brigham Young University
Provo, Utah 84602

Disclaimer

TABLE OF CONTENTS

LIST OF TABLES

LIST OF FIGURES

EXECUTIVE SUMMARY

Objectives

This report documents a recently completed study funded by the U.S. Department of Energy (DE-FG22-93PC93226) to examine the impact of staged combustion on ash formation and deposition while firing pulverized coal. The objectives of the study were:

1) To perform experiments in order to evaluate the impact of staged combustion on ash formation and deposition,

2) To identify key mineral species or reactions which may be problematic, and to quantify the magnitude of their impact,

3) To develop understanding and insight into the mechanisms which control ash formation and deposition under low-NOx firing conditions.

Perspective

In staged combustion of systems firing pulverized coal, particles move through a fuel-rich zone followed by an oxidizing region or zone. The amount of time spent in the reducing zone is limited in practical systems. In this study, a pilot-scale self-sustained combustor was used to approximate the time/temperature/composition history present during staged combustion. Because of this, the study is distinct from other work which has only considered reducing conditions and the impact of such conditions on ash formation.

Accomplishments

Major accomplishments of this study are noted in the number paragraphs below.

1. Coal Selection and Characterization. Two coals with very different properties were selected for use in this study. The first, Black Thunder, was a U.S. subbituminous coal from the Powder River Basin. This coal is a non-swelling coal which has a high concentration of organically-bound inorganic constituents. The second was a Pittsburgh #8 coal, a bituminous coal from the eastern United States. The particular sample used was washed so that its ash content (11%) was considerably lower than expected from a run-of-the-mine fuel. One motivation in the selection of these particular fuels was that they had been used by other DOE investigators in a related study (DE-AC22-

93PC92190). The principal method for characterizing the coals was with use of CCSEM. The coal characterization results were similar to those of others and provided a basis for evaluating the influence of staged combustion on ash formation.

2. Assembly and Use of a Pilot-Scale Combustor. A self-sustained combustor was used for the present study in order to more closely approximate operating conditions in a practical system. One of the key challenges of the study was the assembly, maintenance, and operation of this facility. Although based on an existing combustor, the demands of this study required a new coal feeder and feed system, data acquisition system, burner, particle collection system, and deposition probe, in addition to a myriad of minor modifications. Successful assembly and operation of the combustor was a major accomplishment of this study.

3. Development of Analysis Software. It was necessary to develop a variety of analysis tools in order to accomplish the objectives of this study. Part of this development included improvement of existing CCSEM software and conversion of the software to use on a new microanalytical system. However, the principal part of this effort was spent in the development of new software for data processing and interpretation. Accomplishments in this area include the development of an advanced classification algorithm (NPCA) which was used to quantify the impact of staged combustion on ash composition. An algorithm was also developed to quantify the difference in behavior between discrete inorganic particles included in char and excluded inorganic particles (not associated with the char). In addition, other software tools were developed to assist in data processing, interpretation, and presentation.

4. An Understanding of the Impact of Staged Combustion on Ash Formation from Black Thunder Coal. One of the key technical contributions of the report is an understanding of the impact of staged combustion on ash formation. Specific results for the Black Thunder coal include:

    1) The effect of staged combustion on Black Thunder coal was to cause ash particles to coalesce to a greater extent than they do under conventional conditions. This is believed to be due to slowing of char oxidation leading to reduced fragmentation.

    2) The effect mentioned in (1) is not large. The large effects seen in previous studies occurred because ash and char particles experienced low oxygen concentrations for extended periods of time. When additional oxygen is introduced following a short time under reducing conditions, effects due to the reducing conditions are minimized.

    3) Following (1) and (2), staged combustion of Black Thunder coal is not expected to alter significantly the size or composition of the fly ash in large-

scale systems.

4) Staged combustion did not affect the bulk elemental composition of the Black Thunder ash by selective vaporization. However, a shift in the composition of small ash particles, consistent with less fragmentation of char particles under staged combustion, was observed.

In summary, staged combustion did influence ash formation from this coal. However, the impact was small enough that it is not expected to be important in practice. It should be noted, however, that the observed effect was more significant for particle sizes less than 10 microns; particles in this size range have been implicated in the formation of downstream sulfate-based deposits (Benson et al., 1993).

5. An Understanding of the Impact of Staged Combustion on Ash Formation from the Pittsburgh #8 Coal. Specific results for the Pittsburgh #8 coal include:

   1) Staged combustion temporarily impedes the oxidation of pyrite particles. This effect is particularly evident for included pyrite (as opposed to excluded pyrite which is not associated with the organic matrix).

   2) Following the introduction of staged air into the combustor, the remaining pyrite particles rapidly oxidize.

   3) Staged combustion does not alter the bulk composition of the ash.

   4) The extent of coalescence does not appear to be significantly affected by the initial reducing conditions associated with staged combustion.

6. An Initial Understanding of the Impact of Staged Combustion on Deposits from the Black Thunder Coal. Conclusions from the deposition studies performed to date include:

   1) The oxygen concentration in the gas did not appear to have a significant effect on deposit sintering.

   2) The influence of temperature on deposit sintering was significant. Hence, changes in the radiative heat flux and/or gas temperatures present under low-NOx firing conditions are expected to have a substantial influence on deposition behavior.

   3) Incompletely combusted particles which adhere to the wall will burn out in-

situ to form a high-surface-area structure which is prone to sulfation. Therefore, carbon carryover into the convective pass may influence the formation of sulfate-based deposits.

7. Preliminary Understanding of the Impact of Staged Combustion on Deposits from the Pittsburgh #8 Coal. The deposit studies performed with this coal were quite limited. However, the following observation can be made:

    1) No influence of staged combustion (S.R.=0.85) on deposit composition/ morphology was observed for uncured deposits formed from this coal.

The results listed under numbers 4-7 above indicate that the behavior under staged combustion conditions is different than that observed under reducing conditions alone (see e.g., Bool et al., 1995). Therefore, studies of ash behavior under low-NOx firing conditions should consider the effect of downstream oxygen following the initial fuel-rich zone.

Organization of the Report

These results are described and supported in the remainder of the report which follows. The first two sections of the report provide an introduction and background for the study. Section 3 details the experimental and analytical methods used to obtain the results. Results for ash formation from the Black Thunder coal are described in Section 4, which also contains the characterization results for this coal. Characterization of the Pittsburgh coal and results from the ash formation study for this coal are described in Section 5. Section 6 contains the results related to deposit formation from both coals. A short summary and conclusion section is included at the end of the report.

SECTION 1

INTRODUCTION

The purpose of this report is to document a recently completed four-year study funded by the U.S. Department of Energy (DE-FG22-93PC93226) to examine the impact of low-NOx firing technologies on ash formation and deposition while firing pulverized coal. This is a matter of great concern to those who operate large boilers, as the ash behavior is frequently the dominant factor in the day-to-day operation of such units. In fact, hundreds to thousands of tons of ash per day may pass through a boiler, depending on the size of the unit and the properties of the coal. Most of the ash leaves the boiler as fly ash, but deposits formed from even a small fraction can cause a number of operational problems, which in turn lead to costly maintenance, unplanned outages, increased operating costs, and lower efficiency.

Recently, low-NOx firing technologies have been adopted to meet stringent regulations on NOx emissions. Low-NOx burners and staged combustion inhibit NOx formation by restricting the amount of oxygen available to form a fuel-rich zone in which nitrogen compounds are reduced to molecular nitrogen (N_2) rather than oxidized. Additional oxygen is provided downstream for complete combustion. Consequently, coal and mineral particles encounter different temperatures and oxygen concentrations when they are burned under low-NOx firing conditions than they do in conventionally-fired units.

As mentioned above, the objective of this project was to determine the effect of staged combustion on ash formation and deposition. To that end, two coals with distinctly different inorganic contents and ash characteristics were fired in a pilot-scale laboratory combustor under both conventional and staged combustion conditions. Ash and deposit samples were collected at various locations in the reactor and analyzed in order to assess the influence of staged combustion.

This report is organized as follows. First, a background section provides the foundation needed in order to understand the motivation for and the results of the experimental program. The next section presents a description of the experimental apparatus and procedures, including the development the analytical methods critical to the study. Results of the analyses of coal, ash and deposit samples are then presented and discussed for each of the two coals. Finally, the report ends with a short summary and statement of conclusions.

SECTION 2

BACKGROUND

As stated in the introduction, the object of this work was to understand the effect of staged combustion on ash formation and deposition in units firing pulverized coal. The questions of whether staged combustion produces ash with a different composition, or with a different particle size distribution are specifically addressed. In addition, the impact of staged combustion on deposit behavior is also examined.

Relevant background literature reviewed in this section includes information on low-NOx combustion strategies and their effect on boiler operation. The potential influence of such strategies on ash formation and deposition are also discussed. Finally, a brief background is provided on the key analytical methods used in this study.

2.1 BOILERS AND LOW-NOX FIRING CONDITIONS

Utility boilers burning pulverized coal are typically large, with dimensions on the order of 250 ft in height and 40 ft in width (Figure 2-1). The lower and upper portions of the boilers are called the radiant section and the convective pass, respectively, in reference to the mode of heat transfer that dominates in each. Ash is primarily formed in the radiant section. Deposits can form in either section, but are distinguished by their location. By definition, slagging deposits form in the radiant section and fouling deposits form in the convective pass.

Combustion and NOx formation both take place in the radiant section. In a conventionally-fired unit, coal and an excess of air are introduced through the burners. NOx forms because there is excess oxygen and the flame temperature is high. The amount of NOx that is produced can be decreased by beginning combustion in a fuel-rich mixture. Under reducing conditions, the favored product of nitrogen shifts from NOx to N_2.

Two approaches have been used to implement low-NOx firing as illustrated in Figure 2-2. In staged combustion or overfire air, a large fuel-rich zone is created by blowing less than the stoichiometric amount of air through the burners with the coal. To complete combustion, additional (tertiary) air is injected downstream. When low-NOx burners are used, the amount of air is not decreased, but the flow patterns of the coal and air streams are modified so that mixing is delayed. The reducing zone is relatively small and located within the flame near the burners. In either case, the environment experienced by the

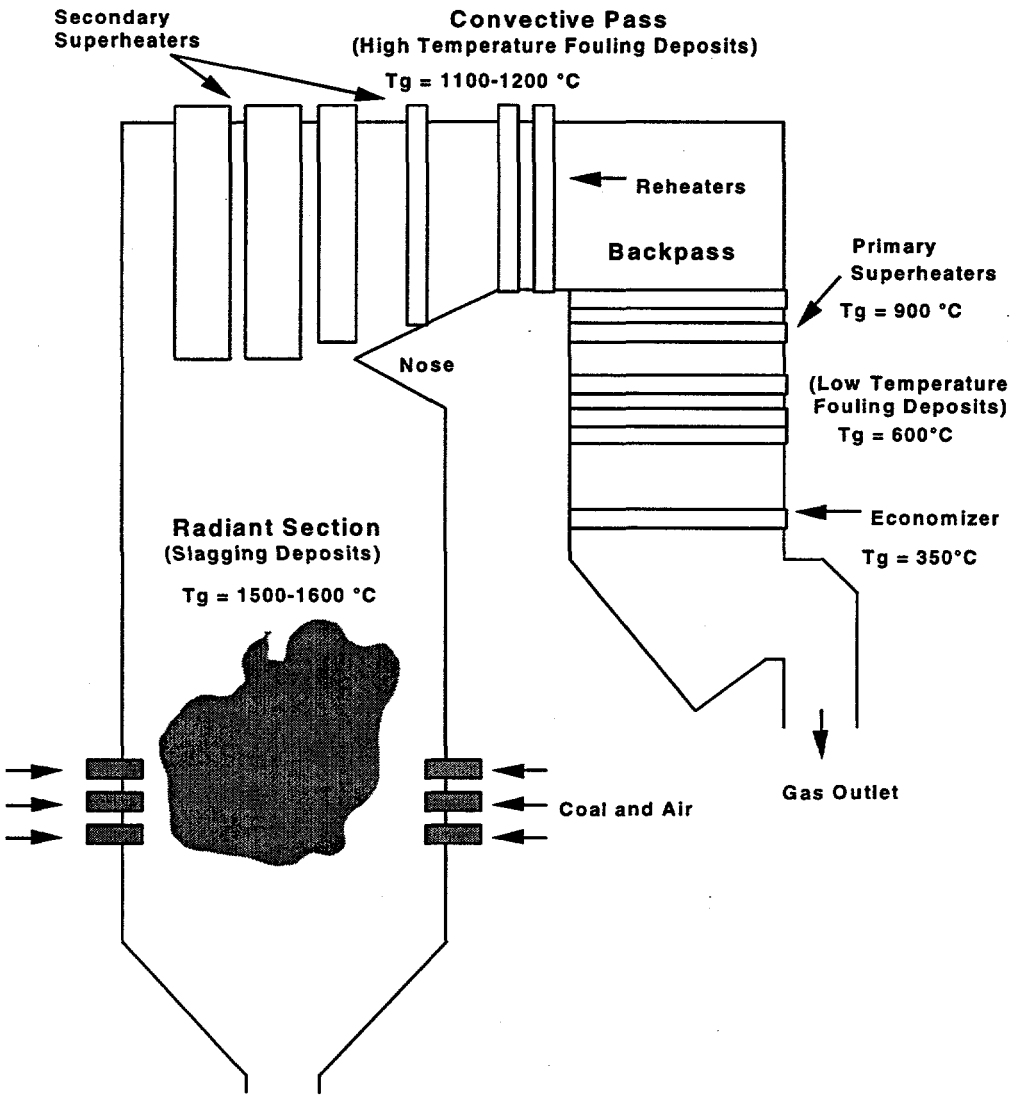

Figure 2-1 Schematic diagram of a generic utility boiler (Richards 1994)

entrained coal particles is different than that present during conventional firing. The residence time in the reducing zone is believed to be relatively short, on the order of 200-300ms.

2.2 EFFECT OF ASH DEPOSITION ON BOILER OPERATION

Ash deposition affects all phases of boiler design and operation. Since deposits insulate the walls, extra surface area must be included to provide sufficient heat transfer. Therefore, the deposition characteristics of the coal sometimes overshadow other factors in the design. For example, low rank coals are more reactive than high rank coals but require larger boilers (reactors) to compensate for their higher tendencies to slag and foul.

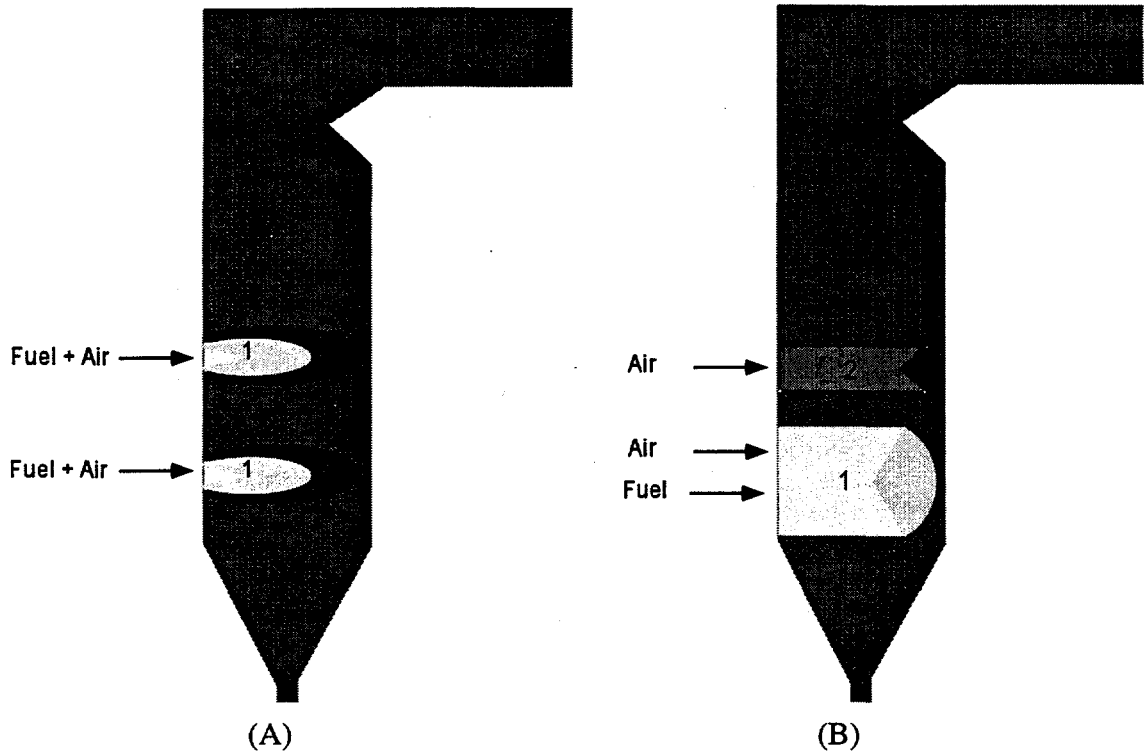

Figure 2-2 A) Low-NOx burners B) Staged air combustion

An important boiler operating parameter is the furnace exit gas temperature (FEGT). This is the temperature of the gas stream at the boundary between the radiant section and the convective pass. An acceptable range of values for FEGT is specified in the design of the unit. FEGT is an indicator of how much heat has been transferred to the steam in the radiant section. The proportions of heat transferred in the two sections of the boiler must be balanced so that the steam raised in the radiant section can be superheated to the proper degree in the convective pass. When ash deposits form on heat transfer surfaces in the radiant section (slag), less heat is transferred and FEGT rises. To compensate, operators use sootblowers installed in the walls of the boiler to remove the deposits. They also spray water directly into the gas stream to cool it. These measures keep the unit within operating parameters for a time, but there is a limit to their efficacy. In cases where there is a continual net accumulation of deposits, the plant must eventually be shut down for deposit removal.

The influence of low-NOx combustion strategies on ash behavior in boilers is not well understood. Initially, there was considerable concern that such strategies would greatly increase the accumlation of ash deposits. It is well known that ash fusion temperatures, a commonly used predictor of slagging, are lower when measured under reducing conditions (Ghosh 1985; Lloyd 1993). In contrast, experience over the past few years has shown these concerns to be largely unwarranted. Although there have been reports of increased deposits near the burners, the authors are unaware of catastrophic problems due to increased deposition that have been attributed to low-NOx firing. In fact, some plants

that have been retrofitted for low-NOx firing have seen FEGT fall over time (Muzio 1996; Richards 1996). In these units, slagging has decreased. As a result, more heat is transferred in the radiant section. This would be an additional benefit of staged combustion had the boiler and steam cycle not been designed for a certain level of slagging. Without the slag to insulate the walls, too much heat is transferred to the steam in the radiant section and the proper balance between boiling and superheating is lost. To restore the balance, some utilities have taken the seemingly odd measure of painting the interior of the radiant section with a reflective coating in order to reduce the net radiant heat flux to the walls.

2.3 ASH FORMATION MECHANISMS AND THE INFLUENCE OF LOW-NOX STRATEGIES

The purpose of this section is to review the mechanisms by which ash is formed and to evaluate the potential impact of low-NOx combustion strategies on those mechanisms. The information included in this review provided a basis for the experiments performed as part of this study.

2.3.1 Inorganic Constituents in Coal

An understanding of the form in which the inorganic matter is found in the coal is critical to an understanding of ash formation. Coals used for generating electricity typically contain from 10 to 25% inorganic impurities by weight (Skorupska and Couch 1993). The forms in which these impurities exist in the coal are illustrated in Figure 2-3. The rank of the coal is a factor in determining what sort of inorganic material it contains. Discrete mineral particles are found in coals of all ranks, but only low rank coals contain significant amounts of organically-associated inorganic elements.

Hundreds of mineral species occur in combination with coal. Many of these are clays, i.e. aluminosilicates with various impurities such as calcium, potassium, and iron. Pyrite and quartz are also commonly associated with coal (Couch 1994). As shown in Figure 2-3, some mineral particles are intimately associated with coal particles while others are not. The term "mineral liberation" refers to the association of minerals with the coal. The inorganic particles which are intimately associated with the coal are called *included* minerals; the separate mineral particles are called *excluded* minerals. This distinction is important since included and excluded mineral particles experience different combustion environments. Excluded particles are exposed to the temperature and composition of the gas phase in the flame, whereas included particles experience the somewhat higher temperature and an oxygen-depleted gas at the surface of the burning coal particle. In addition, it is possible for multiple mineral particles within the same coal particle to coalesce during combustion. No interaction between excluded minerals is possible.

The organically-bound elements include calcium, magnesium, aluminum, iron, and potassium. These elements are dispersed throughout the organic matrix, occurring, for example, as carboxylates bound by the oxygen found in the low rank coals. Sulfur is also organically-bound to the carbon matrix in some coals.

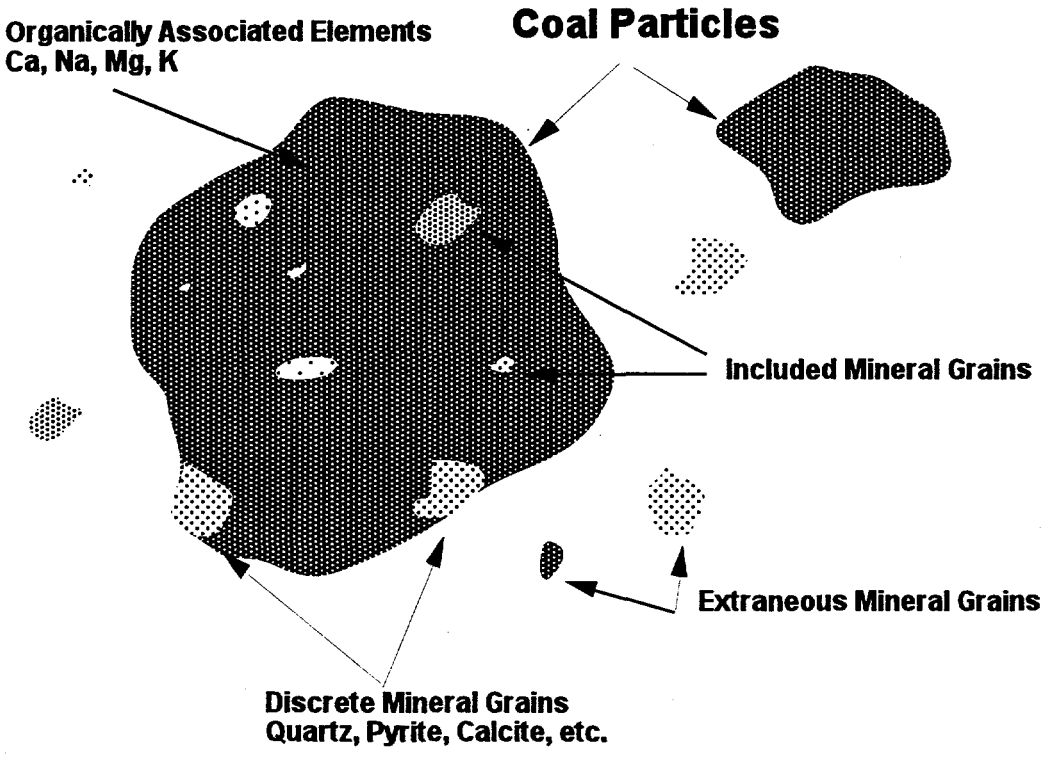

Figure 2-3 Occurrence of mineral matter in coal

2.3.2 Ash Transformations

The minerals and organically-bound elements present with the coal become ash via a complex set of physical and chemical changes that occur as the fuel burns (Figure 2-4). Ash transformations, as these changes are collectively called, are influenced by both the nature of the inorganic constituents and the environment to which these constituents are exposed. Coalescence and fragmentation represent two physical processes which are central to ash formation. Coalescence is used to describe the extent to which inorganic constituents present in a single char particle mix together. Two limiting cases are typically considered: full coalescence where one ash particle is formed per char particle, and no coalescence where there is no interaction and an ash particle is formed from each discrete mineral particle. As long as a char particle remains intact, the inorganic constituents associated with that particle have the opportunity to coalesce.

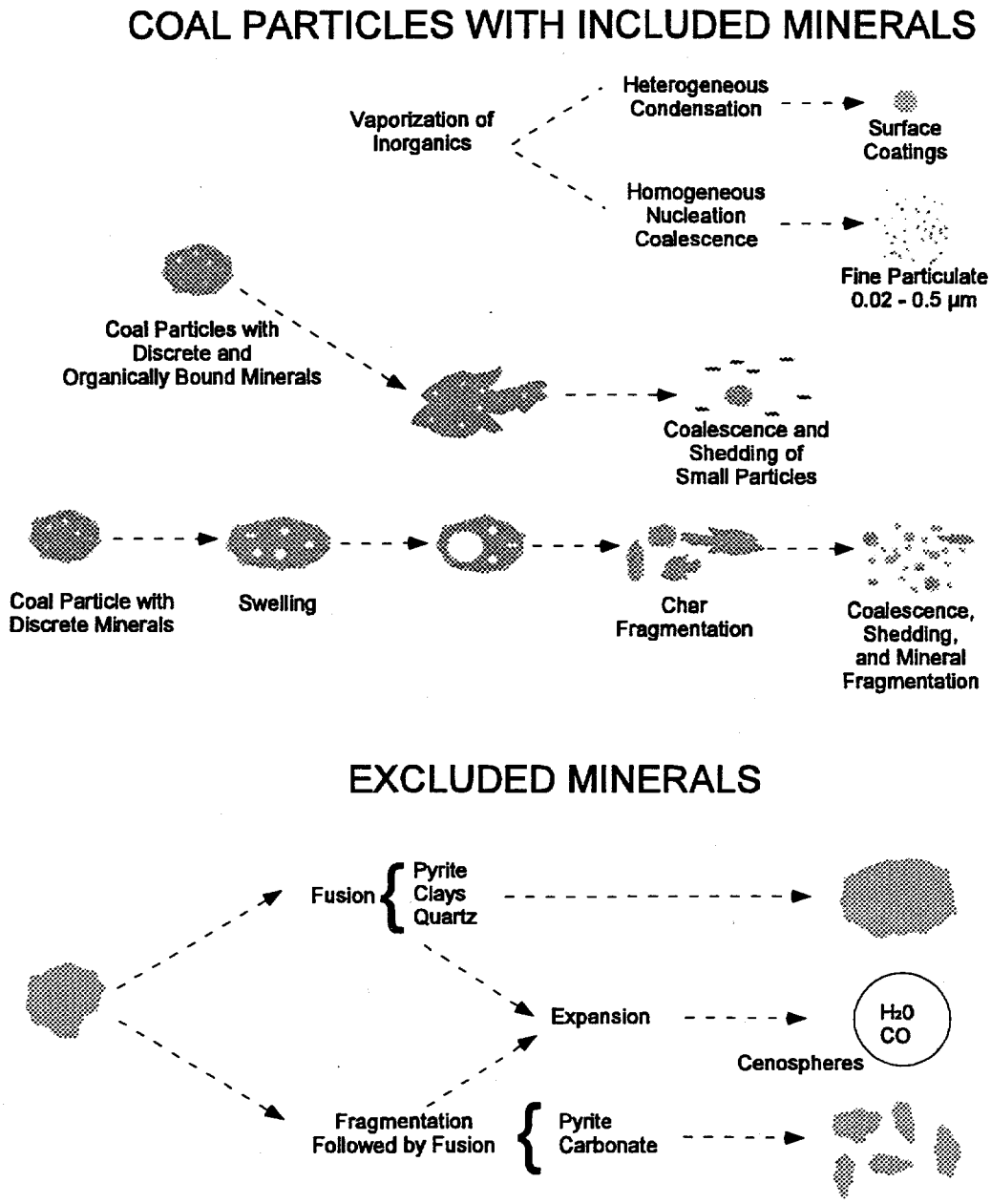

Figure 2-4 Schematic diagram of the transformations of inorganic constituents during coal combustion (Benson, et al., 1993)

Coalescence plays a role in the formation of ash from organically-bound constituents as well. As the combustion of low-rank chars proceeds, the organically-bound constituents leave the organic matrix. Sulfur forms SO_2 and enters the gas stream. Sodium may vaporize and then condense heterogeneously on heat transfer surfaces or other ash particles (Wall 1992). More importantly, calcium, magnesium, and aluminum form small oxide particles (< 1 µm) which coalesce to form larger particles (10-20 µm) as the char recedes (Quann and Sarofim 1986).

Coalescence is disturbed by fragmentation. Swelling chars tend to break into many small pieces before completing combustion. Char also fragments as it oxidizes. Mineral particles fragment due to rapid heating and evolution of gases. Once ash particles become excluded or separated from the char, there is virtually no possibility for them to coalesce with one another. Likewise, particles associated with different fragments have no opportunity to mix.

Therefore, if char particles are somehow kept from fragmenting, the likelihood that the included ash particles will coalesce increases. Staged combustion tends to decrease the rate of char oxidation due to lower temperatures, lower oxygen concentrations, decreased char reactivity, or a combination of the three. Whatever the cause, it follows that more of the individual char particles remain "intact" under staged combustion than under conventional conditions. Therefore, increased coalescence might be expected when firing under staged conditions. The chances for coalescence may be further increased by lowering the viscosity of the ash so that it is more prone to flow and sinter. Such a change may occur in the initial reducing zone during staged combustion.

The driving forces for the physical changes discussed above are provided by chemical transformations occurring in the coal and ash. Specific physical transformations can be related directly to chemical reactions. For example, ash particles fragment when clay minerals lose waters of hydration, when CO_2 evolves from decomposing carbonates, and when pyrite decomposes to pyrrhotite (Raask 1985). The changes in state from solid to gas associated with combustion and decomposition cause density changes which generate enormous forces that contribute to fragmentation and thus affect the size and composition distribution of the ash.

The physical properties which govern the coalescence of ash particles and sintering of deposits, i.e. melting point, viscosity, and surface tension, are functions of composition, temperature, and environment and may therefore be influenced by staged combustion. Therefore, ash chemistry, a complex subject concerned with the composition, reactions, and interactions of many species, is vital in understanding ash behavior.

Fly ash typically contains large fractions of amorphous materials derived from the clay minerals present in coal. While these glasses consist primarily of silicon and aluminum oxides, Benson, Jones, and Harb (Benson, et al., 1993) pointed out that other oxides present as impuritities can significantly alter their properties.

Certain oxides, known as network formers, are capable of building random, three-dimensional networks. Other oxides cannot form a continuous network. When these so-called network modifiers are added to glass melts, weaker networks are formed. Consequently, the viscosity of the material is reduced, making it more prone to coalesce and stick. The oxides of sodium, magnesium, calcium, and potassium are examples of network modifiers encountered in fly ash.

Iron can act as either a network former or a network modifier, depending on its oxidation state. Ferric oxide (Fe_2O_3) is an intermediate oxide and can take part in a glass network with alumina and silica. However, ferrous oxide (FeO) is a network modifier and will introduce nonbridging oxygens which weaken the network. Bool and coworkers (Bool, et al. 1995) have shown that combustion in a drop-tube furnace under reducing conditions can lower the ratio of Fe^{3+} to Fe^{2+} in ash. Presumably, the aluminosilicate melts in which the iron is incorporated have a correspondingly lower viscosity, making them more prone to coalesce and stick to heat transfer surfaces. Clearly, there is a concern that the reducing conditions encountered in staged combustion will have the same effects on iron and aluminosilicate melts in utility boilers.

2.3.3 Pyrite Transformations

Many coals contain appreciable quantities of iron. Much of the iron in eastern U.S. bituminous coals occurs as pyrite (FeS_2) and, to a lesser extent, siderite ($FeCO_3$). Pyrite has been studied extensively because it has been involved in many instances of severe slagging problems. During its transformation from iron sulfide to iron oxide, pyrite passes through a molten state which has been implicated in deposit formation. The mechanism, illustrated in Figure 2-5 has been established by a number of researchers (Bryers

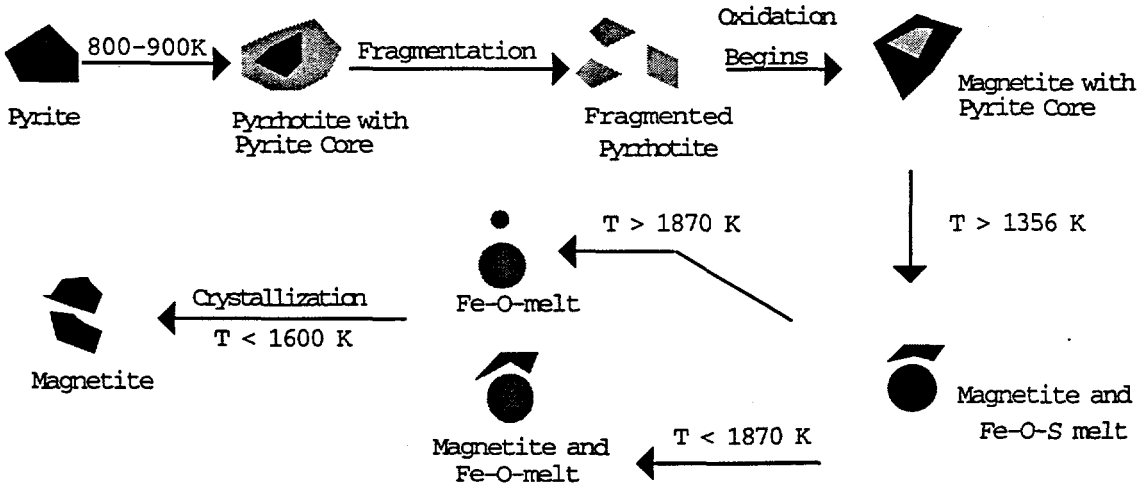

Figure 2-5 Pyrite transformation mechanism (Bool 1995)

1979; Simpson and Bond 1988; Srinivasachar, Helble et al. 1990; Gryglewicz 1992; Wall 1992; Bool, Helble et al. 1995; Bool 1995). Upon heating, pyrite (FeS_2) melts and decomposes, yielding pyrrhotite ($Fe_{0.877}S$). Pyrrhotite then oxidizes. During these initial steps, gaseous sulfur leaves the particle, making it porous and susceptible to fragmentation. The temperature rises as pyrrhotite oxidation continues until the particle melts and forms a

sphere of a molten Fe-S-O mixture. Oxidation of the molten material yields iron oxide, primarily magnetite (Fe_3O_4). Magnetite crystallizes out of the mixture as the particle cools.

The molten Fe-O-S phase has been associated with deposit initiation (Cunningham 1991; Wall 1992). Since it is very sticky, Fe-O-S has the capacity to act as an adhesive and hold itself and other particles to surfaces in the boiler. Therefore, the length of time that molten Fe-O-S takes to oxidize to magnetite is critical in deposition.

Staged combustion may prolong the time for Fe-O-S oxidation and increase deposition. From the kinetics of heterogeneous reactions, it is known that the oxidation rate could be dependent upon temperature, oxygen concentration, and particle size. In staged combustion, both temperature and oxygen concentration are reduced. Lower oxidation rates would be expected. The magnitude of the reduction would, however, depend upon the kinetic regime. In the reaction-controlled regime, reaction rate is very sensitive to temperature and proportional to particle diameter. In the regime controlled by mass transfer, reaction rate is relatively insensitive to temperature but proportional to oxygen concentration and inversely proportional to particle diameter.

There is evidence that Fe-O-S oxidation is controlled by mass-transfer. Experiments have shown that the time spent in the molten phase is proportional to the square of the particle diameter. The utility experience has been that coals which contain pyrite as large particles are more troublesome than fuels with small pyrite particles (Bryers 1979).

If mass transfer is the controlling rate, then staged combustion may tend to prolong the existence of molten Fe-S-O by reason of the lower oxygen concentrations in the reducing region. The difference will not be as large as it could be in the reaction-controlled regime, but it may be enough to influence coalescence of included pyrite particles.

Pyrite frequently occurs as inclusions in combination with other minerals in coal particles. Recently, (Bool 1995) considered the interactions of included pyrite with aluminosilicates as illustrated schematically in Figure 2-6. An important aspect of this mechanism is the dependence of the final product upon temperature and the types of other inclusions the pyrite contacts.

Staged combustion may influence Bool's mechanism in a number of ways. At the elementary level, char will burn more slowly, at least initially, under staged combustion because of the lower oxygen concentration and thereby promote ash coalescence. Char annealing, the loss of reactivity due to the thermal treatment of the char, may also prolong the char burning time (Beeley, Crelling et al. 1996). Temperature will clearly play a role in crystallization, as well as coalescence through its effect on viscosity.

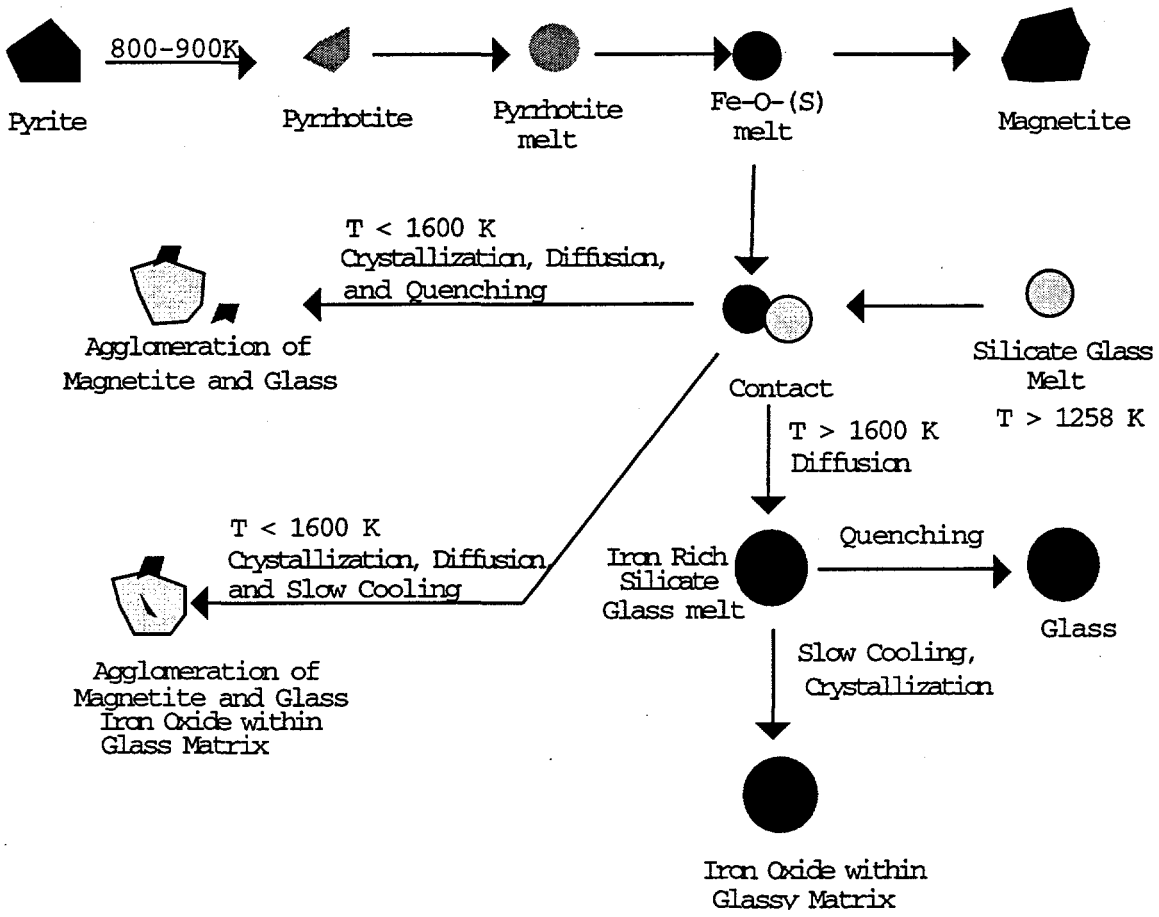

Figure 2-6 Transformation mechanism for included pyrite particles (Bool 1995)

Coalescence may also be promoted by chemical changes in the ash. As noted previously, Bool showed that relatively more of the network-modifying ferrous iron is produced under reducing conditions. This shift, if its effects continue into the oxidizing section of the flame, could result in a ash consisting of larger particles, with lower melting temperatures.

The greatest potential for change, however, is in the lifetime of the Fe-S-O intermediate material. The greater propensity for sticking discussed above for excluded particles translates into greater tendency for coalescence of included particles. In fact, the effect could be magnified since oxygen concentration is typically low at the char surface, even in conventional combustion.

2.3.4 Behavior of Low-rank Coals

In low-rank coals, included minerals interact with ash particles derived from the organically-bound constituents. The oxides of calcium and magnesium are highly reactive and readily combine with quartz and aluminosilicates (Quann and Sarofim 1986; Bool, Helble et al. 1995). Since these oxides are network modifiers, the resulting ash tends to be amorphous.

Again, the effect of staged combustion would seem to be in the extent of coalescence. In tests with two low-rank coals, Zygarlicke and others (Zygarlicke, McCollor et al. 1995) reported that low-NOx firing conditions resulted in increased particle size concurrent with an increase in the fraction of mixed phases and attributed the difference to longer char burning times. The calculated viscosity of the staged combustion ash they produced was significantly lower than that of their conventional ash. Both the larger particles and the mixed phases are consistent with more coalescence. The lower viscosity provides an additional reason for the greater coalescence and portends greater deposition problems with the staged combustion ash.

2.4 THE POTENTIAL IMPACT OF LOW-NOX STRATEGIES ON ASH DEPOSITION

The formation of ash deposits is a function of the size and composition of the impacting ash, as well as boiler conditions such as temperature, particle residence time, radiation heat flux, and the flow patterns and composition of the gas phase. Particle size, momentum, and stickiness are the principal factors which determine whether particles will adhere to a surface to form a deposit. Once formed, the deposit develops strength as the individual particles sinter. The purpose of this section is to discuss ways in which the deposition process may be affected by the use of low-NOx strategies. For a more general description of ash deposition, the reader should refer to reviews such as those found in (Couch 1994, Benson, et al., 1993).

There are several ways in which staged combustion may influence the deposition process. First, slower char oxidation associated with lower oxygen levels may change the nature of the particles which impact on heat transfer surfaces. Specifically, particles will be larger and contain a larger fraction of carbon in some parts of the boiler, affecting both the impaction rate and particle stickiness (Bool, et al., 1995). Much of this additional carbon will burn out after the particle has deposited on the wall, influencing the local gas environment in the deposit. Reducing conditions caused by either the prevailing combustion gases or char oxidation in the deposit may impact the tendency of the deposit to sinter by affecting the oxidation state of the iron as discussed previously with respect to the ash. Incomplete reaction of pyrite may also influence the nature of deposits formed from high pyritic coals. The morphology and surface area of ash formed from in-situ oxidation may also differ from that formed in the bulk combustion stream. These differences may impact sintering rates and/or other chemical reactions that take place within the deposit. As far as

chemical reactions are concerned, Gopalakrishnan and Seehra (1990) found that the extent of sulfation increased with lower oxygen levels. Sulfation has been linked to deposit strength development for some systems.

There is another aspect of low-NOx combustion that is expected to have an important effect on ash deposition. Unpublished calculations by the author and others show an expanded combustion zone and substantially decreased radiation heat fluxes in the burner region when firing under low-NOx conditions. Both the temperature and the extent of sintering of ash deposits are a strong function of the radiation flux levels. Therefore, significant changes in the flux level may have a substantial influence on the deposition behavior in the boiler. This effect may contribute to decreased deposition which has been observed in some utility boilers firing under low-NOx conditions (Muzio, 1996; Richards, 1996).

2.5 ANALYTICAL TECHNIQUES BASED ON SCANNING ELECTRON MICROSCOPY

The two principal analytical techniques used in this study were Computer-Controlled Scanning Electron Microscopy (CCSEM) and Scanning Electron Microscopy Point Count (SEMPC). The details of the techniques have been discussed elsewhere (Jones, et al., 1992), and the reader should refer to these reviews for details.

The two techniques are similar in that they both use image analysis to identify a large number (e.g., 6,000-12,000) of analytical points on the sample of interest. An energy dispersive X-ray spectrum is taken at each of the points in order to determine the weight percent of elements present at that location. In the present study, the measured compositions were ZAF corrected in order to account for element interactions and improve the accuracy of the results. The principal output for both of the techniques is the location of each analytical point and the elemental composition at that point.

The key difference between CCSEM and SEMPC is the method used for selecting the analytical points. In CCSEM, backscattered-electron images are used to identify discrete particles and the measured compositions represent particle compositions. The position, composition, and size (e.g. equivalent diameter) of each particle is recorded. This technique is best suited to the analysis of fly ash particles and discrete minerals in coal. In contrast, analytical points in SEMPC are defined on a uniform grid. Image analysis is then used to distinguish grid points which lie on the sample from those which fall on the mounting material in order to enhance the efficiency of the method. No size information is available and output consists of the location of and composition at each analytical point. SEMPC is best suited to the analysis of deposit samples.

The results of CCSEM and SEMPC are typically reported by classifying the individual compositions according to stoichiometric criteria (Skorupska and Carpenter 1993). The classification systems used in the coal and ash community are based upon mineralogy (Skorupska and Carpenter 1993)(Galbreath, Zygarlicke et al. 1996)(Jones, Kalmanovitch

et al. 1992). Using the compositions of commonly found crystalline materials, criteria have been devised to assign particles to bins based on the information in their X-ray spectra. The amounts of each of the mineral species or phases are reported, as in Figure 2-7.

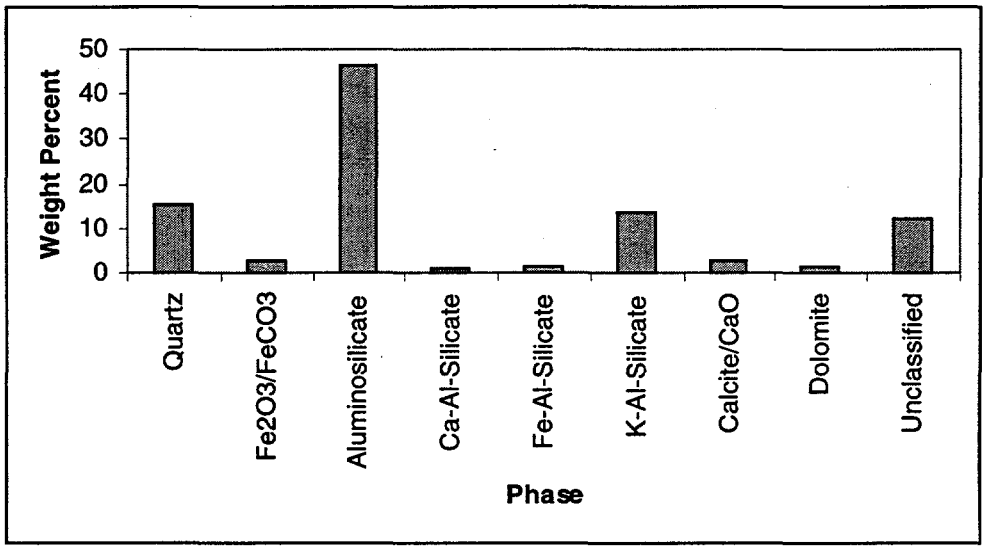

Figure 2-7 Composition (phase) distribution of an Australian coal

Classification with such a phase set based on the stoichiometry of crystalline materials works well when coal minerals are analyzed. In such cases there are relatively few particles that cannot be classified. However, ash samples contain large amounts of amorphous materials with compositions that do not correspond to known crystalline species. This is particularly true of ash from low rank coals. As a result, poor classification results are observed. For example, Benson and others (Benson, Erickson et al. 1991) reported unclassifiable fractions ranging from 40% to 85% of various Black Thunder ash samples.

Poor classification makes the comparison of composition results difficult. Substantial variations between ash samples could be hidden and undetectable in the unknown (unclassifiable) fraction. Consequently, it was necessary to develop a method for characterizing and quantifying the composition of the unclassifiable fraction in order to properly evaluate the effects of staged combustion on the composition of the ash and deposits.

2.6 SUMMARY

Low-NOx firing technologies such as low-NOx burners and staged combustion alter the combustion environment in which fly ash forms. Consequently, altered ash deposition behavior has been observed in boilers. It is possible that the changes in deposition are due to the initial reducing conditions, which have the potential to affect the composition and particle size distribution of the ash. The primary concern is the extent of coales-

cence of ash particles, which is affected by both char oxidation and the properties of the individual ash particles. The behavior of pyrite particles is particularly important in this respect. Low-NOx combustion strategies may also have a direct effect on sintering and chemical reactions in the deposit once it has been formed. A fundamental experimental study is needed in order to understand and quantify the effects of low-NOx combustion on ash behavior.

SECTION 3

EXPERIMENTAL APPARATUS AND PROCEDURE

A series of combustion tests was performed using two coals: 1) Black Thunder, a subbituminous coal from the Powder River Basin of the western United States, and 2) Pittsburgh #8, a bituminous coal from the eastern United States. In addition to the different properties of the two coals, these coals were chosen because they have been used by other DOE investigators in related studies (see e.g., DE-AC22-93PC92190). The coals were fired in a laboratory combustor under both conventional and staged combustion conditions in order to determine the effect of staged combustion on fly ash formation. Fly ash samples were collected and analyzed using computer-controlled scanning electron microscopy. This section describes the experimental apparatus, analytical equipment, computer software, and associated procedures whereby the samples were produced, collected, and analyzed.

3.1 EXPERIMENTAL APPARATUS

3.1.1 Laboratory Combustor

Extensive modifications were made in order to adapt an existing combustor located in the Combustion and Reactions Laboratory at Brigham Young University for the particular needs of this study. A full description of the combustor and the recent modifications is presented elsewhere (Adair 1998). An abbreviated description is included here for completeness.

The facility (Figure 3-1) was designed for the combustion of natural gas and/or pulverized coal in a premixed, non-swirled flame. The main body of the combustor consists of six individual 0.3 m (1 ft) tall sections and one 0.15 m (.5 ft) tall section. Each section consists of a steel cylinder with an inside diameter of 35.5 cm and wall thickness of 0.64 cm lined with castable insulation (National Refractories Purolite). The diameter of the actual combustion chamber is 12.7 cm. The sections are fitted with flanges and O-rings to provide an air-tight seal. The first section has windows for optical access to the flame. The 0.15 m section (staged air injection section) is fitted with four diametrically opposed air injectors for staged air operation. Thermocouples are embedded in the insulated walls over the entire length of the reactor.

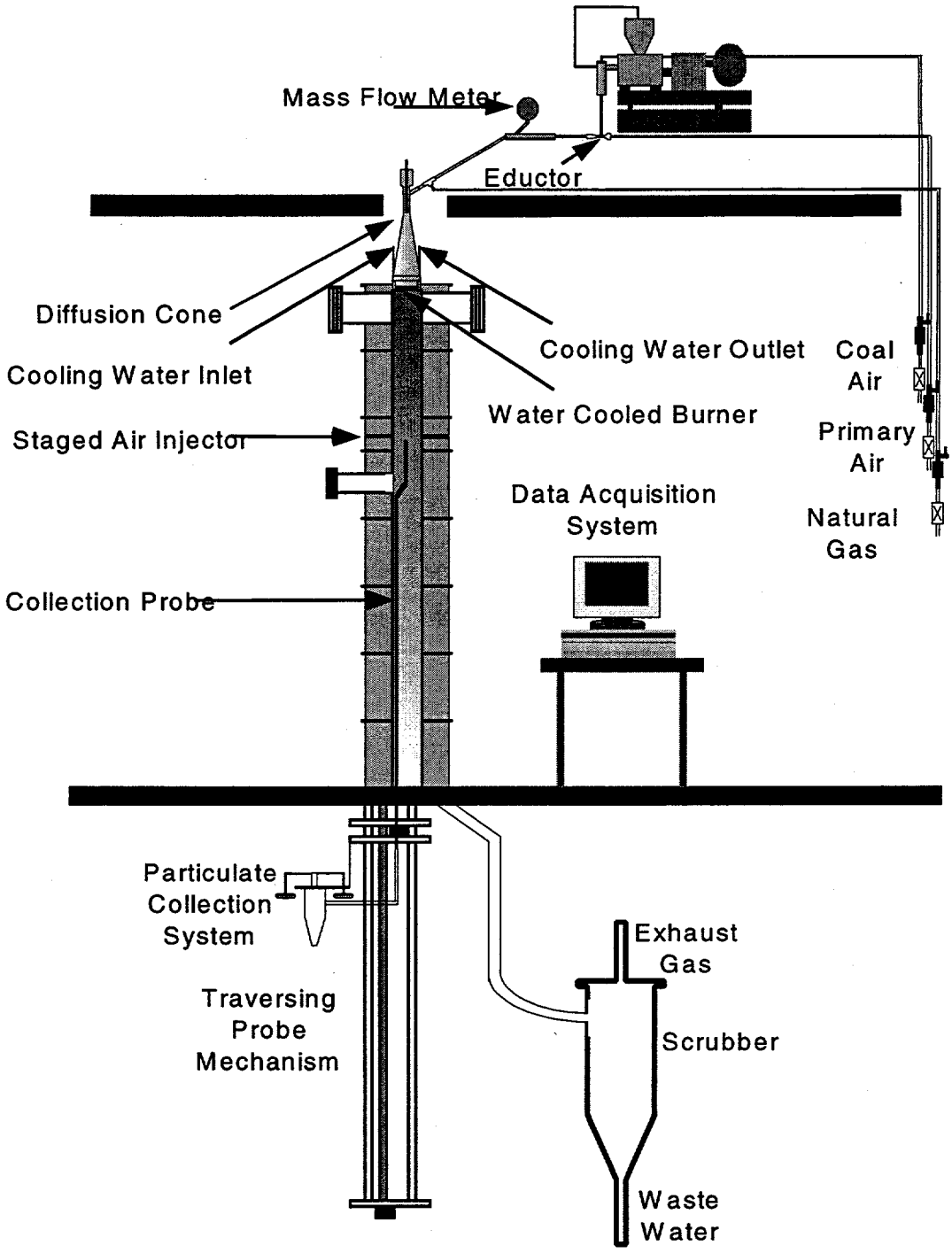

Figure 3-1 Laboratory Combustor

Coal was fed to the reactor at a constant rate by a single-auger gravimetric feeder (Acrison Model 406-BDFM). Feeder operation was monitored and controlled by an Acrison MD-II feedback controller. The coal dropped from the auger into a sealable aluminum funnel attached to the feeder. After passing through the funnel, the coal was entrained in

the primary air stream through an eductor (Fox Valve 2@ 300-SCE-CS). Immediately before entering the combustor, the combined primary coal and air stream went through a tee where it was mixed with natural gas. A flowmeter (Kurz Instruments 502FT thermal element mass flowmeter) located between the eductor and the reactor measured the primary air flow rate. The flow then expanded through the conical inlet section as it approached the burner. A series of screens mounted inside of the cone aided in straightening the flow.

The operation of the facility was monitored online by a data acquisition system (National Instruments) connected to a Macintosh personal computer. The coal feed rate was supplied to the data acquisition system by the feeder controller. The air flow rate was measured and reported by the mass flow meter. Choked-flow orifice meters were used to gauge the feed rate of natural gas and provided a second measure of the air flow rate. A custom-built oxygen meter consisting of an O_2-sensing element (Figaro KE-25) and a pressure transducer (Omega Instruments PX139) was used to provide a secondary check of the firing conditions. It was also used to check for leaks in the reactor.

3.1.2 Particulate Collection System

An isokinetic sampling probe (Figure 3-2) was used to collect fly ash samples from various locations inside the combustor. The probe was constructed of three concentric 304 stainless steel tubes 80" in length. Since the probe insertion point was not at the center of the combustor, the top 6" of the probe were offset 2" to allow sampling from the center of the combustor. A screw mechanism allowed the probe to traverse the combustor axially over a range starting at a point 12" below the burner and extending approximately 60" further toward the bottom.

Particulate samples were drawn through the innermost ¼" OD tube by a vacuum collection system as described below. Quench nitrogen was supplied through the middle tube and entered the sample tube through a ring of ten small holes near the top of the probe. Four 3/32" OD tubes located in the annulus between the middle and outer tubes supplied deionized water to the top of the probe for cooling. The cooling water sprayed into the outer annulus and then dropped to the bottom of the probe, where outlet tubes carried it to the building drain.

Gas and particulates were withdrawn from the probe and pulled through a cyclone separator by a pneumatically actuated vacuum pump (MLL-200, PIAB). The cyclone was custom-machined of aluminum to provide a 2 μm size cut. It was constructed so that it could be quickly removed and disassembled for inspection and cleaning between samples. Fine particles that escaped the cyclone were collected on 47 mm diameter polycarbonate membranes with a 1 μm pore size (Poretics, Livermore, CA). The time required to collect samples for CCSEM analysis ranged from 20 to 45 minutes. Variability was due to sampling position, ash content of the fuel, and the operating conditions.

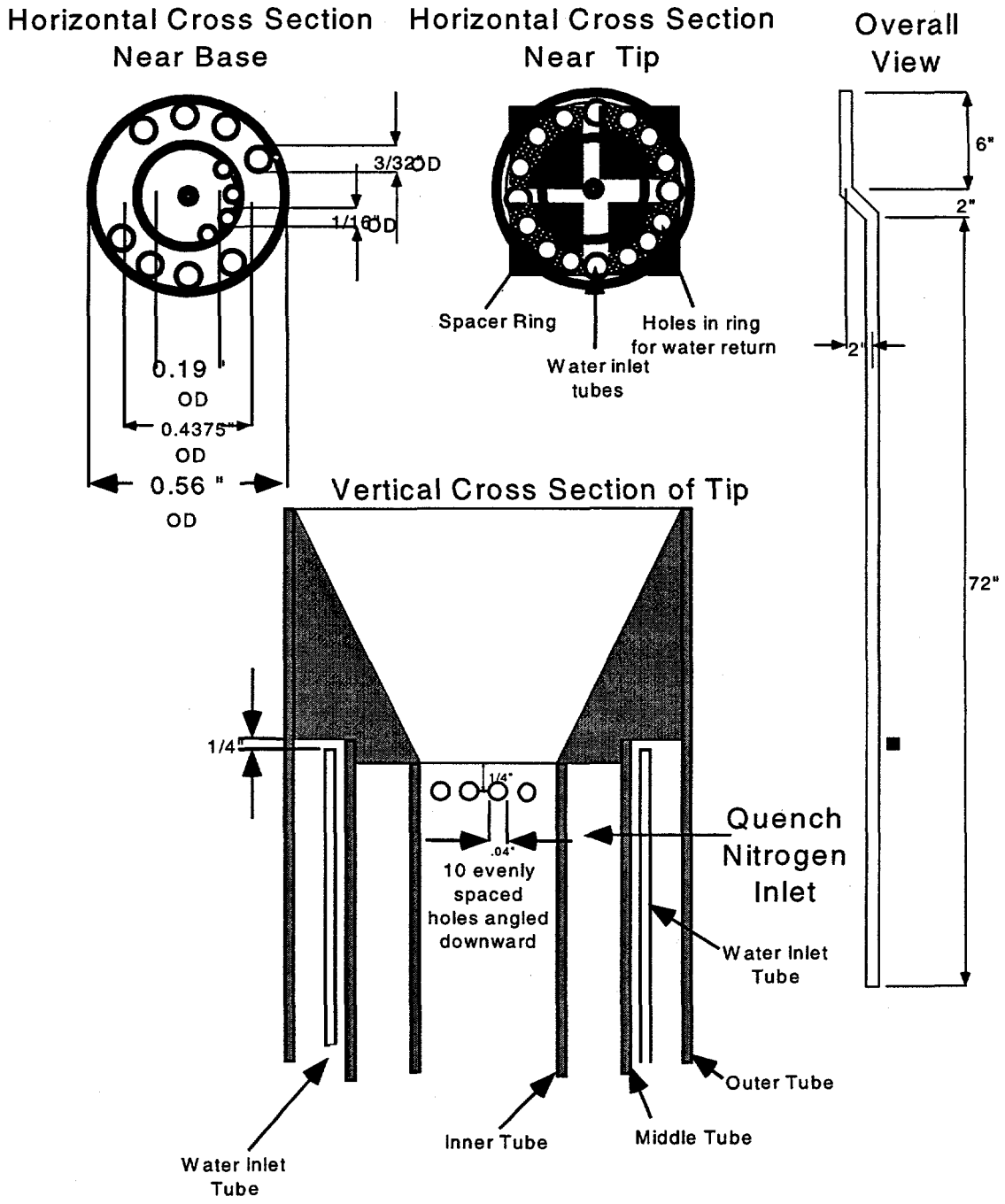

Figure 3-2 Particulate sampling probe

3.1.3 Operating Conditions

The operating conditions under which fly ash samples were collected are shown in Table 3-1. Coal feed rates were chosen to maintain the combustor temperature and to provide reasonable ash sampling times. Pittsburgh #8 has both a larger heating value and more ash per pound. Therefore, it was fired at a lower rate than the Black Thunder.

Since the combustor is laminar and non-swirled, it was necessary to use natural gas to stabilize the flame during the tests. Without natural gas, there is insufficient heat feedback from the flame to ignite the coal. Sustained operation without natural gas is not possible.

Table 3-1 Operating Conditions

Fuel	Condition	Coal (lb/hr)	Natural Gas (kg/hr)	Initial SR	Final SR
Pittsburgh #8	Conv.	1.5	0.37	1.04	1.04
	Staged	1.5	0.37	0.75	1.04
Black Thunder	Conv.	3	0.54	1.04	1.04
	Staged	3	0.54	0.75	1.04

Since the stoichiometric ratios reported in Table 3-1 are based on the combined flow rates of natural gas and coal entering the reactor, they should not be compared directly with operating conditions reported in the literature. The flame is complicated by the premixed natural gas, which reacts very quickly. Under the staged combustion operating conditions in Table 3-1, a large fraction of the oxygen was consumed as the natural gas was converted to water and carbon dioxide. The volatile matter from the coal consumed still more oxygen very quickly. Consequently, the char was oxidized at a local stoichiometric ratio much lower than the reported value. Under the conventional operating conditions, an excess of oxygen was available. However, it was diluted by the water and carbon dioxide produced from the natural gas.

3.1.4 Deposit Probe and Collection

Deposit samples were also collected and analyzed as part of this study. To accomplish this, one of the reactor stages (1 ft. long) was modified to provide access for a deposit probe. The deposit probe, shown in Figure 3-3, consisted of a ¾ inch schedule 40 mild steel pipe with connection fittings for air or water cooling. Coupons of mild steel with an inner diameter slightly larger than the outer diameter of the pipe were designed to fit over this pipe. The deposit samples were collected on these coupons. This configuration permitted sample collection and removal without destruction of the probe. A thermocouple was placed between the pipe and the coupon to provide a measurement of the coupon temperature. A window was installed perpendicular to the probe, allowing for visual observation of deposit buildup. Deposit probes were inserted through a large port

designed to be sealed during deposit collection. This eliminated the contamination of the sample by additional air entering the reactor through the probe port. The port was large enough to allow for probe removal with the deposit intact. The deposit probe stage was designed to replace any of the existing reactor sections, facilitating the placement of the deposition probe stage at various locations in the reactor.

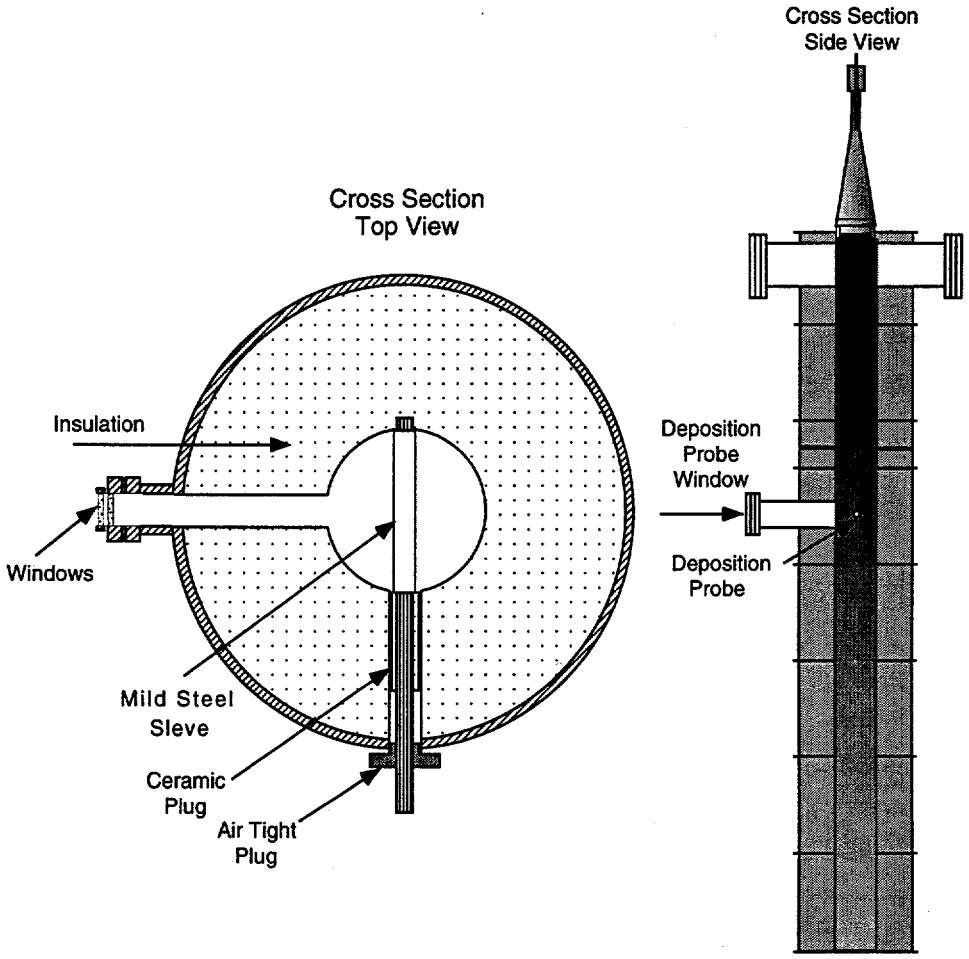

Figure 3-3 Deposition probe stage design

As deposits were collected, it was observed that deposit formation began almost immediately when the probe was inserted in the reactor. After insertion, the temperature between the coupon and the probe tube increased steadily to about 400 °C over a 5 minute period of time. As a deposit continued to build up on the probe, this temperature fell because of the insulating nature of the deposit. Therefore, the coolant flow was manually decreased during operation to keep the temperature approximately constant. Deposits were allowed to grow on the probe for approximately 45 minutes.

A direct comparison of deposits collected under different operating conditions was complicated by the fact that changes in the heating rate and SR result in different particle velocities, burnouts, and particle loading at the collection position. The gas velocity in the reactor was higher at higher stoichiometric ratios and heating rates because of the increased mass flow rates and higher temperatures. In particular, the higher flow rates led to increased erosion of the deposits which made sample comparisons difficult.

Consequently, an alternate strategy was developed to establish the effect of gas phase oxygen concentration on deposit behavior. To do this, several samples were collected at a specific SR and coal feed rate. These samples differed from each other only by the environment they experienced after deposit accumulation was stopped. After deposit growth, two samples were allowed to mature (cure) in a natural gas flame under either (a) oxidizing or (b) reducing conditions. In other words, deposits were grown under the same conditions, but matured in different environments. A few samples were also removed from the reactor after the deposit growth without curing in order to provide a reference point for comparison of the deposit samples. The maturation time was typically 3 hours.

3.2 ANALYTICAL EQUIPMENT AND PROCEDURES

The equipment and procedures used for CCSEM and SEMPC analysis of the parent coals, fly ash samples and deposits collected in the laboratory combustor are briefly described in this section. In addition, two novel CCSEM techniques, developed as part of this study, are also described. The nearest phase classification algorithm (NPCA) is a tool for interpretation of amorphous particle compositions. It is applicable to SEMPC results as well as those obtained from CCSEM. The char/ash association algorithm determines whether ash particles are included in cenospheric ash particles, much as the AMCA algorithms of Yu (1992) and Richards (1994) determine the liberation of minerals in coal. Documentation of the development of these algorithms is also included here, along with a brief description of some additional software.

3.2.1 Equipment

SEM analyses are performed on a JEOL JSM840A scanning electron microscope. The SEM is equipped with a Pentafet light element EDS detector, a Link ISIS X-ray analyzer, and a Link Tetra retractable backscattered electron detector. The EDS detector is equipped with a three-window turret. A standard beryllium window and a MOXTEK ultrathin window occupy the first two positions; the third is empty. The ultrathin window is used during analyses to allow detection of sodium and magnesium. A Link LEMSAS system connected to the ISIS provides computer control of the motion of the X and Y axes of the SEM sample stage. A 150 MHz Hewlett-Packard Vectra personal computer running ISIS Suite 3.1 software under Windows 95 provides the operator interface to the analysis system.

The ISIS system produces composition data and digital images which are processed on Hewlett-Packard 9000 Series 700 computer workstations. The custom-written software used to process these data and interpret the results is described later in Section 3.3.

3.2.2 Sample Preparation

Coal and fly ash samples were prepared in accordance with the coal sample preparation procedure developed by Yu (Yu 1992) and modified by Richards (Richards 1994). Sample material consisting of coal or fly ash and char was blended into a molten mixture of Carnauba wax and Cerita wax (approximately 1:1 by weight) and then allowed to cool while rotating horizontally to prevent the settling of particles. After hardening, sample and wax composites were cast into 1" diameter epoxy plugs. The epoxy plugs were sectioned on a diamond saw (Buehler ISOMET 1000) and then polished to a 1 micron finish (Buehler ECOMET 2/AUTOMET 2). After cleaning to remove the Buehler METADI fluid used as a lubricant during polishing, the polished surface was made conductive by applying a thin carbon layer in a vacuum evaporator.

The procedure used for sample preparation of deposits was essentially that developed and described by West (1996). Since the deposit samples were often only lightly attached to the deposit coupons, the coupons were cast into an epoxy plug soon after collection. To do this, a low viscosity resin epoxy (Buehler No. 20-8149-128 resin and No. 20-8142-064 hardener) was used in order to avoid the presence of large air bubbles in the mounted sample. Once mounted, the samples were cross-sectioned, polished, and carbon coated by the same procedure described for the ash and coal samples.

3.2.3 Microscopic Analysis

The details of the microscopic analysis have been documented by Slater (1998), West (1996) and Adair (1998), and will not be repeated here. Automated runs typically required 6 to 12 hours to complete and were performed overnight. CCSEM runs yielded from 6,000 to 12,000 particle analyses each. Typical numbers of analysis points for SEMPC ranged from 5,000 to 15,000. At the conclusion of a run, a tab-separated variable (TSV) file containing the composition (and size) information for each point analyzed was transferred via network to an HP workstation, along with the stored BSE image of each field in compressed TIFF format.

3.3 SOFTWARE FOR PROCESSING CCSEM AND SEMPC DATA

Extensive modifications were made to the existing BYU software as a part of this study as documented by Slater (1998). Important new capabilities, such as classification of amorphous compositions and liberation determination for swelling chars, were also added to the software. In addition, a number of tools for visualization and interpretation, including an interactive application for creating sophisticated ternary diagrams, were developed. The new capabilities were critical to the successful completion of this work and are therefore described in the sections which follow.

3.3.1 Nearest Phase Classification Algorithm

As mentioned previously, many ash samples, particularly those of low-rank coals, contain significant fractions of amorphous materials which cannot be classified by crystalline phase criteria. Indeed, analyses of Black Thunder ash samples obtained during this project contained as much as 67% unclassifiable material. This made it impossible to compare the composition of ash samples obtained under conventional and staged combustion and necessitated that an alternate means of classification be found.

Automated electron microscopy techniques have been employed in a number of fields of study besides coal and ash analysis. Examples include the study of environmental airborne particulates (Casuccio, Janocko et al. 1983; van Borm and Adams 1988; Kim, Hopke et al. 1989), automotive emissions (Kim, Hopke et al. 1987), and household lead particles (Hunt, Johnson et al. 1993). Researchers in these fields have employed multivariate classification methods instead of mineralogy to interpret their composition data. The NPC algorithm is a combination of such methods with mineralogy.

Methods for classification by grouping of similar objects have been reviewed by (Massart and Kaufman 1983). An object is a multivariate data point, such as a vector of elemental compositions. Similarity is some measure of how alike two objects are. The most commonly used metric is the Euclidean distance between the objects

$$d = \sqrt{\sum_{i=1}^{n} (x_i - y_i)^2}$$

where n is the number of variables or the dimension of the data (Massart and Kaufman 1983). In contrast to phase identification by mineralogy, grouping in clusters proceeds without any preconceived notions about the composition of the phases or even how many there should be. Clusters are formed as the data are examined. Afterwards, a classification scheme can be devised to compare different samples (Hunt, Johnson et al. 1993).

One drawback of using a classification scheme such as this is that the phases do not necessarily have any physical significance. The nearest phase classification (NPC) algorithm described here uses similarity but retains much of the physical significance of the mineralogical phases. Mineralogy is used where possible for the classifiable compositions. When this fails, similarity or nearness is used to group the amorphous or unclassifiable compositions with clusters associated with the mineralogical phases.

3.3.1.1 Theory

As discussed above, the composition results from CCSEM analyses are usually presented in terms of a set of predefined mineralogical species or phases. Typically, a set of 30-60 phases is used. Each phase is associated with a set of criteria. As illustrated in Table 3-2, each of the criteria which define phases is a linear inequality involving one or more of the analyzed elements.

Table 3-2 Mullite Criteria

	Criterion		Criterion
1	$Al + Si \geq 85$	6	$S \leq 5$
2	$(Al)/(Si) \leq 4$	7	$Ti \leq 5$
3	$(Al)/(Si) \geq 2.4$	8	$Mg \leq 5$
4	$Ca \leq 5$	9	$Na \leq 5$
5	$Fe \leq 5$	10	$K \leq 5$

To be classified, a composition must satisfy all of the criteria for one of the phases. Classified compositions are said to "belong" to a phase. If a composition fails to satisfy the criteria of any phase, it is identified as unclassifiable. The NPC algorithm is applied only to these unclassified particles.

The primary concept behind the NPC algorithm is that the composition can be interpreted geometrically in a real number space of dimension n, where n is the number of analyzed elements. Each composition is an n-vector corresponding to a point in n-space. Phases are polyhedral regions in n-space (polygonal in two dimensions) whose boundaries are expressed algebraically by the constraints. Compositions which "belong" to a phase lie inside of the corresponding region. Unclassifiable particles are those which lie outside of the boundaries of all phases. This is illustrated, in two dimensions, in Figure 3-4. Two phases, mullite and quartz, are marked in the silicon-aluminum plane. The points inside of the shaded areas belong to the corresponding phase. The clusters of points outside of the shaded areas are unclassified. It is apparent that while unclassifiable compositions lie outside of both phases, they are closer to one phase than the other. This is shown explicitly in Figure 3-5, where the distances from one of the unclassifiable compositions to the phases have been computed.

The distance between an unclassifiable composition $\mathbf{x}^*$ and a phase is found by finding the composition $\mathbf{x}$ that is closest to $\mathbf{x}^*$ but still belongs to the phase. Finding $\mathbf{x}$ is an optimization problem with a quadratic objective function (the square of the Euclidean distance) and a set of linear constraints (the phase criteria). Such problems are called quadratic programs or QP's.

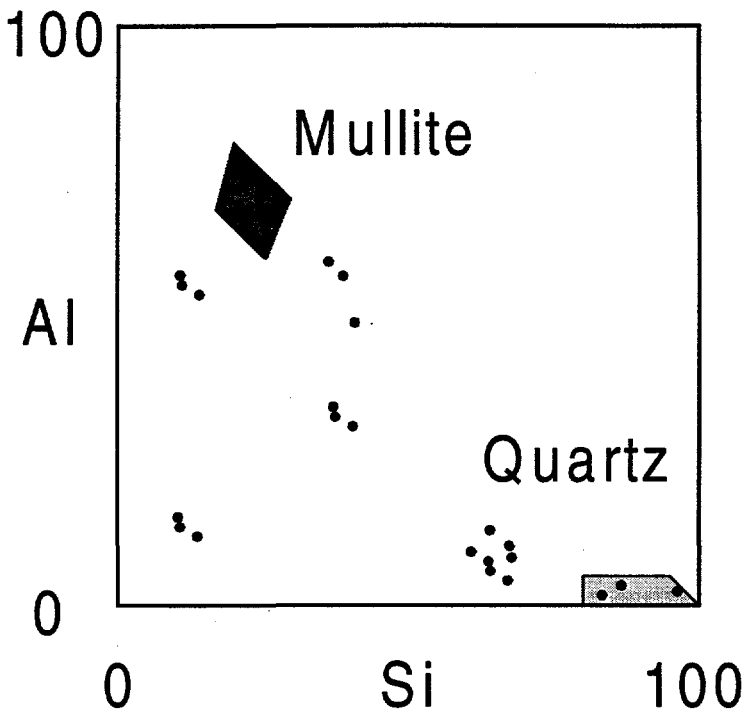

Figure 3-4 Example of two phases in the Si-Al plane

Since QP's often include numerous constraints, it is common practice to use matrix notation to describe them. This means that instead of writing out a list of many linear inequalities, one would collect all of the coefficients into matrices and vectors and write one compact vector inequality.

For example, consider the mullite criteria in Table 3-2. There are ten criteria, each of which is a simple linear inequality, or a ratio, which can be rearranged into a linear inequality.

To transform into matrix notation, each criterion is cast into the standard form:

$$a_1 Na + a_2 Mg + a_3 Al + a_4 Si + a_5 P + a_6 S + a_7 Cl + a_8 K + a_9 Ca + a_{10} Ti + a_{11} Fe + a_{12} Ti \leq b$$

Thus, the first criterion becomes

$$0Na + 0Mg - Al - Si + 0P + 0S + 0Cl + 0K + 0Ca + 0Ti + 0Fe + 0Ba \leq -85$$

After all the criteria are written in standard form, the coefficients are collected into matrices, with one row per criterion:

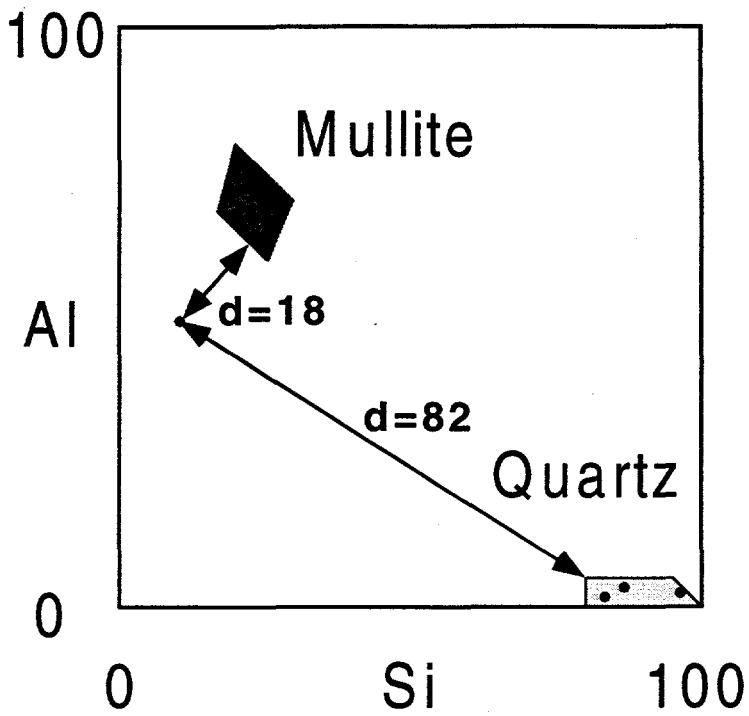

Figure 3-5 Distance to phases in the Si-Al plane

$$\begin{bmatrix} 0 & 0 & -1 & -1 & 0 & 0 & 0 & 0 & 0 & 0 & 0 & 0 \\ 0 & 0 & 1 & -4 & 0 & 0 & 0 & 0 & 0 & 0 & 0 & 0 \\ 0 & 0 & -1 & 2.4 & 0 & 0 & 0 & 0 & 0 & 0 & 0 & 0 \\ 0 & 0 & 0 & 0 & 0 & 0 & 0 & 0 & 1 & 0 & 0 & 0 \\ 0 & 0 & 0 & 0 & 0 & 0 & 0 & 0 & 0 & 0 & 1 & 0 \\ 0 & 0 & 0 & 0 & 0 & 1 & 0 & 0 & 0 & 0 & 0 & 0 \\ 0 & 0 & 0 & 0 & 0 & 0 & 0 & 0 & 0 & 1 & 0 & 0 \\ 0 & 1 & 0 & 0 & 0 & 0 & 0 & 0 & 0 & 0 & 0 & 0 \\ 1 & 0 & 0 & 0 & 0 & 0 & 0 & 0 & 0 & 0 & 0 & 0 \\ 0 & 0 & 0 & 0 & 0 & 0 & 0 & 1 & 0 & 0 & 0 & 0 \end{bmatrix} \begin{bmatrix} Na \\ Mg \\ Al \\ Si \\ P \\ S \\ Cl \\ K \\ Ca \\ Ti \\ Fe \\ Ba \end{bmatrix} \leq \begin{bmatrix} -85 \\ 0 \\ 0 \\ 5 \\ 5 \\ 5 \\ 5 \\ 5 \\ 5 \\ 5 \\ 5 \\ 5 \end{bmatrix}$$

This matrix inequality is written symbolically as $\mathbf{Ax} \leq \mathbf{b}$, where the definitions of **A**, **x**, and **b** can be inferred from the example.

Using this notation, a QP to minimize some quadratic function f of a composition **x** subject to the constraint that **x** belong to a phase with criteria $\mathbf{Ax} \leq \mathbf{b}$ is written as

$$\min f(\mathbf{x})$$

$$\text{subject to } \mathbf{Ax} \leq \mathbf{b}$$

If the function f(**x**) is defined as the square of Euclidean distance between the unclassifiable composition $\mathbf{x}^*$ and a member composition **x**

$$f(\mathbf{x}) = \sum_{i=1}^{12} (x_i^* - x_i)^2$$

then the solution of the above QP will be the distance from the unclassifiable composition to the phase. A similar QP can then be solved for each phase in order to determine the nearest phase.

After the nearest phase is determined, the residual vector $\mathbf{r} = \mathbf{Ax} - \mathbf{b}$ can be computed to reveal why **x** was not classified. Elements of **r** with positive values indicate violated constraints. There are two possible uses for this information. First, it could be used to guide revision of the criteria. For example, if a number of compositions were found to violate one constraint by a small amount, it might be advantageous to relax that constraint so that the phase will be slightly more inclusive. It might also be advantageous to define a new phase similar to the original but with the violated criterion removed or relaxed. Second, the violated criteria could be used as a means of subclassifying the compositions in a nearest phase group. For example, in Figure 3-4 there were two clusters of unclassified particles, each with an aluminum content of slightly greater than 50% near the mullite phase. NPC would lump all of the particles in these two clusters into the near mullite group even though they are clearly different, having dissimilar silicon contents. However, since they lie off of different faces of the mullite polygon, they can be differentiated by noting which criterion they violate. The distance to the phase could also be used in this respect.

3.3.1.2 Implementation and Performance

The NPC algorithm was implemented as a set of FORTRAN subroutines. To minimize memory and time requirements, a sparse matrix data structure was used to eliminate the large number of zeros in the coefficient matrices. QP's were solved using the Sequential Quadratic Programming (SQP) subroutine from OptdesX (Design Synthesis, Orem, Utah). The criteria for a set of 53 mineral phases were translated into the matrix notation and packed into the sparse matrix data structure. The subroutines were incorporated into both CCSEM and SEMPC, and compiled for use on a Hewlett-Packard VISUALIZE

the NPC algorithm requires approximately 0.5 seconds per unclassifiable composition. Thus, a CCSEM or SEMPC run containing 10,000 particles with 60% unclassifiable would take 50 minutes to process.

3.3.2 Char and Ash Associations

CCSEM results and stored BSE images of Pittsburgh #8 samples were used to investigate the effect of liberation on the transformation of pyrite during staged combustion. The analyses were performed using an algorithm specifically designed for use with the swollen char of Pittsburgh #8.

Richards and Slater (Richards 1994) developed an AMCA routine for liberation analysis of coal minerals. Their algorithm assumed that the cross sections of coal particles seen in BSE images were continuous and that included minerals were immediately adjacent to the coal. Minerals could not be matched with their parent coal particles if there appeared to be a gap between the mineral and the coal.

This assumption made the algorithm unsuitable for use with the Pittsburgh #8 samples. Due to swelling nature of this coal, the char it forms is highly vesicular and porous. The problem is illustrated in Figure 3-6. Although the large char particle is a single entity, it appears as several different pieces in cross section. Most of its ash inclusions seem to be adjacent to char areas, but there are several inclusions in the interior of the particle which do not appear to be connected to the char. There may also be single-pixel gaps between the included particle and the adjacent char which cannot be seen without magnification. Because of these features, the algorithm would fail to properly identify included and excluded ash particles.

However, a human observer could make the distinction manually by noting which areas of the image are occupied by char and which are not, and then identifying ash particles located inside of char areas as included. For example, boundaries such as those in Figure 3-7 might be drawn around the char.

Since manual analysis of the large number of fields required to obtain enough data to be meaningful would be too tedious, a computer program was written to perform the task automatically.

The program is used as a post-processor for CCSEM analyses. The locations of individual ash particles are determined from BSE images of the sample and output files from the standard CCSEM analysis. Other input data, such as threshold values and the range of fields to examine, are provided at runtime via a graphical user-interface.

On each field, the program proceeds in much in the same manner that a human operator would in performing the job manually. First, char is identified by brightness in the BSE image. Any pixel whose brightness is between user-specified threshold values is taken as char. Ranges of continuous char pixels are identified as char particles. To account for the vesicular morphology of the chars, the continuity requirement is relaxed so

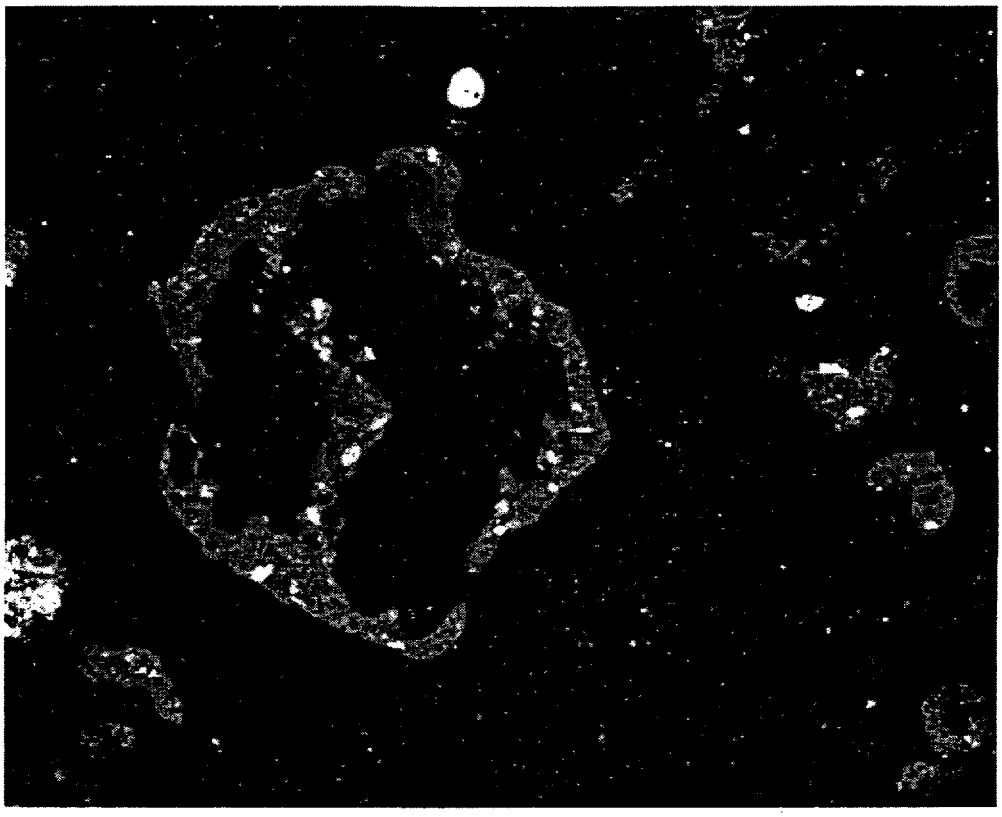

Figure 3-6 BSE image of char and ash mounted in wax

that char pixels separated by as many as five "empty" pixels can still be considered continuous. This allows large, porous char such as that in Figure 3-6 to be identified as single features, as demonstrated in Figure 3-8. Note that the value of five for the continuity relaxation factor was determined by trial and error on BSE images taken at 250X. Different values may be suitable at other magnifications.

Following the first step, each char particle is represented by a set of pixels. To properly identify inclusions, a set of pixels that all of the area that is associated with the char particle, including interior spaces and the areas between apparently separate pieces of char in addition to the char pixels, is required. This set is obtained by determining the convex hull of the char pixel set. For a set X in two dimensions, the convex hull [X] is the minimum convex polygon that contains X (Sugakkai 1985). This task is accomplished using the MATLAB toolkit function `convhull`, which returns the vertices of the convex hull as a set of (x,y) coordinates.

The correspondence between convex hulls and the char areas in Figure 3-7 is shown in Figure 3-9. Hulls have not been shown around small char particles. (The definition of small is a user-specified number of pixels.) It is apparent that the large char particle was erroneously identified as two particles. However, the included area of the particle has been correctly represented. Therefore, the error has no significance for the determina-

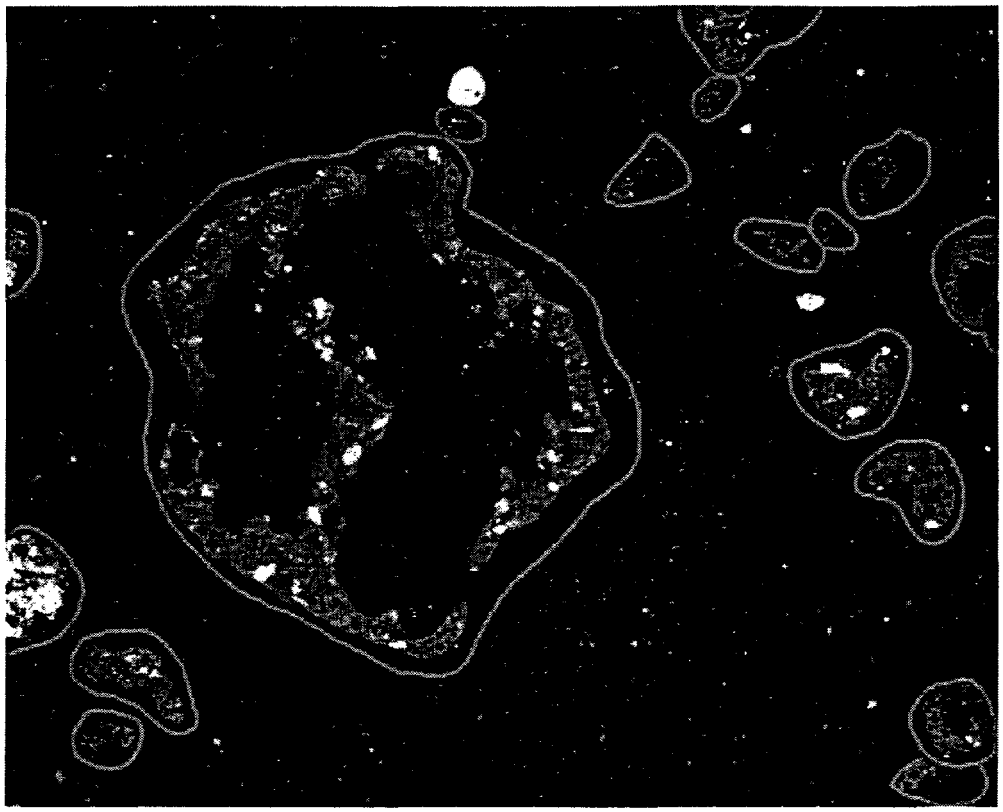

Figure 3-7 BSE image of char and ash with hand-drawn boundaries

tion of liberation data. Were the data to be used as input to an ash formation model, it would be necessary to correctly identify all of the particles that could coalescence with one another. This might be accomplished by adjusting the continuity relaxation factor to allow larger gaps when the char particle appears to be large.

The locations of ash particles are checked against the convex hulls using the MATLAB toolkit function `inpolygon`. Particles are flagged with a feature number corresponding to the appropriate char particle if they are included and with a zero otherwise.

After each field is processed, the program creates a visual representation or image of its results, comparable to Figure 3-9. Included particles are marked with a plus (+) so that the program's findings can be manually verified. Each image is stored, occupying slightly more than one quarter-megabyte of disk space.

The program was implemented as a set of user-defined functions in MATLAB 5.0. Running on an HP VISUALIZE C180 workstation, each field requires approximately 30 seconds of CPU time for processing. To date, ash liberation analyses have been performed using typical CCSEM runs of approximately 100 fields at 250X magnification.

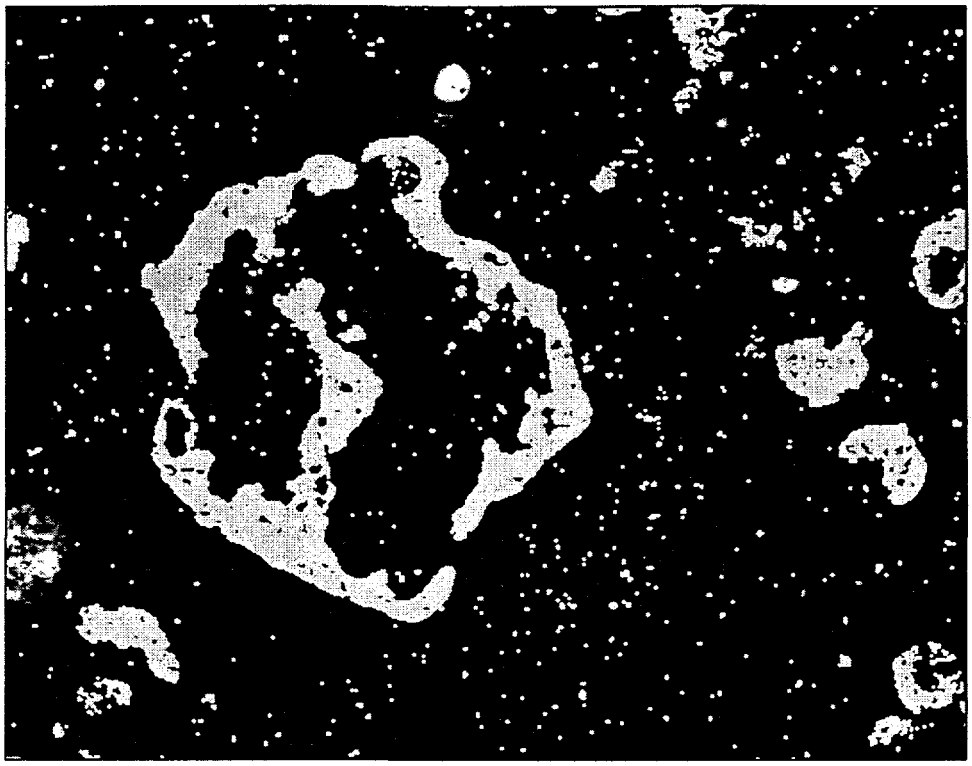

Figure 3-8 Binary image showing the locations of char particles

3.3.3 Ternary Diagram Software

A program to generate 3D triangular diagrams such as that shown in Figure 3-10 was also developed as part of this work. Others have used similar types of diagrams to display results. However, the software developed as part of this study has several attractive features. First, it includes a user-friendly graphical interface which facilitates its use for routine examination of data, as well as for generation of final presentation quality figures. Also, it is based on commercial software (MATLAB) which is available on a variety of computational platforms. It has a number of features, described briefly below, that provide flexibility and power for the user. It is believed that the program represents a useful analysis tool; therefore, it is documented briefly in the paragraphs which follow.

The program has two interface windows. The first (Figure 3-11) is the primary control panel. From it, the user specifies which elements to plot, the names of the data sets to plot (two can be viewed simultaneously in adjacent plot windows), and several parameters pertaining to the appearance of the plots. A popup menu allow the user to set the plotting cutoff level specifying which compositions from the data set will be included in the diagram. Only particles whose mole or weight percents of the selected elements sum to at

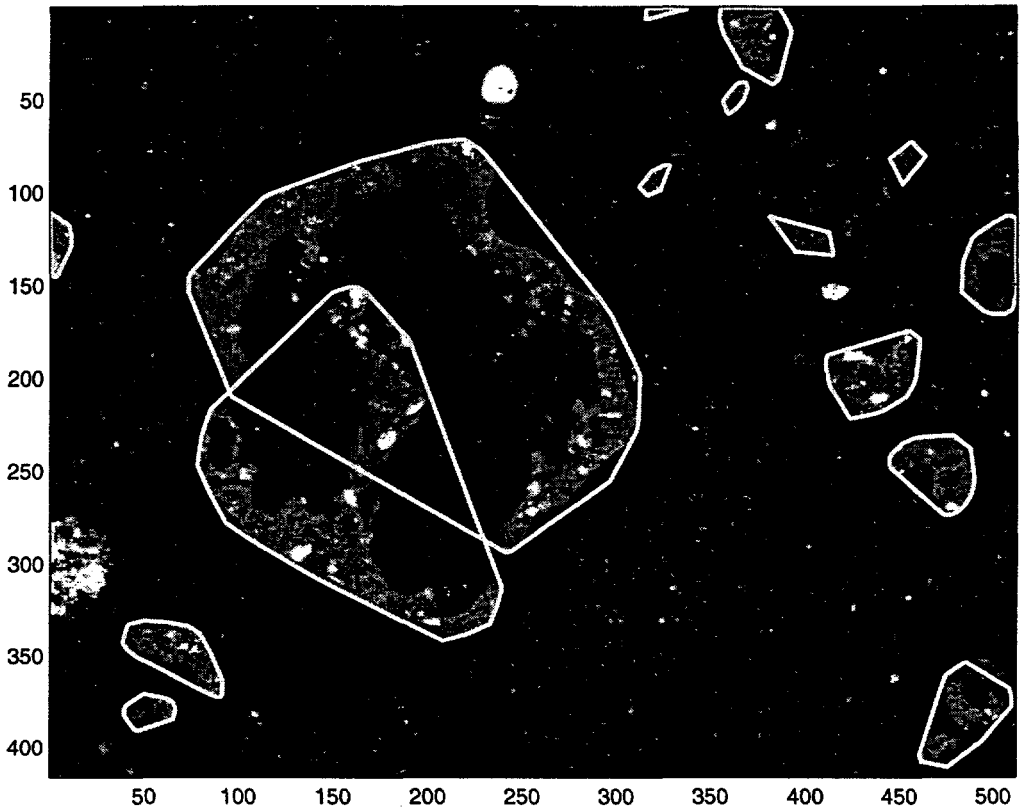

Figure 3-9 BSE image of char with convex hulls

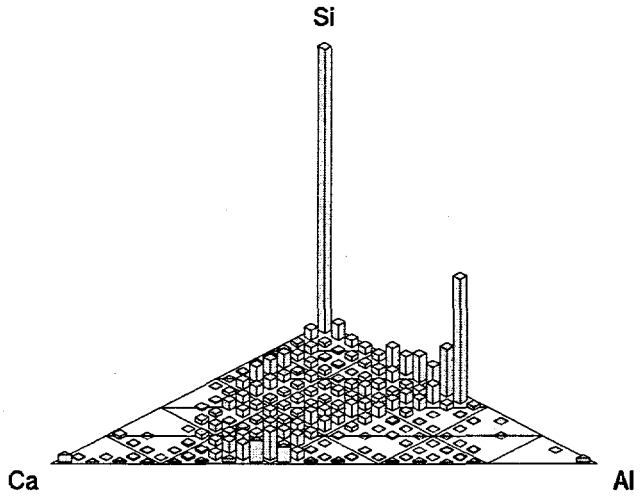

Figure 3-10 Example of a 3D ternary diagram.

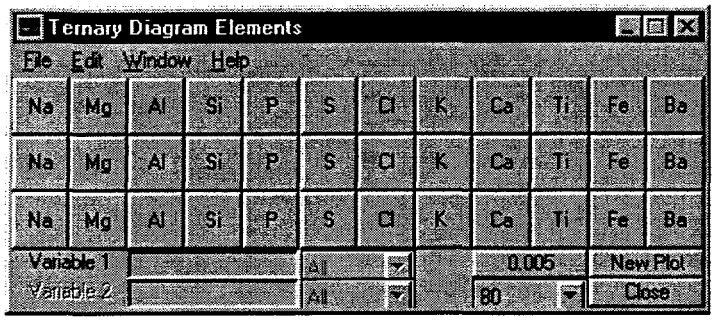

Figure 3-11 Ternary diagram control

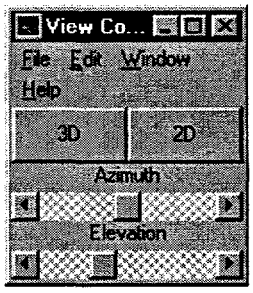

Figure 3-12 View control

least the cutoff value are plotted. The default is eighty percent. Another cutoff value specifies the weight fraction that a composition bin must meet before it will be plotted. The default for this value is 0.005.

The second interface window (Figure 3-12) is used to control the viewing height and angle. A default three-dimensional view and a two-dimensional (overhead) view can be accessed directly via pushbuttons. Alternatively, the height and azimuth can be controlled via the two sliders.

A number of features were included in the program to aid in exploring data. When two data sets are viewed simultaneously, height axis scaling is synchronized so that the plots can be compared. More than one element can be placed on a vertex so that pseudo-ternary diagrams can be created.

Since it is unlikely that all of the particles in a particular data set will meet the plotting cutoff, the program reports the cumulative weight fraction of those that are included on the diagram after each plot change. This information is useful when comparing data sets. If the fractions of the two data sets that are plotted are not the same, the data sets are different even though their diagrams may appear otherwise. A facility is also provided for determining which compositions in a data set do not meet the current plotting criteria.

The diagrams can be saved or printed in a variety of common formats via MATLAB's standard printing functions.

The program was written in MATLAB 5.1 and has been tested on Hewlett-Packard HP 9000 Series 700 workstations and personal computers running Windows 95. The diagrams presented in the following sections were created on a workstation.

SECTION 4

BLACK THUNDER ASH RESULTS AND DISCUSSION

Black Thunder coal was used in this study to determine the effects of staged combustion on the formation of fly ash from low-rank coals containing organically-bound inorganic constituents. The coal was burned in a pilot-scale combustor under both conventional and staged combustion conditions to investigate whether the latter caused differences in the particle size distribution or composition of the resulting ash. Results for Pittsburgh #8 ash are given in Section 5.

The coal was analyzed by CCSEM to determine the size and composition of the discrete minerals it contained. Minerals are one of the starting materials from which ash is formed. During combustion, the organically-bound inorganic constituents also form ash particles, some of which coalesce with ash particles derived from discrete minerals. The extent of coalescence is one of the variables that could be affected by staged combustion.

The composition and particle size distributions of fly ash samples were also determined by CCSEM analysis. Results of the Black Thunder coal and ash analyses are presented and discussed in this section.

4.1 COAL ANALYSIS

A proximate analysis of Black Thunder coal was performed by a commercial laboratory. The results (Table 4-1) show that the ash content of Black Thunder is small, less than 5% by weight, and that there is a significant amount of water in the fuel.

The results of two ash elemental analyses are also presented in Table 4-1. The bulk analysis in the column to the left was obtained by ashing a coal sample at low temperature and analyzing the residue by X-ray fluorescence (XRF). It reflects all of the inorganic constituents in the coal, including the organically-bound elements. In contrast, only discrete minerals were considered in the CCSEM analysis.

Both analyses indicate significant quantities of silicon, aluminum, iron, calcium, and sulfur in the coal. The differing proportions are due to the large fraction of organically-bound material, which was detected only in the bulk analysis. The majority of the calcium and magnesium and some of the aluminum, sulfur, and iron are organically-bound (Bool, et al., 1995; Erikson, 1994; Richards, 1994).

Table 4-1 Bulk analyses of Black Thunder coal

Proximate Analysis (As received)	
Moisture	23.91%
Ash	4.73%
High Heating Value (BTU/lb)	8849
Sulfur	0.42%

Ash Analysis (Weight percent)		
	Bulk	**CCSEM**
Silica, SiO_2	29.87	50.68
Alumina, Al_2O_3	15.53	22.49
Titania, TiO_2	1.21	1.19
Ferric Oxide, Fe_2O_3	6.00	2.92
Lime, CaO	23.14	8.37
Magnesia, MgO	5.19	0.82
Potassium Oxide, K_2O	0.37	0.29
Sodium Oxide, Na_2O	1.06	0.29
Sulfur Trioxide, SO_3	13.21	3.4
Phosphorus Pentoxide, P_2O_5	1.06	7.19
Strontium Oxide, SrO	0.46	-
Barium Oxide, BaO	0.76	2.35
Manganese Oxide, Mn_3O_4	0.00	-
Undetermined	2.14	-

Mass balance calculations applied to the bulk analysis and chemical fractionation results for Black Thunder indicate that approximately half of the total inorganic constituents are discrete minerals (Bool, et al., 1995; Richards, 1994). The phase distribution of the discrete minerals (Table 4-1) was determined by CCSEM. Quartz and clays (aluminosilicates) are the prevalent minerals found in the coal. There is also a calcium-aluminum phosphate. The composition of the Ca-Al-P phase seen in these results corresponds to the mineral crandallite $(CaAl_3)(PO_4)_2(OH)\bullet H_2O$ (Pierrot, 1979). Huggins and Huffman (Bool, et al., 1995) have also reported crandallite in Black Thunder. However, the composition of the phases that they reported does not match the crystalline stoichiometry.

A small quantity (2%) of pyrite (FeS_2) was also detected in the coal. A slightly lesser amount of either pyrrhotite (FeS) or iron sulfate ($FeSO_4$) was also detected. CCSEM cannot distinguish the two because it does not analyze for oxygen. There is so little of this phase (<2% of the minerals) that it was not considered necessary to determine its true composition. However, given the high water content of Black Thunder, it is possible that the material was $FeSO_4$ formed by oxidizing some of the pyrite.

For reasons discussed below, the particle size distribution of the coal was determined using a Coulter counter. As illustrated in Figure 4-1, the coal was ground to 70% under 200 mesh (74 μm), a typical utility grind. Note that the largest coal particles observed were on the order of 300 μm in diameter.

Table 4-2 Phase distribution of minerals in Black Thunder coal

Phase	Weight Percent of Mineral Matter
Quartz	28
Fe2O3/FeCO3	1.66
Aluminosilicate	32.97
Ca-Al-Silicate	6.62
Pyrite	2.04
Barite	1.05
Calcite/CaO	1.21
Dolomite	1.11
FeS/FeSO4	1.68
Ca-Al-P	12.91
Unclassified	7.02

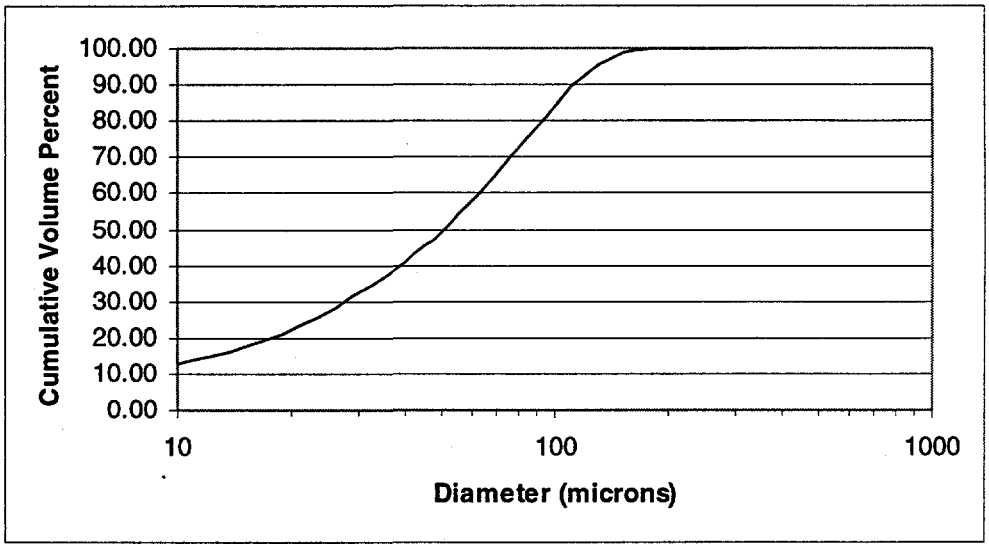

Figure 4-1 Particle size distribution of Black Thunder coal

4.2 SIGNIFICANCE OF COAL PROPERTIES

It was demonstrated in the preceding section that Black Thunder coal contains both discrete minerals and organically-bound constituents. Since the organically-bound fraction is relatively large there is a particularly close relationship between char combustion and ash formation. Indeed, half or more of the ash is actually created as the char burns and leaves the organically-bound elements behind.

As discussed in Section 2, full coalescence and no coalescence are the two limiting cases used for modeling ash formation. Richards (Richards, 1994) modeled the formation of ash from Black Thunder coal by full coalescence using CCSEM and chemical fraction-

ation results as input, as illustrated in Figure 4-2. CCSEM provided the size of coal particles, and the size and composition of the minerals. Chemical fractionation provided the composition of the organically-bound constituents, which were assumed to be evenly distributed in the coal.

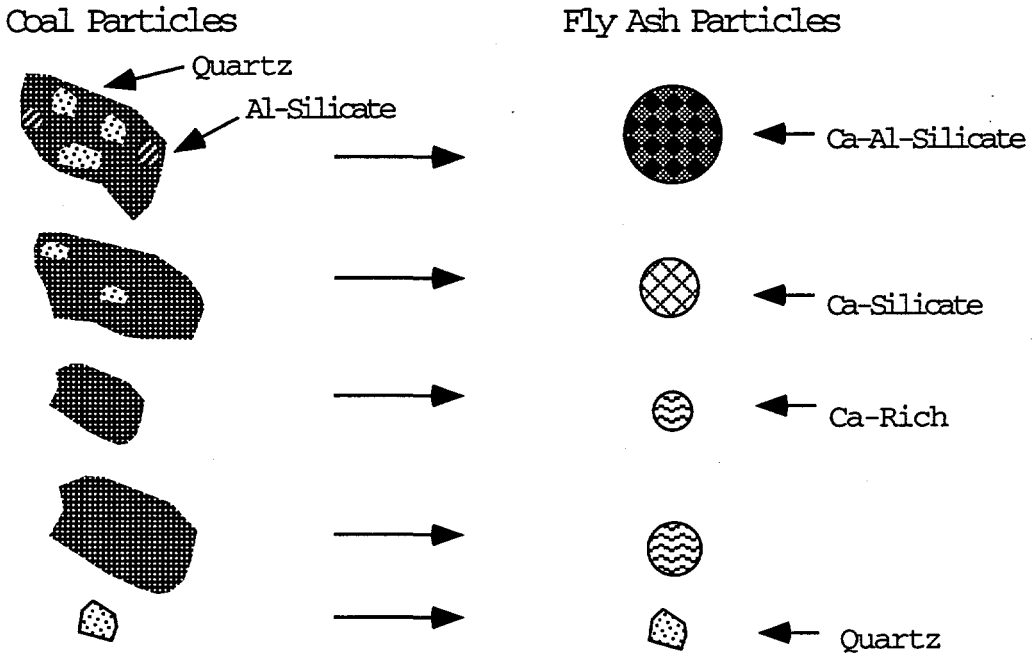

Figure 4-2 Full coalescence assumption for ash formation

Qualitatively then, the ash will consist of three types of particles:

1) Particles derived solely from the discrete minerals,

2) Particles derived solely from the organically-bound material, and

3) Particles derived from both discrete minerals and the organically-bound material.

Excluded particles will not combine with the organically-bound material, since they are not associated with the char particles from which it originates. Included particles will interact with organically-bound material to some extent. Therefore, only excluded minerals will contribute to the formation of ash particles derived solely from minerals. In the remainder of this section, Richards' approach will be used with the coal and mineral data presented in the previous section to estimate some of the properties of the other two types of ash particles. This information will be useful in interpreting the results.

4.2.1 Maximum Particle Size

First, an upper limit on the size of an ash particle formed solely from organically-bound constituents will be established. Since ash from separate coal particles does not interact during combustion, the largest ash particle will be formed by coalesce of the inorganic constituents bound in the largest coal particle. Therefore, the calculation will be based on coal particle with a diameter of 300 μm. The properties of the coal and organically-bound constituents listed in Table 4-3 are taken from Richards (Richards, 1994).

Table 4-3 Properties of inorganic constituents in Black Thunder Coal

Element	Weight Fraction of Coal * 10^4
Na	9.004
Mg	27.86
Al	38.92
Si	0
P	0
S	0
Cl	0
K	0
Ca	131.9
Ti	0
Fe	20.73
Ba	0
Total	228.5
Densities (g/cc)	
Organic	1.3*
Ash	2.6
*(Gan, et al., 1972)	

The mass of this 300 μm particle is

$$m = \rho V_c = \left(1.3 \cdot \frac{g}{cm^3}\right)\left(\frac{\pi}{6} \cdot 0.03 \cdot \mathrm{cm}^3\right) = 1.83 \cdot 10^{-5} \cdot g$$

Using the total oxide mass fraction from Table 4-3 the ash content of this particle is

$$m_a = mw = (1.83 \cdot 10^{-5} \cdot g)\left(2.285 \cdot 10^{-2} \cdot \frac{g}{g}\right) = 4.20 \cdot 10^{-7} \cdot g$$

The hypothetical volume of the ash particle is simply the mass divided by the density

$$V = \frac{m_a}{\rho_a} = \frac{4.20 \cdot 10^{-7} \cdot g}{2.6 \cdot \frac{g}{cm^3}} = 1.61 \cdot 10^{-7} \cdot cm^3$$

Finally, the diameter is

$$d = \sqrt[3]{\frac{6V}{\pi}} = 6.76 \cdot 10^{-3} \cdot cm$$

Thus, in the absence of mineral inclusions, the maximum ash particle diameter expected to form from organically-bound constituents during the combustion of Black Thunder is approximately 68 μm. This is an upper limit, since the few 300 μm particles present in the coal would likely fragment during combustion.

4.2.2 Detection Limit

The same modeling approach can also be used to estimate the fraction of the total ash will be of sufficient size to analyze by CCSEM. Particles with diameters less than about 1 μm cannot be analyzed by CCSEM. Therefore, the volume and mass of the smallest ash particle that can be analyzed are

$$V = \frac{\pi}{6} d^3 = 5.236 \cdot 10^{-13} \cdot cm^3$$

and

$$m_a = \rho V = \left(2.6 \cdot \frac{g}{cm^3}\right)(5.236 \cdot 10^{-13} \cdot \mathrm{cm}^3) = 1.361 \cdot 10^{12} \cdot g$$

The mass of the parent coal particle is then

$$m_c = \frac{m_a}{w} = \frac{1.361 \cdot 10^{-12} \cdot g}{2.285 \cdot 10^{-2} \cdot \frac{g}{g}} = 5.956 \cdot 10^{-11} \cdot g$$

The volume and diameter are then found directly:

$$V_c = \frac{m_c}{\rho_c} = \frac{5.956 \cdot 10^{-11} \cdot g}{1.3 \cdot \frac{g}{cm^3}} = 4.58 \cdot 10^{-11} \cdot cm^3$$

$$d = \sqrt[3]{\frac{6V_c}{\pi}} = 4.44 \cdot 10^{-4} \cdot cm$$

Thus, under full coalescence, a 4.5 μm particle of Black Thunder coal will yield a 1 μm ash particle. Since only slightly less than 6% of the coal is under this size, most of the organic material will yield ash particles which can be analyzed by CCSEM. Again, fragmentation of the char during combustion and ash shedding will lead to some smaller, submicron particles. However, coalescence with mineral particles, which are typically larger than one micron, will tend to keep a portion of the organically-bound constituents in a form that is subject to CCSEM analysis.

4.2.3 Ash Composition

The composition of the ash particles formed by coalescence can be predicted from the composition of the minerals and the organically-bound constituents. The compositions of the major mineral phases (See Table 4-2) observed in the Black Thunder coal are plotted in Figure 4-3, along with the bulk composition of the organically-bound material from Table 4-3. This figure is not realistic in that it represents the organically-bound constituents as having a single composition. In actuality, the organically-bound constituents span a range of compositions, as will be seen in the ash results that follow. As combustion proceeds, mixing or coalescence of the particles will occur to some extent. The extent of coalescence is one of the factors that could be affected by staged combustion.

The lines between the phases indicate the mass balances that must be satisfied during coalescence. Particles derived solely from excluded minerals must have essentially the same composition as the minerals from which they formed. Likewise, the particles derived solely from organically-bound material must have the same composition as the organically-bound material in the coal. The composition of particles formed by coalescence of organically-bound material and mineral matter must be averages of the compositions of the initial materials weighted by the relative amounts that coalesced. Since mass balances must be satisfied during ash transformation, mass will seem to shift along the indicated lines as coalescence proceeds. Thus, movement along the lines can be taken as evidence of the amount of coalescence that took place in the formation of a given ash sample.

4.3 ASH ANALYSES

4.3.1 Carbon Content (Burnout)

The burnout (percent carbon loss) of fly ash samples collected in the experimental program was determined using a modification of ASTM Procedure D 3682. The results are presented in Table 4-4. The most important samples are those collected at the bottom of the reactor. These have the longest residence times and are the samples most representative of the fly ash that forms in utility boilers. From Table 4-4, it can be seen that the conventional and staged combustion samples collected at the bottom of the reactor had comparable levels of burnout. This facilitates comparison of results for the two samples.

4.3.2 Particle Size Distribution

One indicator of the extent of coalescence is the size of the final ash particles. Indeed, Zygarlicke and others (Zygarlicke, et al., 1995) reported the formation of substantially larger ash particles during low-NOx combustion of Black Thunder in a drop-tube furnace and attributed the difference to the increased coalescence due to the initial reducing conditions. However, the CCSEM particle size distributions of the conventional and staged combustion samples in this study shown in Figure 4-4 do not indicate this. If there is a change in particle size, it is too small to be detected by CCSEM.

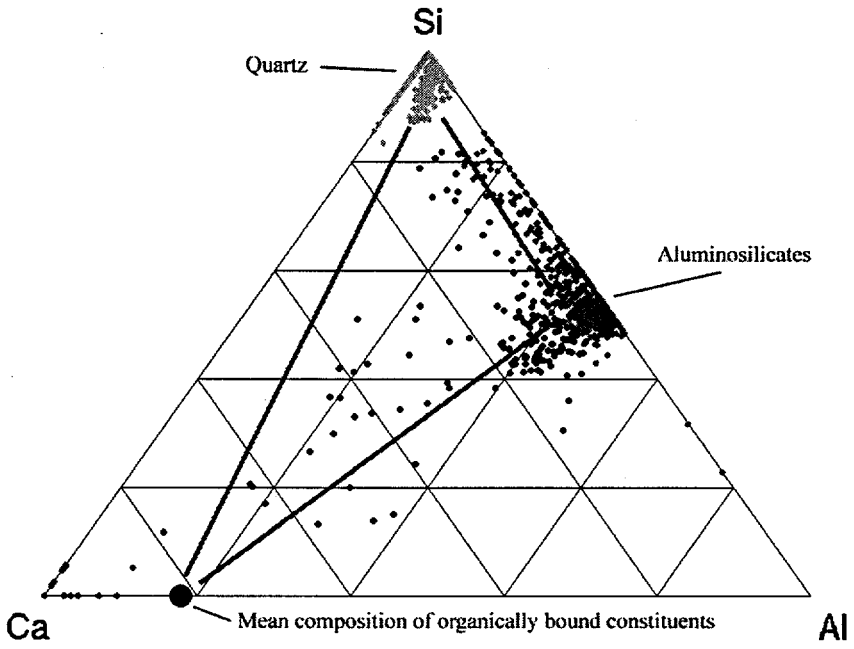

Figure 4-3 Ternary diagram of the ash-forming material in Black Thunder coal with lines indicating compositions that could occur as the result of coalescence

Table 4-4 Burnout (percent carbon loss) of Black Thunder samples

Sample Date	Position	Staged	Conventional
5-22-97	Top	87	
5-22-97	Bottom	99	
5-23-97	Middle		94
5-23-97	Bottom		98
6-24-97	Bottom	98	

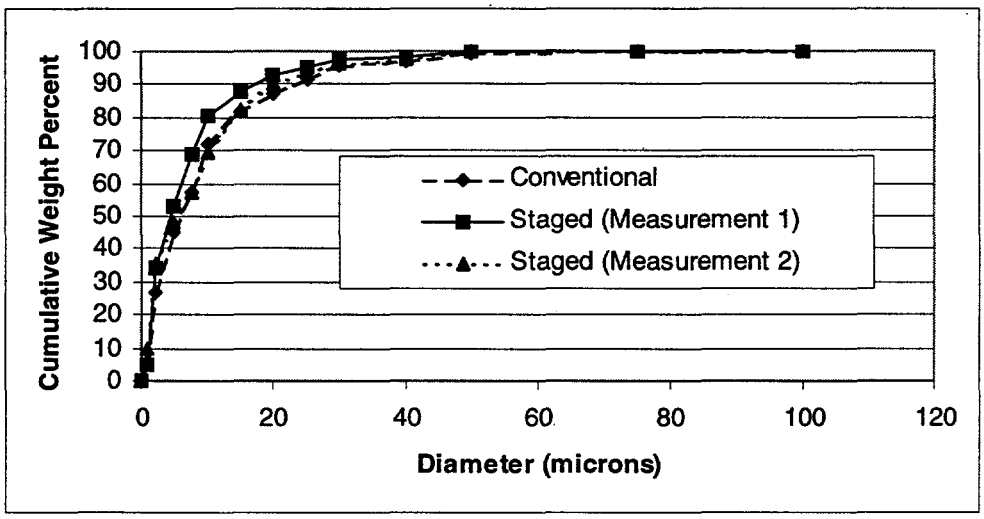

Figure 4-4 Particle size distributions of Black Thunder ash produced under conventional and staged combustion conditions

In the present staged combustion study, particles experienced reducing conditions for only a few hundred milliseconds. Most of the char oxidation occurred in an oxygen-rich environment after the staged air is introduced. In contrast, particles remained in a low-oxygen environment for as long as two or three seconds in drop-tube experiments. Consequently, there was more opportunity for coalescence in drop-tube experiments. This may explain why a shift in particle size distribution was observed by Zygarlicke and others (Zygarlicke, et al., 1995) but not in the present study.

4.3.3 CCSEM (Bulk Composition)

The bulk oxide composition of the ashes as analyzed by CCSEM are presented Figure 4-5. Confidence limits (95%) are included for the staged combustion composition. The organically-bound constituents which were not present in the coal minerals, specifically calcium and magnesium, account for a significant portion of the ash. Conservation of mass requires that the bulk elemental composition of the conventional and staged combustion ash samples be identical except for two cases. If different amounts of inorganic material vaporized under conventional and staged combustion, one sample would appear to be depleted in the elements that vaporized. Likewise, if one set of combustion condi-

tions resulted in more of the organically-bound constituents forming more submicron ash particles, which were neither collected nor analyzed by CCSEM, there would be a difference in bulk composition as well. However, since the bulk compositions of the two samples are identical to within analytical accuracy, staged combustion does not significantly alter the vaporization of inorganics or change the proportion of submicron ash.

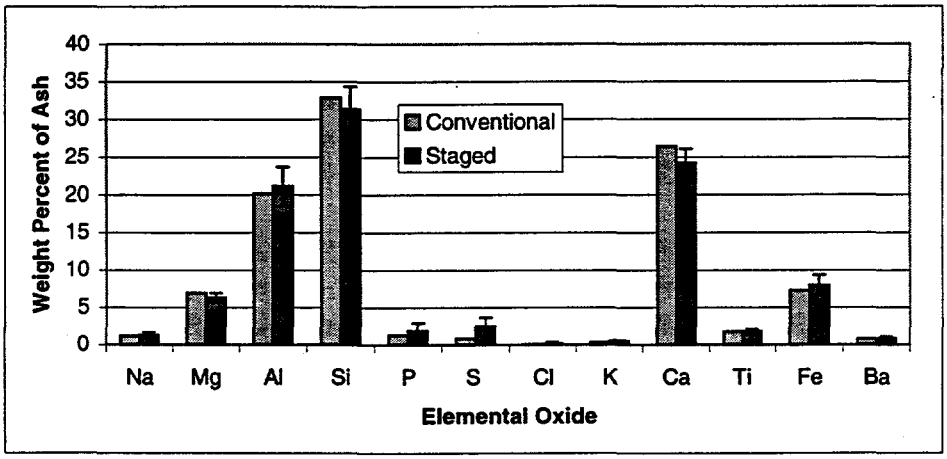

Figure 4-5 Composition of Black Thunder ash samples as determined by CCSEM

Small amounts of sulfur (1% and 2.5%) were detected in the ash samples. The presence of sulfur in combination with a calcium-rich ash is not unexpected, since CaO is used as a sorbent for reducing SO_2 emissions from boilers. The difference in amount, though not substantial, is in agreement with the literature on the kinetics of CaO sulfation which suggests that the sample contained under staged combustion would contain more sulfur. Gopalakrishnan and Seehra (Gopalakrishnan and Seehra, 1990) reported that the effect of increasing O_2 concentration on the rate of sulfation at high temperature is to lower conversion. Clearly, the oxygen concentration was higher during the conventional tests. Dam-Johansen and Østergaard (Dam-Johansen and Oestergaard, 1991) observed that ferric oxide is the only calcium oxide impurity that seems to reduce sulfur-bearing capacity. Although the ratio of ferric to ferrous iron oxide in the samples was not determined, it is reasonable to assume that if there were any difference, the conventional sample would contain relatively more ferric oxide because of the availability of oxygen.

Calcium sulfate is the important adhesive in the formation of deposits in Black Thunder ash (Benson, et al., 1993; Richards, 1994). Therefore, the elevated sulfation in the ash from staged combustion could lead to increased coalescence and larger ash particles. There may also be implications for deposit formation under staged combustion.

In contrast to the foregoing results for the entire range of particle sizes, differences in bulk elemental composition between the conventional ash and staged combustion ash are evident in particular size fractions of the ash. Average elemental compositions of particles with diameters less than 10 microns are presented in Figure 4-6, along with 95% confidence limits obtained from multiple analyses.

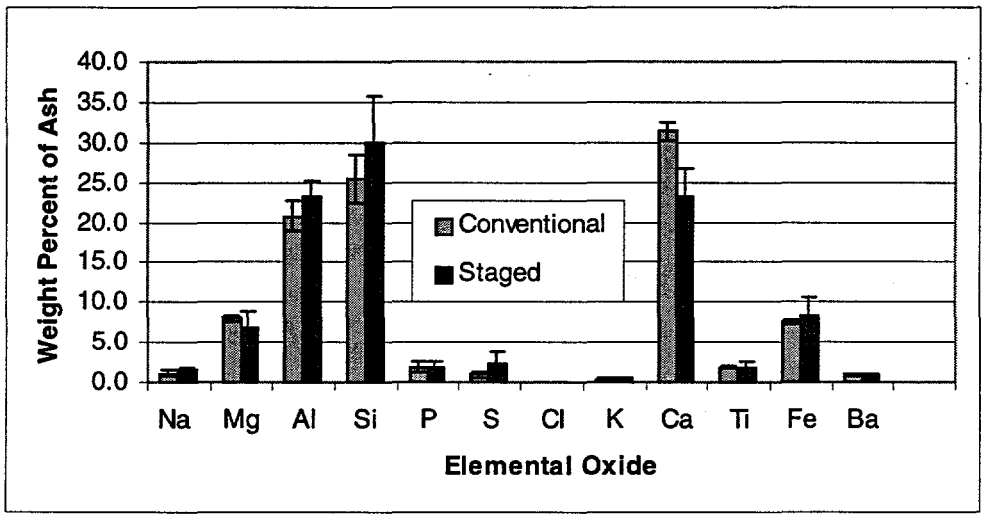

Figure 4-6 Composition of small (<10 μm) Black Thunder ash particles

There is clearly a measurable difference in the calcium content of the two ashes. The conventional ash contains slightly more calcium than the coal, while the staged combustion ash contains slightly less. The width of the confidence intervals is indicative of substantial variation in the calcium and silicon. Since the results are normalized, it is not clear which element is driving the variation. If it is silicon, then the difference is probably insignificant, since the variations would be due to the detection of quartz, which tends to be noisy in CCSEM analyses. In the case of calcium-driven variation, the mechanism could be due to increased fragmentation of large char particles under conventional combustion. Under excess oxygen conditions, the char would burn rapidly and fragment to a greater extent than under staged combustion. The final size of ash derived from these particles would then be limited because the particles would not be able to coalesce into a single large particle. Instead, several smaller particles would result. These would increase the calcium content of the small size fraction of the ash without affecting the overall content

As illustrated in Table 4-5, the smallest particles analyzed by CCSEM are more abundant in the conventional ash by a factor of 50%. Furthermore, examination of the composition of the particles with diameter less than 2 μm showed that they are almost entirely derived from the organically-bound constituents. Therefore, it seems likely that

increased char fragmentation under conventional conditions played a role in shifting the bulk composition of the small particles. Helble and others noted previously (Helble, 1993) that char fragmentation increases with the stoichiometric ratio.

Table 4-5 Number of particles detected in CCSEM analyses of Black Thunder ash performed at the same magnification

Size Cut	Number of particles	
	Conventional	Staged
<2μm	2740	1552
<5μm	2689	2393

The composition of the Black Thunder ash particles with diameter greater than 10 μm shown in Figure 4-7 indicates that the organically associated constituents coalesce with the discrete minerals to a large degree under both firing conditions, as evidenced by the presence of both calcium and silicon in the particles. Note that the calcium content of the large particles is much smaller than that of the small particles. This demonstrates that the small particles are more heavily influenced by the organically-bound constituents than the large particles.

The only clear difference evident in Figure 4-7 is in the amount of silicon, which is not a reliable indicator, as discussed above. The slightly lower calcium concentration in the conventional ash is consistent with the hypothesis above that some of the organically-bound material enters the smaller size fraction of the ash due to fragmentation of the large char particles. The difference is not as evident in the larger size cut of the ash because it is dominated by the particles derived from discrete minerals.

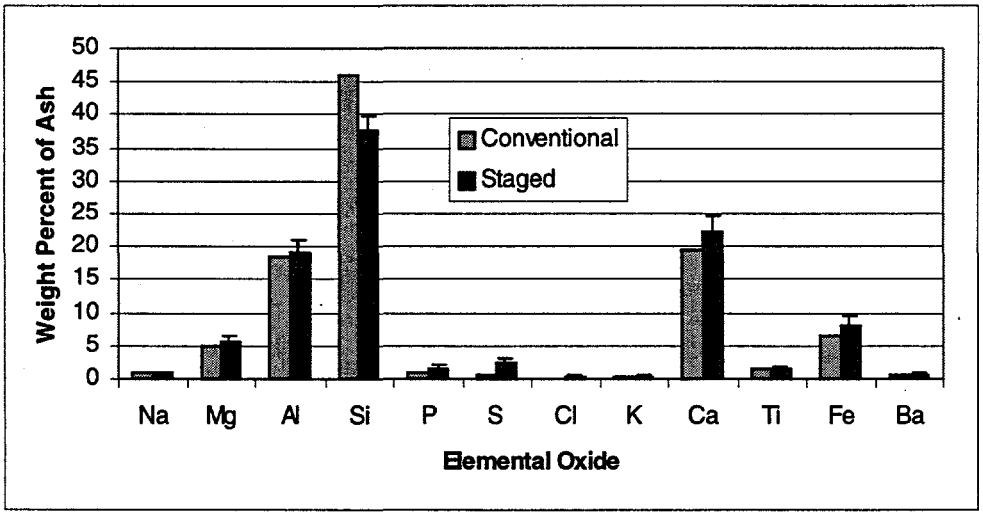

Figure 4-7 Composition of large (>10 μm) Black Thunder ash particles

In summary, the bulk composition results for Black Thunder show no evidence of partitioning by vaporization or the formation of submicron particles associated with staged combustion. Coalescence between ash particles derived from discrete minerals was observed in both large and small ash particles. A difference in composition between large and small particles can be explained by decreased fragmentation of the char during staged combustion.

4.3.4 CCSEM (Phase Distribution)

As discussed previously, the extent of coalescence of ash particles derived from organically-bound constituents with ash particles derived from mineral matter is one of the mechanisms that could be affected by staged combustion. A change in the extent of coalescence would be manifest as a shift in the phase distribution of the ash. Indeed, Zygarlicke and others (Zygarlicke, et al., 1995) noted the disappearance of "pure" phases offset by an increase in mixed phases under low-NOx firing conditions in a drop-tube furnace.

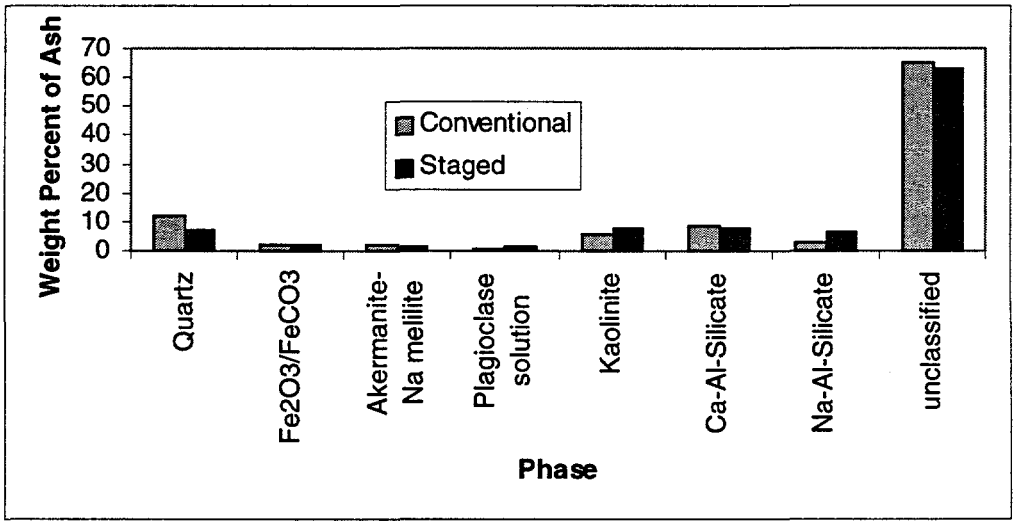

Figure 4-8 Phase distribution of Black Thunder ash

The phase distributions of the ashes as determined by CCSEM are presented in Figure 4-8. For clarity, only phases which represented one percent or more of the total ash are included. The phases that are included account for 99% and 97%, respectively, of the conventional and staged combustion ash samples. It would appear from Figure 4-8 that the compositions of the two ashes are identical. However, the significance of that conclusion is substantially weakened by the large (>60%) fractions of unclassified ash. Since there are no constraints on the unclassified category, a substantial amount of variation may exist within it.

The extent of the variation in the unclassified fraction of the ash can be seen in the Ca-Al-Si ternary histograms. Figure 4-9 and Figure 4-10 show, respectively, the unclassified compositions from the conventional and staged combustion samples. Both diagrams show a group of peaks corresponding to the organically-bound constituents. These are located just off the calcium-aluminum axis at about Ca = 60%. Also evident are compositions similar to quartz (near the silicon vertex) and the aluminosilicates (near the midpoint of the silicon-aluminum axis.)

Two differences between Figure 4-9 and Figure 4-10 point toward greater coalescence under staged combustion. Note first the large peak at the silicon vertex in Figure 4-10 which is missing in Figure 4-9. This peak is due to the dilution of quartz (SiO_2), with organically-bound constituents, particularly calcium and magnesium. Under conventional conditions, the quartz remains pure and thus does not appear as unclassified. Because of the variability in the analysis of silicon noted in the previous section, the presence of this peak alone is not sufficient evidence that coalescence has proceeded further under staged combustion. Stronger support is provided by examining the region lying between the organically-bound material and the silicon-aluminum axis. This is one of the regions that would be most affected by coalescence as aluminosilicates are diluted by organically-bound constituents. The staged combustion ash (Figure 4-10) clearly shows more coalescence products in this region than the conventional ash (Figure 4-9). Furthermore, the decrease in the height of the "pure" organically-bound material in the staged combustion ash relative to the conventional ash is consistent with the hypothesis that the organically-bound constituents have mixed to a greater extent.

It is difficult to quantify the difference based on ternary diagrams. Therefore, the NPC algorithm (Section 3.3.1) was used to classify the unclassified particles in each of the ash samples into groups which could be compared. The results of the NPC classification can be seen in Figure 4-11 and Figure 4-12, which show the same data presented in Figure 4-9 and Figure 4-10, but with color added to indicate the nearest phases. Note that not all of the peak heights in the colored diagrams match those in the originals because some groups overlap. The ternary histogram program is not able to stack markers on top of one another to show multiple phases occurring in the same space on the diagram. Instead, markers are replaced. Therefore, some of the markers appear to contain more than one color. In such instances, the NPC algorithm has found a distinction between compositions which appear to be identical on the ternary diagram. Demarcations reflect composition differences detected in the 12-dimensional element space. These differences involve minor constituents which cannot otherwise not be seen on the diagram. It can be clearly seen from these figures that NPC was able to separate the unclassified compositions into a number of groups.

For comparing the conventional and staged combustion ash samples, the amount and composition of the material lumped into each nearest phase grouping are presented in Table 4-6. Each entry in Table 4-6 consists of two rows. The first is the conventional sample and the second is the staged combustion sample. Each entry is labeled with the number of its nearest phase. Numbers are used rather than names to avoid confusion with the original phases. The second column in each entry is the area percent of the analyzed

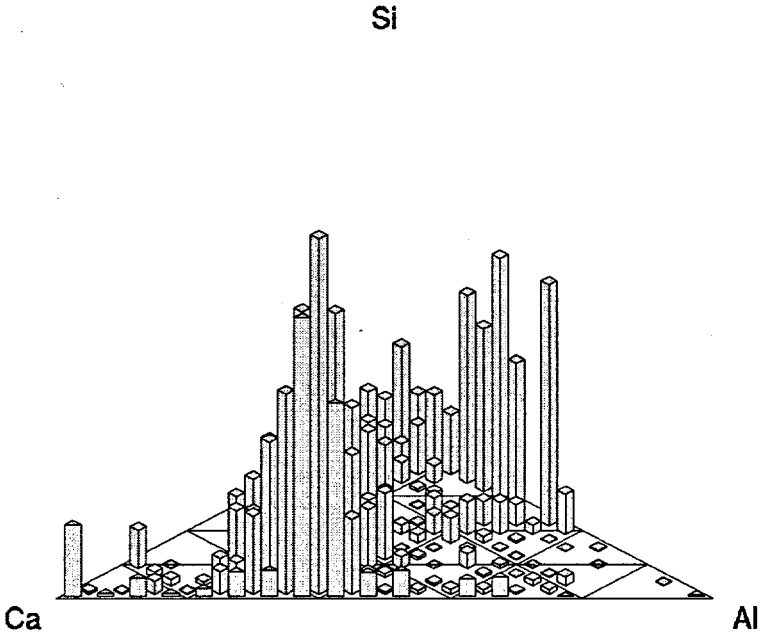

Figure 4-9 Ca-Al-Si ternary histogram of unclassified particles in conventional Black Thunder ash

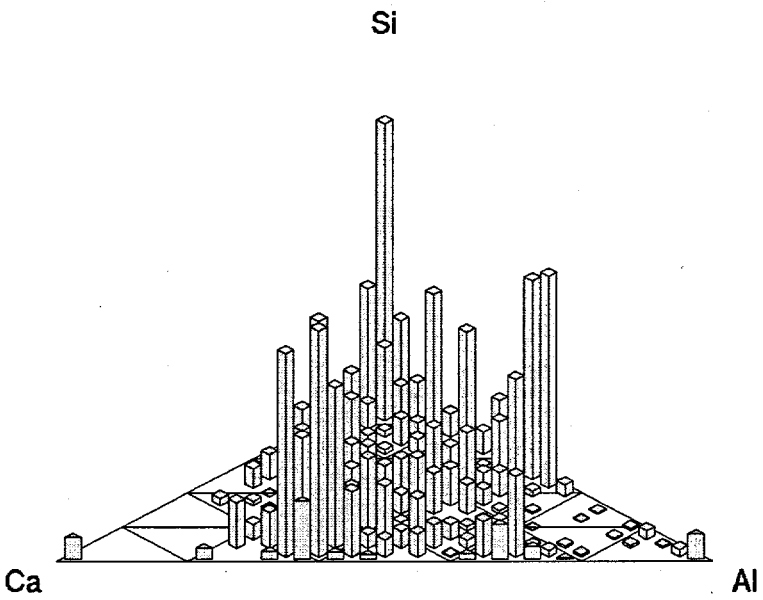

Figure 4-10 Ca-Al-Si ternary histogram of unclassified particles in staged combustion Black Thunder ash

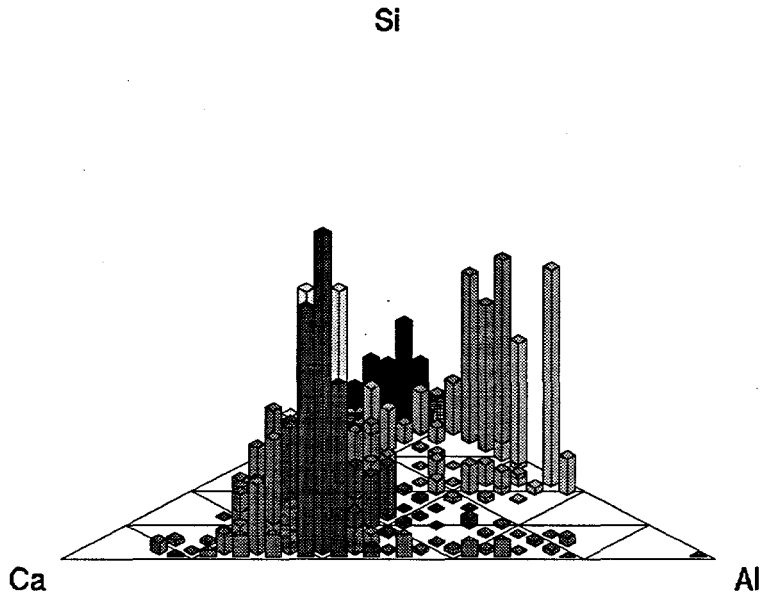

Figure 3-15 NPC results for conventional ash

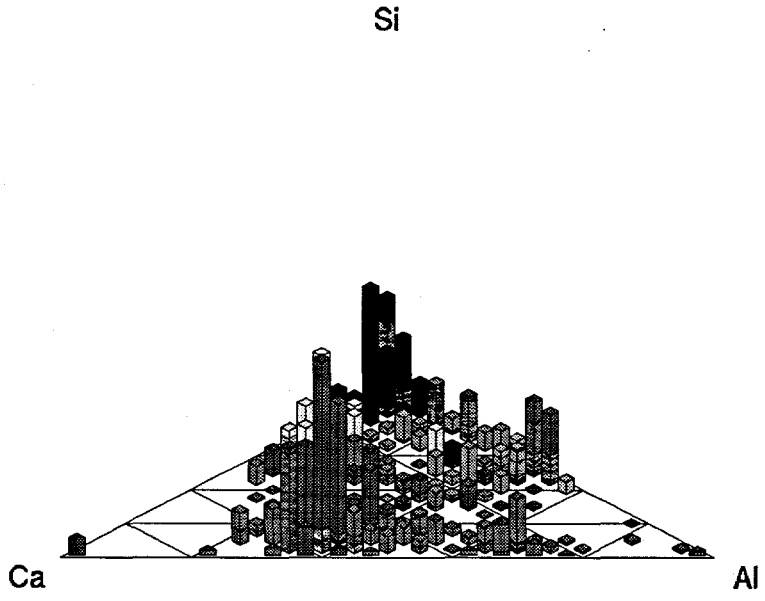

Figure 3-16 NPC results for staged combustion ash

particles that the groupings represent. Again, only phases which represented one percent or more of the total ash area are included in the table. These phases represent 94% and 92%, respectively, of the unclassified particles. The remaining columns contain the mean composition of the particles in each grouping. For example, 2% of the total ash area in the conventional sample was covered by particles which were unclassifiable but similar to phase 1, which happens to be quartz. By way of comparison, the staged combustion sample contained 2.9% near phase 1. This difference is consistent with the observation regarding impure quartz in Figure 4-9 and Figure 4-10.

Table 4-6 Amounts and compositions of NPC groups in unclassified particles in conventional and staged combustion Black Thunder ash

Phase	Area % of ash	Na	Mg	Al	Si	P	S	Ca	Fe
1c	2	5	2.3	5.2	76	1	0.6	5.9	1.8
1s	2.9	4.7	2.1	5	75.4	1.7	1.6	5.8	1.6
10c	1.2	0.7	11.7	12.9	18.1	0.4	0.3	47.2	6
10s	0.1	0.3	8.4	12	15.7	3	1.7	47	7
23c	25.8	0.7	16.5	24.4	4.6	1.2	0.5	43.7	6.7
23s	22	0.4	17	24	4.3	1.2	1.7	42.8	7
24c	8.6	1.1	9.6	30.3	4.3	6.6	0.9	40.2	4.8
24s	7.6	0.7	7.7	36.9	3.6	7.4	2.3	35	4.3
35c	2.7	3	7	6.7	53.5	0.4	0.2	22.3	4.5
35s	2.1	2.7	6.9	6.5	52.4	0.6	0.7	23.1	4.8
41c	3.1	0.8	11.8	25.9	14.3	1.3	0.3	37.8	6
41s	3.1	0.6	12.2	26.9	13.2	1.5	0.8	36.5	6.8
44c	2.2	3.1	8.9	27.8	16	3.8	1.3	28.6	7.5
44s	3.1	2.6	9	26.5	16.7	2.6	3.6	28.9	7
45c	10.1	2.1	17.4	16	21.7	0.7	0.5	32.2	6.3
45s	10.1	1.9	17.3	17.3	20.6	1	2.5	30.2	6.6
48c	4.9	8.7	4.2	27.6	43.4	0.5	0.3	9.7	2.7
48s	4.8	8.6	4.3	27.3	41.8	0.8	1.3	8.8	4.3
49c	1.7	2.9	1.6	46	44.5	0.2	0.1	2.3	0.9
49s	0.7	2.1	1.4	41.6	45.7	0.7	0.4	2.1	2.3

Suffixes: c - conventional sample, s - staged combustion sample

For the two samples shown, there is relatively little intersample difference in the composition of nearest phase groupings. Except for the groups near phases 10, 24, and 49, the mean amounts of the dominant elements differ by only about two percent. Wider variation in the minor constituents is seen, but it is driven by small relative variations in the dominant elements when the compositions are normalized. There is also a certain amount of noise, as much as 5%, in the compositions determined by EDS. Note that the sulfur content of the staged combustion ash is higher in all groupings, consistent with the bulk composition results discussed previously.

The close intersample agreement in group composition allows comparisons to be made on the amount of material in each group. On that basis, only one difference is evident. The conventional sample contained 25.8% near phase 23 while the staged combustion sample contained only 22%. The near phase 23 group is by far the largest classification in both samples and corresponds with the organically-bound constituents that have formed ash but have not coalesced significantly with other species.

The fact that less of this material appears in the staged combustion ash supports the more coalescence hypothesis. Further support is offered by the groups near phase 24. Although the amounts of these groups are not significantly different (8.6% vs. 7.6%), the average compositions vary substantially. The conventional ash contains less silicon (30% vs. 37%) and more calcium (40% vs. 35%) than the staged combustion ash.

A difference in bulk elemental composition for the particles less than 10 μm in diameter was discussed in Section 4.3.3. Particles in this size range are responsible for much of the fouling on the backside of the tubes in boilers firing low-rank coals. Consequently, a change in the composition of the small particles could be significant for deposition behavior. Therefore, the NPC algorithm was applied to the small unclassified particles. The results are presented in Table 4-7.

Table 4-7 Amounts and compositions of NPC groups in unclassified small (< 10 μm) particles in conventional and staged combustion Black Thunder ash

Phase	Area % of Ash	Na	Mg	Al	Si	S	Ca	Fe
1c	2.3	5.5	2.3	4.9	75.9	0.7	5.9	1.9
1s	5.2	5.2	2.1	4.6	75.1	2.2	5.1	1.7
10c	1.6	0.7	12.8	13.2	16.1	0.5	47.6	6.2
10s	2.1	0.1	9.6	12.7	14.1	3.2	46.7	5.9
21c	1.4	1.9	7.1	51.1	1.5	0.7	20.7	2.4
21s	2.5	1.1	8.6	50.7	2.2	2	20.7	3.3
23c	34.6	0.7	15.4	24.7	4.7	0.6	43.6	6.5
23s	23.4	0.4	15.2	25.8	4.4	2	42.1	6.6
34c	3.3	3.7	6.7	6.5	53.5	0.4	20.5	5.8
34s	2.1	3.6	7.9	5.9	53.8	1.2	20.9	3.6
40c	3.5	0.9	11.5	27.6	13.5	0.4	36.8	5.9
40s	3.1	0.6	11.7	30.1	12.1	0.7	35	5.9
43c	2.8	3.2	7.8	31.7	12	1.4	27.3	6.1
43s	3.6	2.6	8.1	29.6	14.2	4.1	27.1	5.7
44c	9.4	2.2	18	16.4	20.3	0.6	32	6.5
44s	9.7	2.1	18	18	19.4	2.8	29.2	6.7
47c	4.2	9.9	4.6	28.3	39.7	0.4	10.8	2.9
47s	6.6	9.6	4.7	27.5	39.1	1.4	9.4	4.5
48c	0.9	4.2	1.7	44.7	42.1	0.2	4.2	0.9
48s	1.5	2.1	1.5	41.9	45.1	0.3	2	2.7

Suffixes: c - conventional sample, s - staged combustion sample

The major difference is again in the amount of ash in the near phase 23 groups. However, the magnitude of the difference is far larger because it is not buffered by the presence of the large silicate and aluminosilicate minerals. The conventional ash contains substantially more of the "pure" organically-bound material than the staged combustion ash. The near phase 23 group is low in silicon (<5%), indicating that it does not contain much ash derived from minerals, while most the other groups contain appreciable quantities, ranging from 12% to 75%.

Still more evidence of enhanced coalescence under staged combustion can be seen in the Ca-Al-P ternary histograms which show the interaction between the organically-bound constituents and crandallite. In the diagram for conventional ash (Figure 4-13), the organically-bound constituents give rise to the cluster of peaks along the calcium-aluminum axis near Ca = 60%. Crandallite gives rise to the cluster of peaks between Al = 40% and Al = 60% along the Ca = 20% line.

The same data for the staged combustion sample are plotted in Figure 4-14. In comparison to Figure 4-13, the organically-bound peaks are shorter and the crandallite peaks are taller. This indicates a shift due to the coalescence of the organically-bound constituents with the minerals. Obviously, crandallite has not been formed during combustion. It is merely coincidental that it has the same proportions of calcium and aluminum as the coalesced ash. A small decrease in phosphorus consistent with increased mixing can also be seen in the position of the crandallite cluster in Figure 4-14.

While the differences between Figure 4-13 and Figure 4-14 are substantial, their significance is not. The diagrams included only 5.7% and 6.3% of their respective samples. That is, only 5.7% of the ash in the conventional sample met the criterion that Ca+Al+P≥80%. Therefore, the two diagrams indicate that there is a substantial difference in a small fraction of the ash.

A more complete view is given by Figure 4-15 and Figure 4-16, which are similar to Figure 4-9 and Figure 4-10 but include all compositions instead of just the unclassified ash. The two diagrams appear very similar. The most apparent difference is the height of the pure silicon peak, but this is not necessarily significant because of the difficulty in analyzing quartz mentioned before. Other, barely discernible differences between the samples can be seen in the height of the peaks between the organically-bound cluster (Ca:Al = 60:40) and the silicon-aluminum axis. The staged combustion sample appears to have more material in the region lying between the organically bound constituents and the aluminosilicates. However, the amounts appear to be small and it would be an overstatement to say that the ash compositions are different on that basis.

A firmer basis for that conclusion is provided by the fractions of the ash that appear on the ternary diagrams. Figure 4-15 includes 52.2% of the conventional ash but Figure 4-16 contains only 45.1% of the staged combustion ash. This disparity is a clear indicator that there is a difference between the samples. As some minerals blend with the organically-bound constituents, they leave the diagram since their compositions become unable to satisfy the Ca+Al+Si ≥ 80% criterion for inclusion on the diagram.

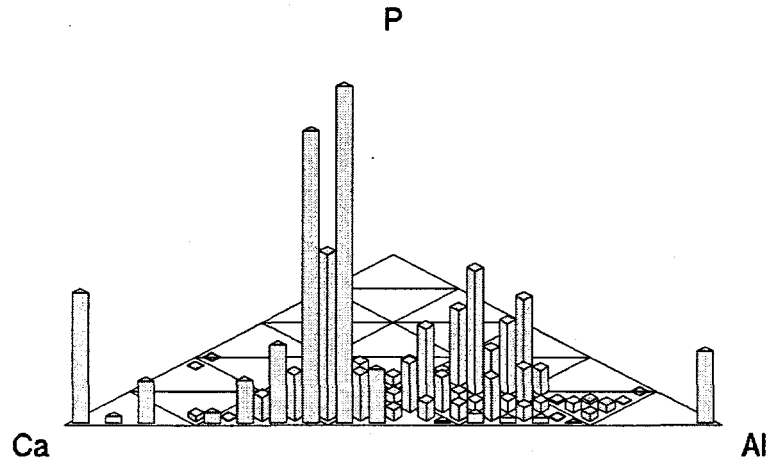

Figure 4-13 Ca-Al-P ternary histogram of conventional ash

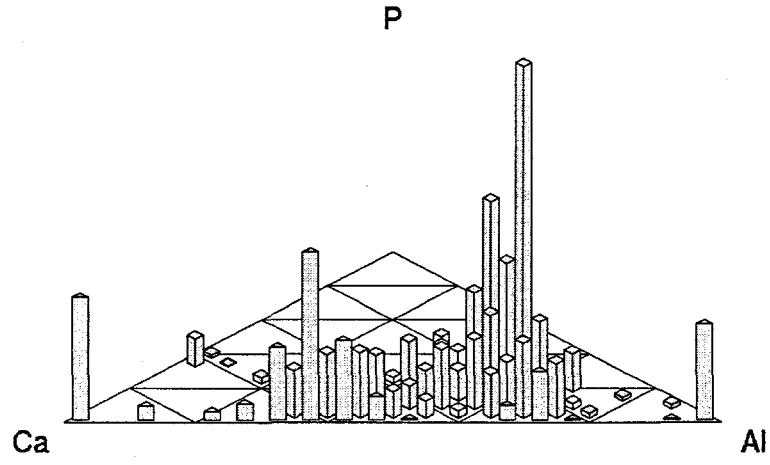

Figure 4-14 Ca-Al-P ternary histogram of staged combustion ash

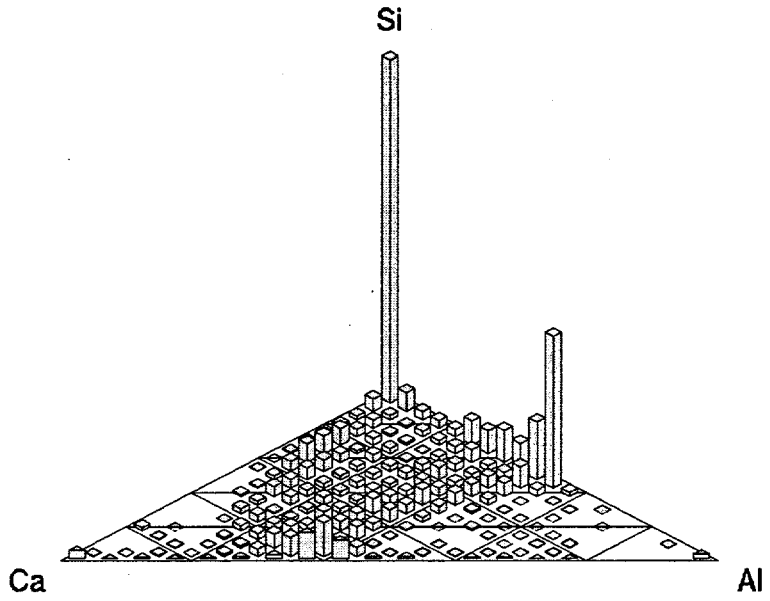

Figure 4-15 Ca-Al-Si diagram of conventional Black Thunder ash

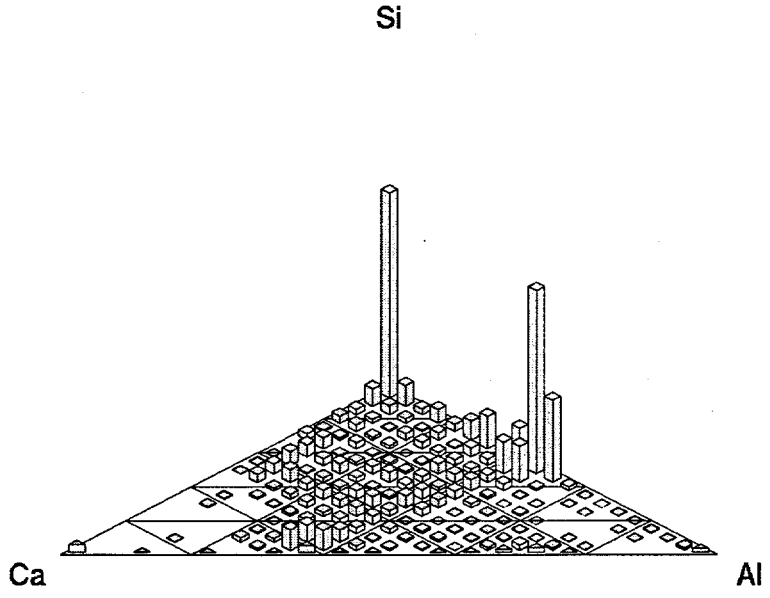

Figure 4-16 Ca-Al-Si diagram of staged combustion Black Thunder ash

The most complete picture available is provided by pseudo-ternary diagrams. In Figure 4-17 and Figure 4-18, sodium, magnesium, phosphorus, and iron have been lumped with the calcium to include more of the ash derived from organically-bound constituents on the diagrams. Figure 4-17 contains 98.3% of the conventional ash and Figure 4-18 contains 95.1% of the staged combustion ash. These diagrams clearly show the importance of the organically-bound constituents in determining the composition and properties of Black Thunder's ash. Again, the differences between the two samples are not large. Nevertheless, a small shift from "pure" organically-bound to mixed compositions can be seen in the height of the peaks along the line connecting aluminosilicates (Si:Al = 50:50) to the organically-bound constituents (Ca:Al = 60:40).

4.4 SUMMARY

Close examination of the results of CCSEM analyses of Black Thunder ash produced under both conventional and staged combustion has determined that staged combustion causes a minor shift in the composition of the ash due to a greater extent of coalescence. The difference is most evident in the results of the nearest phase classification algorithm applied to unclassifiable compositions. Those results show that conventional ash contained relatively more "pure" organically-bound particles. Subsequent study of ternary and pseudo-ternary diagrams indicated that the organically-bound material had mixed with aluminosilicates and quartz.

The increased coalescence observed under staged combustion is most likely due to slower char oxidation, which allowed char particles to stay intact longer before fragmenting. Although increased coalescence must result in larger ash particles, the effect is not large enough to be evident in the particle size distribution of the ash.

As discussed, this finding contradicts that of earlier research which found that low-NOx firing conditions result in a much larger ash with lower viscosity. The earlier findings suggest that altered deposition behavior associated with low-NOx firing could be attributed to changes in the ash. In contrast, it has been shown here that staged combustion does not significantly alter the properties of the ash.

The distinction between reducing conditions and staged combustion is of fundamental importance in understanding these results. Previously reported work was performed in a drop-tube furnace under conditions in which the temperature was set externally, residence times were long, and the oxygen concentration was kept constantly low. In the combustor used in this work, the temperature was controlled by the flame, residence times were relatively short, particularly in the reducing zone, and abundant oxygen was available for char oxidation.

Therefore, based on these results, it is expected that low-NOx firing in practical systems will not produce fly ash with significantly different properties. Altered deposition behavior must be explained in terms of temperature, carbon content of the ash, or other factors.

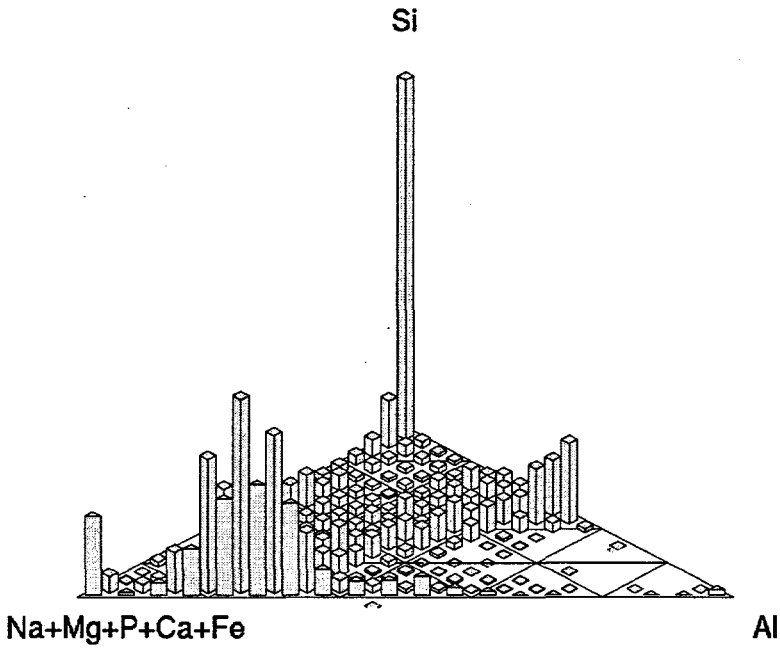

Figure 4-17 Pseudo-ternary diagram of conventional ash

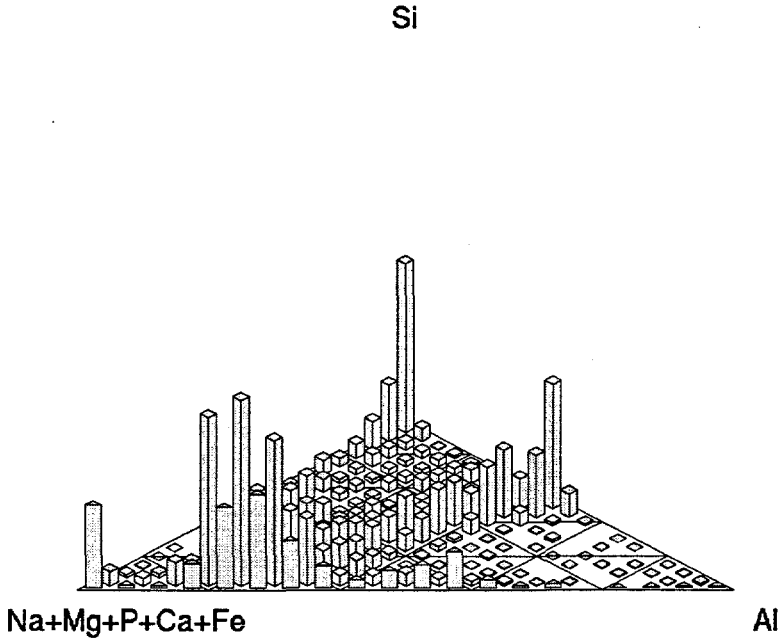

Figure 4-18 Pseudo-ternary diagram of staged combustion ash

SECTION 5

PITTSBURGH #8 ASH RESULTS AND DISCUSSION

Pittsburgh #8 coal was used in this study to investigate the effect of staged combustion on the behavior of pyrite. As discussed in Section 2, pyrite is a key factor in ash formation and has the potential to be affected by the initial reducing conditions experienced under staged combustion. Differences in pyrite behavior could be manifest in the rate at which sulfur is released and in the composition of the final ash.

5.1 COAL MINERAL CHARACTERIZATION

A sample of Pittsburgh #8 coal was sent to Commercial Testing and Engineering for proximate and ash elemental oxide analysis. The results of those analyses are presented in Table 5-1, along with the elemental oxide composition of the minerals determined by CCSEM and a bulk analysis of the same coal performed by another research group. In principle, the elemental oxide compositions determined by bulk analysis and CCSEM should match, since the coal contains very little organically-bound material. As Table 5-1 indicates, CCSEM detected significantly more iron in the coal than was expected from the bulk analyses, which agree closely with one another. The high iron content reported by CCSEM is most likely due to the analysis of too few large particles, which heavily influence the results. When an inadequate number of large particles are analyzed, the composition results are biased towards the composition of the particles that were analyzed. In this case, a number of pyrite particles were analyzed.

The composition distribution of the coal minerals as determined by CCSEM is presented in Figure 5-1. Major mineral constituents of Pittsburgh #8 are quartz, aluminosilicates (clays), and pyrite. Lesser amounts of other minerals, including calcite or calcium carbonate are also present. The unclassified particles in Pittsburgh #8 are primarily mixed silicates. The coal was pulverized after the analyses presented here were performed in order to make it easier to feed into the reactor but this would not have changed the composition of its mineral content.

Table 5-1 Proximate and elemental oxide analyses of Pittsburgh #8 coal

Proximate Analysis			
Weight Percent Ash	11.01		
High Heating Value (BTU/lb)	13346		
Weight Percent Sulfur	2.27		
Elemental Oxides			
	ASTM	**BYU CCSEM**	**PSIT ASTM***
Silica, SiO_2	48.09	40.07	48.77
Alumina, Al_2O_3	21.89	18.21	26.08
Titania, TiO2	1.06	0.74	0.75
Ferric Oxide, Fe_2O_3	18.10	25.6	15.38
Lime, CaO	6.72	11.00	5.00
Magnesia, MgO	1.16	1.06	1.78
Potassium Oxide, K_2O	1.74	1.40	1.06
Sodium Oxide, Na_2O	0.75	0.74	0.98
Phosphorus Pentoxide, P_2O_5	0.38	0.60	0.20
Barium Oxide, BaO	0.11	0.47	n/d

*(Bool, et al., 1995)

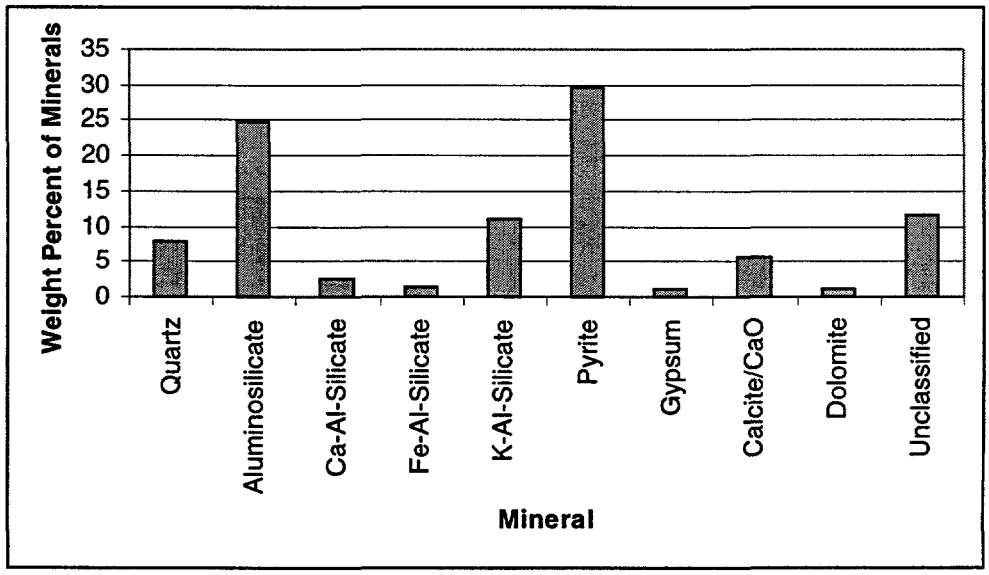

Figure 5-1 Phase distribution of minerals in Pittsburgh #8 coal

The extent to which the coalescence of the discrete minerals will be altered by staged combustion is a primary question to be answered in this investigation. A fundamental factor in the extent of coalescence is the behavior of pyrite under staged combus-

tion. Bool and coworkers (Bool, et al., 1995) reported that reducing conditions significantly affect the oxidation state of iron and the particle size distribution of the final ash.

5.2 ASH ANALYSES

5.2.1 Carbon Content (Burnout)

The burnout (percent carbon loss) for each of the Pittsburgh #8 ash samples is presented in Table 5-2 below. The trends are correct in that the samples collected at the top of the reactor are less completely combusted than those taken at the bottom. Also, the staged combustion sample taken at the bottom of the reactor has a lower burnout than its conventional counterpart.

Table 5-2 Burnouts of Pittsburgh #8 samples

Sample Date	Position	SR = 0.75	SR = 1.04
4-10-97	Top	74	69
4-10-97	Bottom	82	-
5-29-97	Top	70	-
5-29-97	Bottom	78	-
6-4-97	Top	-	73
6-4-97	Bottom	-	90
6-9-97	Top	69	-
6-9-97	Bottom	75	-

Comparisons of samples from the top of the reactor can be made on the basis that the conventional and staged combustion samples have the same level of burnout. Comparisons of the bottom samples are less direct because of the different and relatively low burnouts. The bottom samples from the staged combustion tests clearly are not representative of final ash. Nevertheless, they are used in the following section to show the effect of staged combustion on sulfur release in intermediate ash.

5.2.2 Sulfur Release

As discussed in Section 2, the transformation of pyrite to iron oxide could be slowed by the lower temperature and oxygen concentration that the particles experience in the initial reducing zone during staged combustion. The critical factor in the transformation is the length of time that the molten, sticky iron oxysulfide phase persists. If staged combustion prolongs this time, there is the potential for greater coalescence of ash particles. There is also greater potential for sticking to the boiler walls should the particles impact.

A related issue is the influence of mineral liberation on pyrite transformation. Even in conventional combustion, included particles experience lower oxygen concentrations and higher temperatures than excluded particles. Under staged combustion, the differences in environment could become more pronounced.

These issues were investigated using the char/ash association algorithm described in Section 3.3.2 with Pittsburgh #8 coal ash samples. Short and long residence time samples collected under both conventional and staged combustion conditions, a total of four samples, were studied. The long residence time samples under both operating conditions were obtained at the bottom of the reactor. The short residence time samples were collected several inches below the burner, at a position that was in the initial reducing zone during staged combustion.

Although the association of every particle in the samples was determined, only particles derived from pyrite were of interest. Therefore, only "pyritic" particles, defined as those whose oxygen-free mole fractions of iron and sulfur summed to eighty-percent or more of the total composition, were examined for sulfur release. For each pyritic particle, the extent of pyrite conversion to iron oxide was calculated assuming that the particle began as iron sulfide (FeS_2):

$$\xi = 1 - \frac{S}{2Fe}$$

where ξ is bounded at zero for pyrite and at one for iron oxide.

The distributions of ξ in the four samples are presented in Figure 5-2 through Figure 5-5. The data are presented as histograms, where the height of each peak is proportional to the fraction of the total pyritic particle surface area covered by particles with ξ in the corresponding range.

Recently published results on the kinetics of pyrite oxidation (ten Brink, et al., 1996) indicate that the initial decomposition of pyrite to pyrrhotite is very fast. This is reflected in Figure 5-1 and Figure 5-2, which show the distribution of ξ in the top samples. There is relatively little unreacted pyrite ($\xi = 0$) evident in either diagram. The presence of pyrrhotite and the oxysulfide is indicated by the peaks in the $0.5 \leq \xi \leq 0.6$ range. An appreciable quantity of completely combusted ($\xi = 1$) particles is also seen. Note that some of these may be due to small amounts of iron oxide present in the coal, and not pyrite.

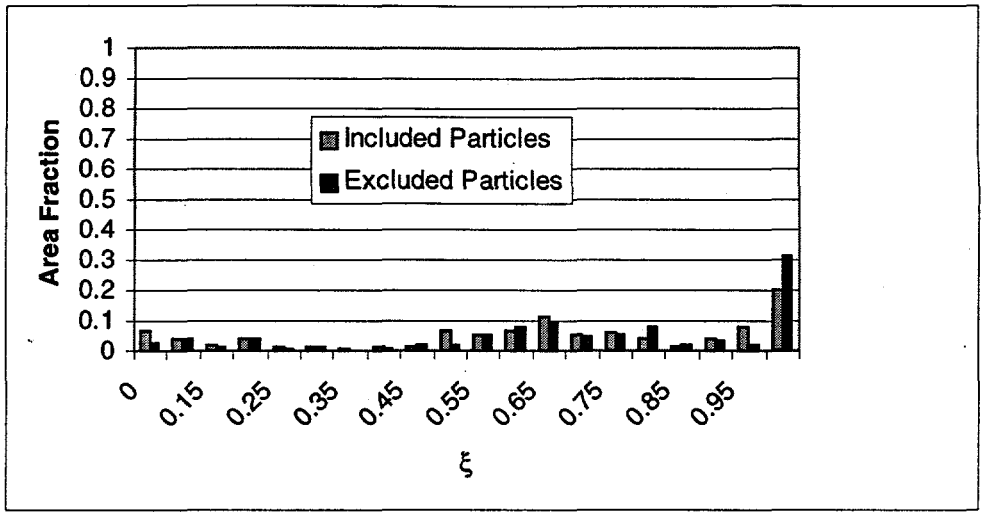

Figure 5-2 Pyrite conversion of conventional top sample

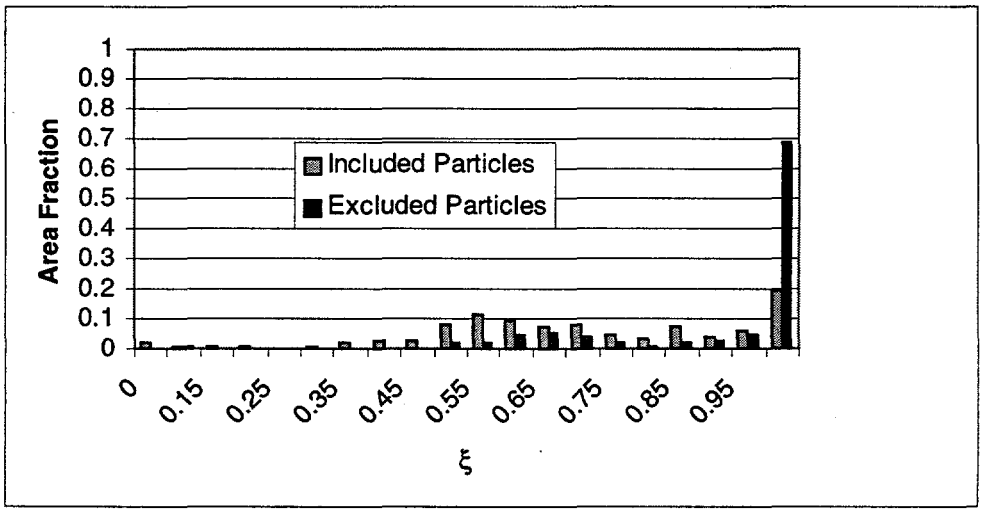

Figure 5-3 Pyrite conversion of staged combustion top sample

Paradoxically, it appears that the staged combustion top sample Figure 5-2 contains less low ξ material than the conventional sample Figure 5-2. This is in contrast to physical intuition that suggests that the sample burned in the high-oxygen environment would react more quickly. However, the staged combustion sample has a longer residence time than the conventional sample. This is due to the difference in the amount of air, and hence the velocity, in the top section of the reactor during the staged combustion test. Therefore, for the same sampling position, the staged combustion sample has been in the reactor longer and has reacted further, despite the lower oxygen concentration.

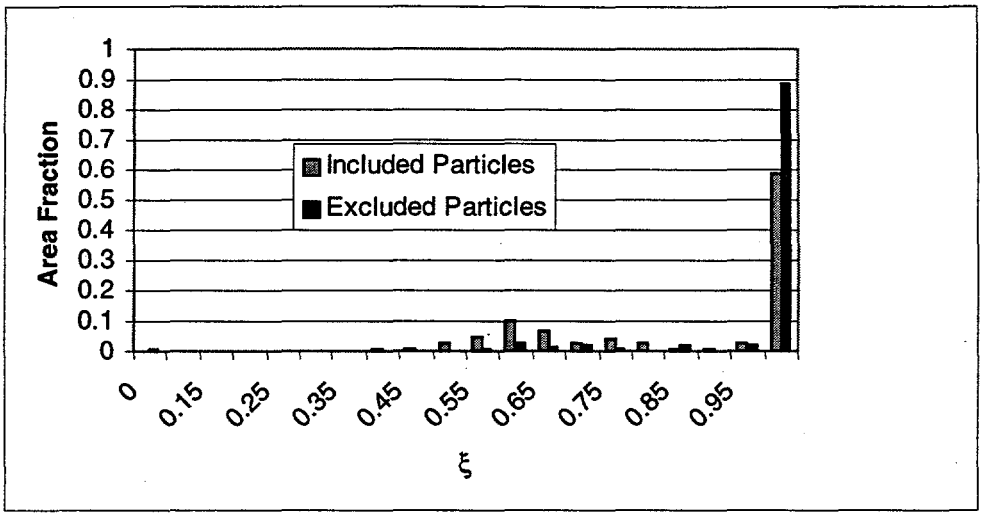

Figure 5-4 Pyrite conversion of conventional bottom sample

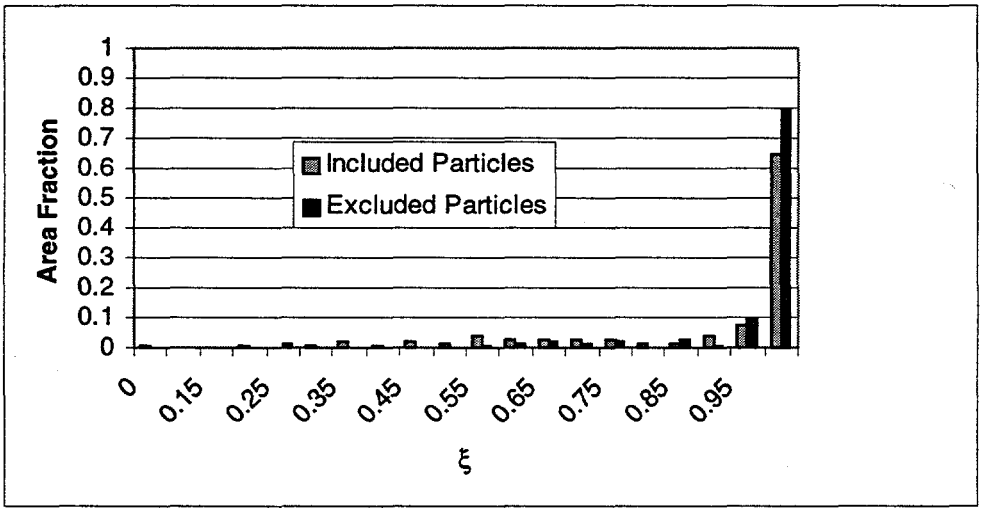

Figure 5-5 Pyrite conversion of staged combustion bottom sample

At complete combustion, all pyrite would be completely converted to iron oxide and no sulfur would remain in the ash. All pyritic particles would have $\xi = 1$. However, the bottom samples in this study are not completely combusted; the maximum burnout is 90% for the conventional bottom sample. It is apparent from the amount of pyritic material in the $\xi = 1$ bin that pyrite combustion is also incomplete. Sulfur remains, as indicated by the peaks in the 0.6 - 0.8 range in Figure 5-4 and Figure 5-5. Residence time seems to play a role in the bottom samples as well. Even at the bottom of the reactor, the staged combustion sample appears to be more completely converted than the conventional sample. This is evidenced by the fraction of the pyritic ash in the range $0.55 \leq \xi \leq 0.65$. Comparing Figure 5-4 with Figure 5-5, it is clear that the conventional sample contains more

pyrrhotite and oxysulfide than the staged combustion sample. This is despite the fact that the burnout of the conventional sample is 15% larger than the burnout of the staged combustion sample.

It is clear that sulfur is released more quickly from excluded than from included pyrite particles. In each sample, the distribution of ξ in the included particles is shifted to the left. The included particles contain more material in the 0.6 - 0.7 ξ range, indicating that the included pyrite has not reacted as completely as the excluded pyrite. The effect is greatest in the top staged sample, which was collected in a reducing environment.

The same sort of difference between included and excluded particles under reducing conditions was observed by ten Brink and coworkers (ten Brink, et al., 1996) who manually tracked the ratio of sulfur to iron as a function of residence time for a few included and excluded particles. The transformation of included pyrite halted at pyrrhotite under reducing conditions but went to completion under oxygen-rich conditions. The difference was explained by the combustion of the surrounding char, which consumed the available oxygen and prevented it from penetrating to the pyrrhotite.

Figure 5-5 shows that the included pyrrhotite continues to combust after the addition of staged air. Relatively little unreacted included pyrrhotite remains at the bottom of the reactor. Instead, approximately 65% of the included pyritic particle area is completely converted to iron oxide. Although this is far from completely converted, it is in line with the 69% conversion of the carbon. As the char recedes, oxygen becomes available to complete oxidation of the pyritic particles.

With regard to the conventional bottom sample illustrated in Figure 5-4, the conversion of excluded particles correlates with carbon burnout. However, the included particles seem to lag. Air was premixed with the coal and an excess of oxygen was available throughout the reactor during the conventional tests; therefore the difference is probably due to residence time as discussed above.

The differences between included and excluded particles can also be seen in the average pyrite conversion of each of the samples, which are tabulated below (Table 5-3). In all of the samples, excluded particles have a higher mean ξ value than included particles. This is not surprising, following the discussion above.

The last column in Table 5-3 contains the difference between the mean values of ξ for included and excluded particles in each sample. For all but one sample, the difference is 0.06 or 0.07. For the top staged sample, it is 0.26. Two conclusions can be drawn from this finding. First, as discussed above, the initial reducing conditions have a marked effect

Table 5-3 Mean values of ξ for included and excluded particles

	Included	Excluded	Difference
Conventional, Top	0.64	0.71	0.07
Conventional, Bottom	0.86	0.92	0.06
Staged combustion, Top	0.65	0.91	0.26
Staged combustion, Bottom	0.89	0.96	0.07

on the conversion of included pyrite particles. Second, following the introduction of the staged air, the included pyrite particles resume combustion and follow the same transformation pathway as the they would under conventional conditions.

These conclusions suggest that the effect of staged combustion on pyrite is short-lived. In the near-burner region, where the concentration of oxygen is low, pyrite remains in the pyrrhotite or oxysulfide state which could lead to increased slagging. However, once the particles enter the oxidizing region, the oxysulfide quickly disappears.

In summary, although the sulfur release results are somewhat obscured by differing residence times, it appears that staged combustion has an effect on pyrite conversion in the reducing zone but that the effect rapidly disappears after the addition of the staged air.

5.3 COMPOSITION

The results of the foregoing section showed that effects of the initial reducing conditions that pyrite experiences during staged combustion quickly dissipate after the introduction of the staged air. Since the particles spent so little time under reducing conditions, there was little reason to expect that the altered pyrite behavior would have a significant impact on the ash as a whole. However, there remained the possibility of altered ash composition due to other effects, such as slowed char oxidation. Therefore, the CCSEM composition results were examined to determine if there was such an effect.

5.3.1 Bulk Composition

Since the inorganic constituents of Pittsburgh #8 coal are primarily silicates, aluminosilicates, and pyrite, with very little organically-bound matter, no selective loss of elements by vaporization due to staged combustion was expected. This was confirmed by the bulk compositions of the Pittsburgh #8 ash samples taken at the bottom of the reactor (Figure 5-6), which are nearly identical. The variation is within the accuracy of CCSEM. The major elements are silicon, aluminum, iron, and calcium as expected from the analysis of the coal.

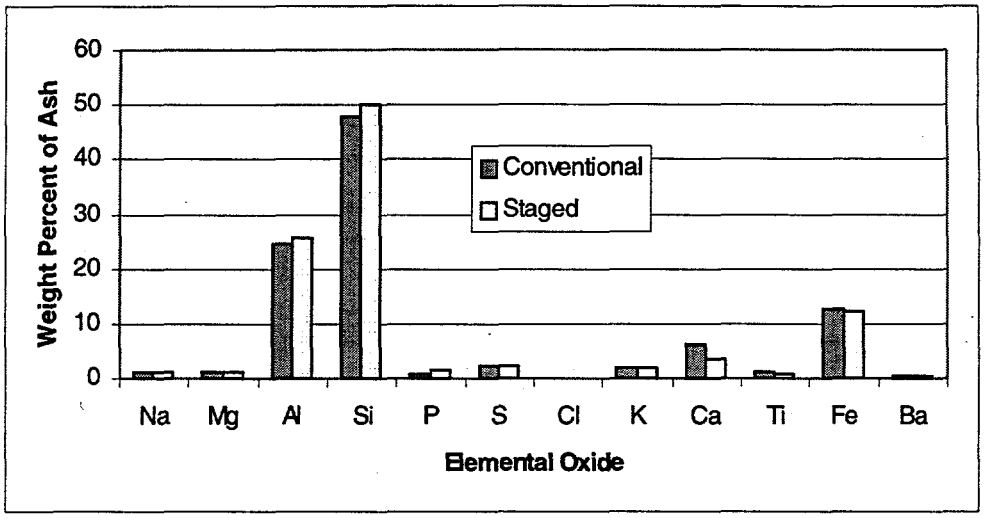

Figure 5-6 Bulk composition of Pittsburgh #8 ash samples

5.3.2 Phase Distribution

The phase distributions of the conventional and staged combustion bottom samples (Figure 5-7) were examined for evidence of a different extent of mixing during staged combustion. Little difference between the two was seen, but the conventional sample did contain a somewhat lesser amount of the pure phases (quartz, iron oxide, kaolinite) and somewhat more of the mixed phases (Fe-Al-Silicate and Unclassified) than the staged combustion sample. This contrasts with the results of experiments performed by other researchers (Bool, et al., 1995; Zygarlicke, et al., 1995) which showed greater mixing under reducing conditions. This can be attributed to the difference in residence time and burnout level of the samples. The conventional sample from the bottom of the reactor was 90% burned out while the comparable staged combustion sample was only 75% burned out.

Greater mixing in the conventional sample is also evident in the Fe-Al-Si diagrams of the two samples (Figure 5-8 and Figure 5-9). Quartz and kaolinite are represented as the groups of peaks near the silicon vertex and midway between the silicon and aluminum vertices, respectively. The iron derived from pyrite gives rise to the pure iron peak. The extent of mixing is gauged by noting the amount of silicate and aluminosilicate material that has incorporated iron. Although the extent of mixing is small, it is clear that more coalescence has occurred in the conventional sample.

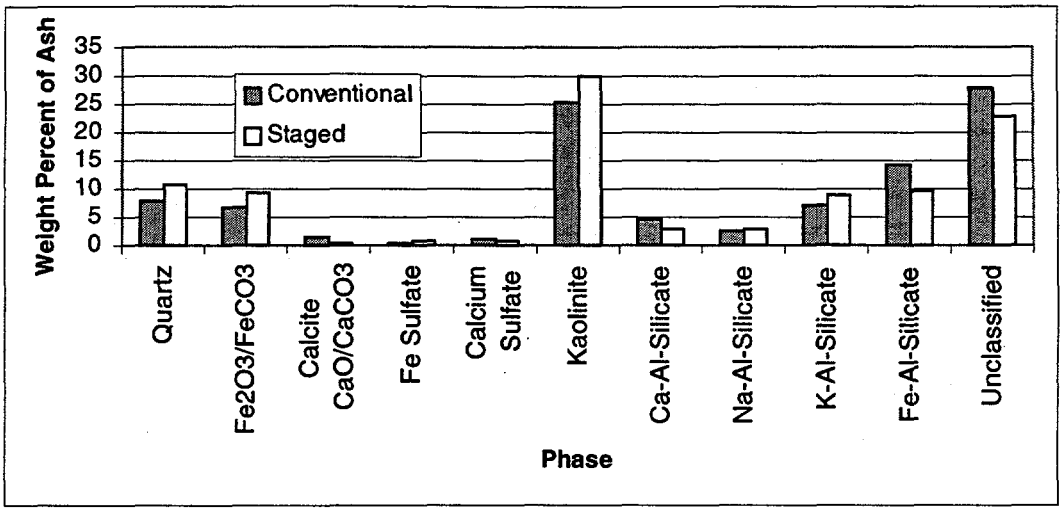

Figure 5-7 Phase distribution of Pittsburgh #8 ash samples

It is also notable that Figure 5-8 includes only 85% of the total ash while Figure 5-9 includes 89% of the total staged combustion ash. This difference is further evidence for greater mixing in the conventional ash. As mixing proceeds, the aluminum, silicon, and iron are diluted so that fewer particles meet the criteria for inclusion in the ternary diagram.

The preceding results indicate that in order to assess the impact of staged combustion on mixing, it is necessary to compare samples at the same burnout. The only samples with the same burnout were taken at the top of the reactor and have a very low burnout level of 69%. Since the staged combustion sample was obtained at the end of the reducing zone, where any differences due to the altered combustion conditions would be most evident, comparison of these samples is meaningful despite the low burnout level. The Fe-Al-Si ternary histograms (Figure 5-10 and Figure 5-11) indeed show that little mixing has occurred in either sample, although the staged combustion sample has mixed to a slightly greater degree due to its longer residence time. No significant difference that can be attributed to the initial reducing conditions is evident.

It is unlikely that changes in composition would manifest themselves following the introduction of the staged air. Indeed, comparison of the nearly identical ternary diagrams for the staged combustion top and bottom samples shown in Figure 5-11 and Figure 5-9, respectively, shows that practically no change occurred after the particles entered the oxidizing zone.

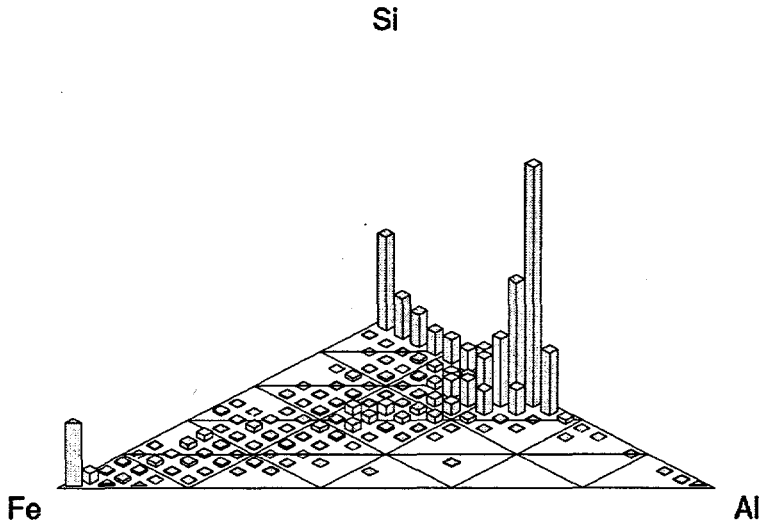

Figure 5-8 Fe-Al-Si ternary histogram of conventional Pittsburgh #8 ash (bottom, 90% burnout)

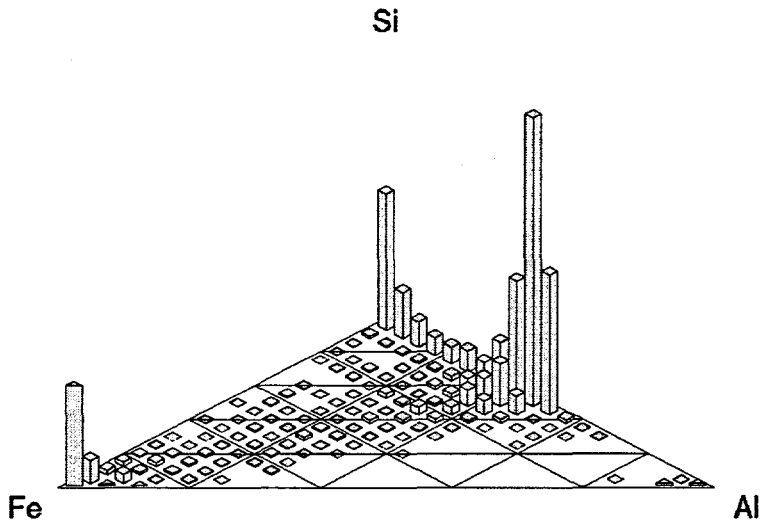

Figure 5-9 Fe-Al-Si ternary histogram of staged combustion Pittsburgh #8 ash (bottom, 75% burnout)

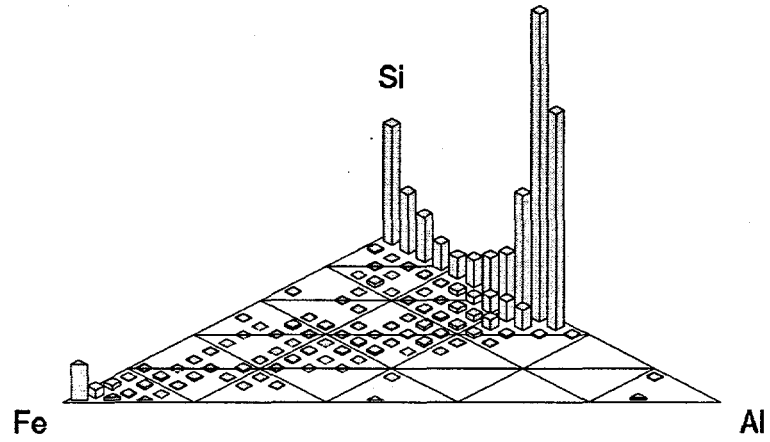

Figure 5-10 Fe-Al-Si ternary histogram of conventional Pittsburgh #8 ash (top, 69% burnout)

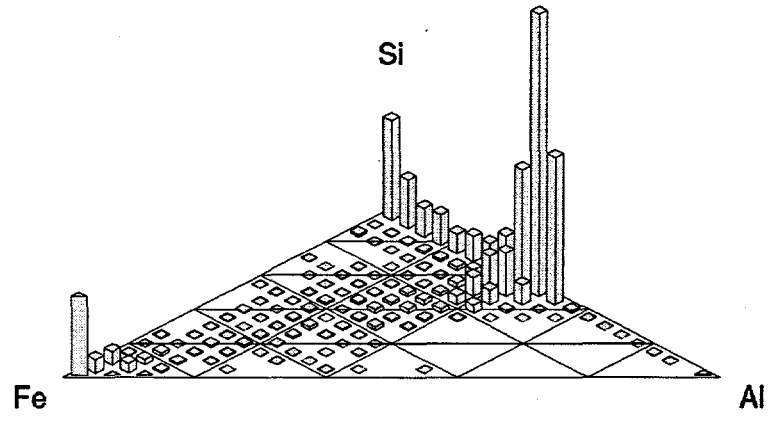

Figure 5-11 Fe-Al-Si ternary histogram of staged combustion Pittsburgh #8 ash (top, 69% burnout)

These findings are in agreement with the results of previous workers (Laitinen, 1993; Zygarlicke, et al., 1995) who found that staged combustion only had a minor effect on the properties of the ash of high-rank coals. The conflict with the results of Bool (Bool, et al., 1995), in which a much larger particle size distribution was observed for Pittsburgh #8 ash formed under reducing conditions, can be explained by the nature of the experiments. While the particles in this work were premixed with oxygen and then experienced reducing conditions for only a few hundred milliseconds and finally finished combustion with excess oxygen, the particles in Bool's drop tube experiments experienced extremely reducing conditions for 2.5 seconds or more, causing combustion to occur so slowly that the included minerals had time to coalesce to a large degree.

5.4 CONCLUSIONS

Staged combustion has a short-duration effect on the release of sulfur from pyrite during the combustion of Pittsburgh #8 coal. Use of a novel char/associations algorithm showed that the effect is most pronounced for included ash particles. Following the initial reducing conditions, pyrite transformation appears to resume quickly. Therefore, additional sticking due to the molten oxysulfide phase should only be an effect in the region near the burners of practical units.

Differing burnout levels in the samples obtained at the bottom of the reactor made it difficult to see the effect of staged combustion on the overall composition of Pittsburgh #8 ash. Coalescence correlated with burnout level. However, no signficance difference in ash composition was noted in the samples taken at the top of the reactor, where the differing combustion conditions would be expected to have the most pronounced effect. These results indicate that altered deposition behavior in utility boilers is not due to changes in the properties of the ash and must be explained by other mechanisms such as temperature, char annealing (Beeley, et al., 1996) or carbon content of the ash.

SECTION 6

RESULTS OF DEPOSITION STUDIES

This section presents the results from the Black Thunder and Pittsburgh #8 deposit samples. The objective of the section was to evaluate the influence of staged combustion on the composition and morphology of the deposits. Deposit composition was characterized with use of SEMPC as described in Section 3 of this report. Backscattered electron images of deposit cross-sections were used to characterize deposit morphology. Both the morphology and composition provide measures of the extent of sintering present in the deposit. Sintering affects the thermal properties and strength of a deposit. The strength of deposits formed from low-rank U.S. coals can also be influenced by sulfate formation. Therefore, sulfate formation was examined in deposits formed from the Black Thunder coal.

As mentioned above, one measure of sintering is the size distribution of "clusters" in the 2-D cross-sectional images of the deposit. A cluster is defined as a contiguous group of pixels whose brightness in the backscattered image corresponds to that of ash. Clusters can range from individual particles in the inner layer to highly sintered, irregularly shaped features in the outer deposit. As sintering occurs, individual particles and small clusters combine to form increasingly large clusters. Figure 6-1 shows a deposit comprised of small clusters (individual particles) at 500 X. This is contrasted by Figure 6-2, which shows a highly sintered deposit with a much larger cluster size at 250 X.

One of the primary results of sintering is a movement away from individually identifiable particles with a composition distribution resembling that of the ash, toward a set of large clusters with a highly mixed chemical composition. As particles sinter, they form a cluster whose composition is the weighted average of the composition of the original particles. Consequently, another measure of the extent of sintering is the extent of mixing which has occurred in the deposit. This mixing is frequently manifest in an increased amount of unclassifiable compositions in SEMPC analysis.

Experiments were designed to examine the effect of gas phase oxygen concentrations on the composition and morphology of deposits. Furthermore, since staged air combustion in practical systems tends to lower the incident heat flux to the furnace walls and lower the temperature of the deposits, the effect of deposit temperature on composition and morphology was also examined. The results for the Black Thunder and Pittsburgh #8 samples are provided in the following sections.

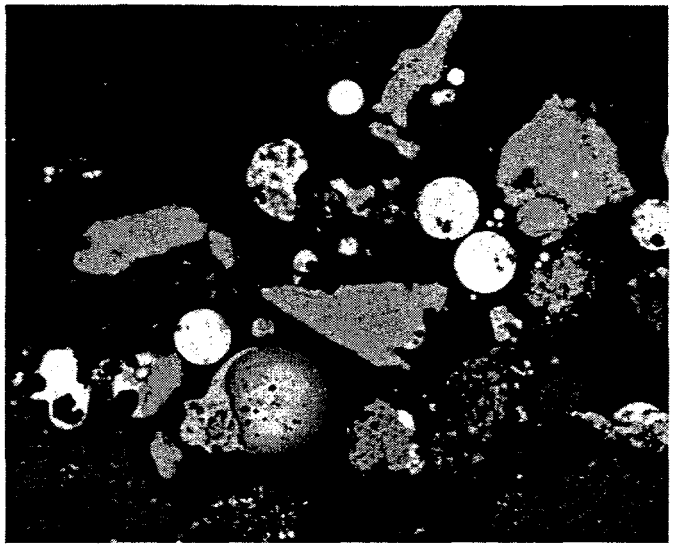

Figure 6-1 Backscattered electron image showing small clusters (500X)

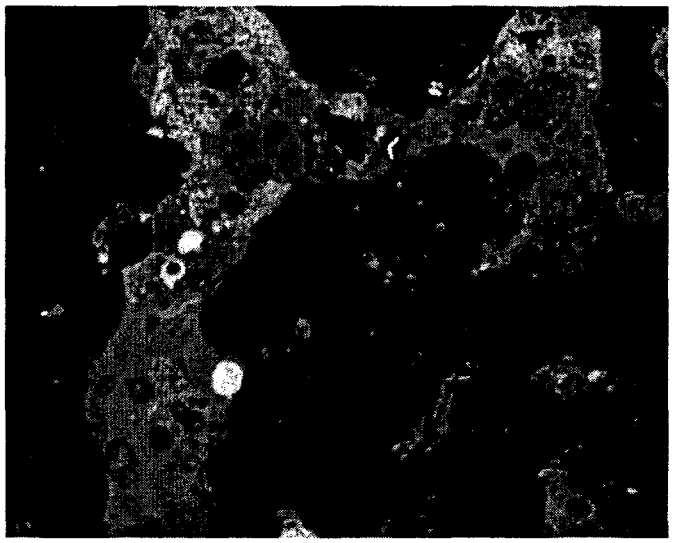

Figure 6-2 Backscattered electron image showing large clusters after sintering (250X)

6.1 BLACK THUNDER RESULTS

As mentioned in Section 3.1.4, the Black Thunder deposit samples were collected under similar conditions and allowed to mature (cure) in a natural gas flame under either oxidizing or reducing conditions. Furthermore, in order to investigate the effect of temperature on deposit composition and morphology, samples were collected at two rates of heat addition (40,500 BTU/hr and 58,000 BTU/hr). Curing of the samples was performed

at approximately the same heat rate at which they were collected. However, since the coal flames were more efficient in transferring heat to the probe than the natural gas flames, it was necessary to adjust the natural gas flow rate during curing in order to maintain a constant deposit temperature. The temperature measured at the deposit-probe interface was kept constant at about 350°C during both deposit collection and curing.

Table 6-1 shows the specific test conditions for Black Thunder deposit samples collected in this study. The sample collection positions (see Figure 6-3) correspond to locations just above the staged air injection stage (43 cm from the burner), below the staged air injection stage (89 cm from the burner), and at the end of the reactor (180 cm from the burner).

Table 6-1 Experimental conditions for Black Thunder deposit samples

	SR	Cure SR			
Coal	**Initial/ Final**	**Position 1**	**Position 2**	**Position 3**	**Heat rate**
Black Thunder	0.75 / 1.2	Unc. / 0.75 / 1.2	Unc. / 1.2		Low
Black Thunder	0.75 / 1.2	Unc. / 0.75 / 1.2		Uncured	High
Black Thunder	1.2 / 1.2			Uncured	High

While collecting deposits it was observed that every deposit contained at least some carbon-rich particles. In all cases, the outer portion of the deposit was composed of highly burned-out particles. However, even in the most oxidizing cases, the inner layers of the deposits contained some carbon. The level of carbon incorporated in the deposit was proportional to the burnout at the sample collection point (see Table 4-4). The cold tube surface probably quenched the oxidation of the impacting particles resulting in the high carbon content of the inner layers. It was interesting to note that the thickness of this carbon-rich layer increased with decreasing SR. For the samples collected under low SR conditions, the combination of lower temperatures and low oxygen concentrations resulted in more residual carbon in the deposit.

6.1.1 Deposit Sintering

Both the composition and morphology of the deposits were characterized in order to estimate the degree of sintering for all of the samples described in Table 6-1. This section presents the results for samples collected at all three sampling locations.

The cluster size distributions for the Black Thunder deposits collected at position 1 at a low heat rate are shown in Figure 6-4. These data represent the cluster size distribution for the outer layer of the deposit where the extent of sintering is expected to be the greatest. As seen in the figure, the cluster size distribution of each of the two cured sam-

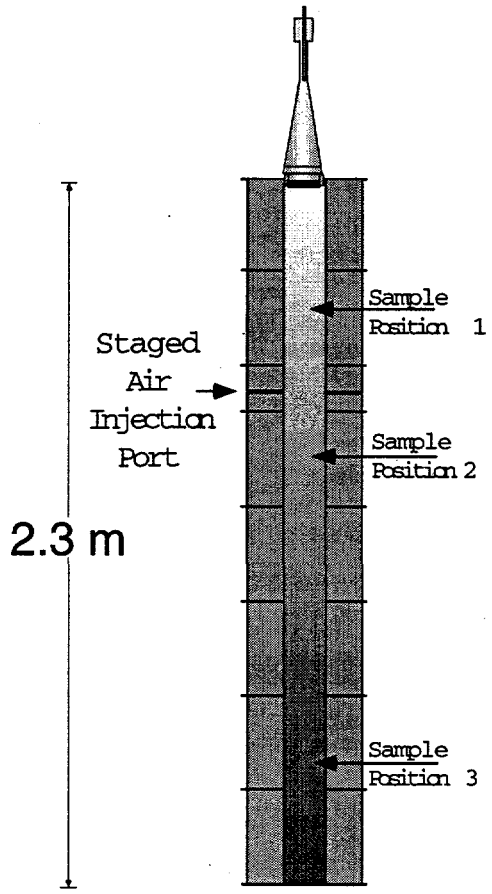

Figure 6-3 Schematic diagram showing the sample collection positions

ples is very close to that of the uncured sample. In fact, the difference between these samples is believed to represent sample-to-sample variation. Thus, based on the morphology, there is little evidence of sintering. In contrast, the composition information for these samples (not shown) indicated that a slightly greater amount of mixing may have occurred in the cured samples. However, the oxygen concentration of the gas had no apparent effect on the size or morphology of the deposits. Note that we can conclude from these results that the composition is a more sensitive measure of sintering.

Figure 6-5 shows the cluster size distributions for the outer layer of the Black Thunder deposit samples collected at the same position under a high rate of heat input. This figure shows a significantly larger cluster size distribution than that shown in Figure 6-4. It is also apparent from Figure 4 that the cluster sizes for the sample cured under oxidizing conditions were significantly larger than those of the uncured sample. This difference was found to be statistically valid (Mann-Whitney rank-sum test with a 99% confidence interval). In contrast, the sample cured under reducing conditions appeared to have a smaller cluster size distribution than the uncured sample. Clearly this result is not physically reasonable. Close examination of the situation showed that the problem was

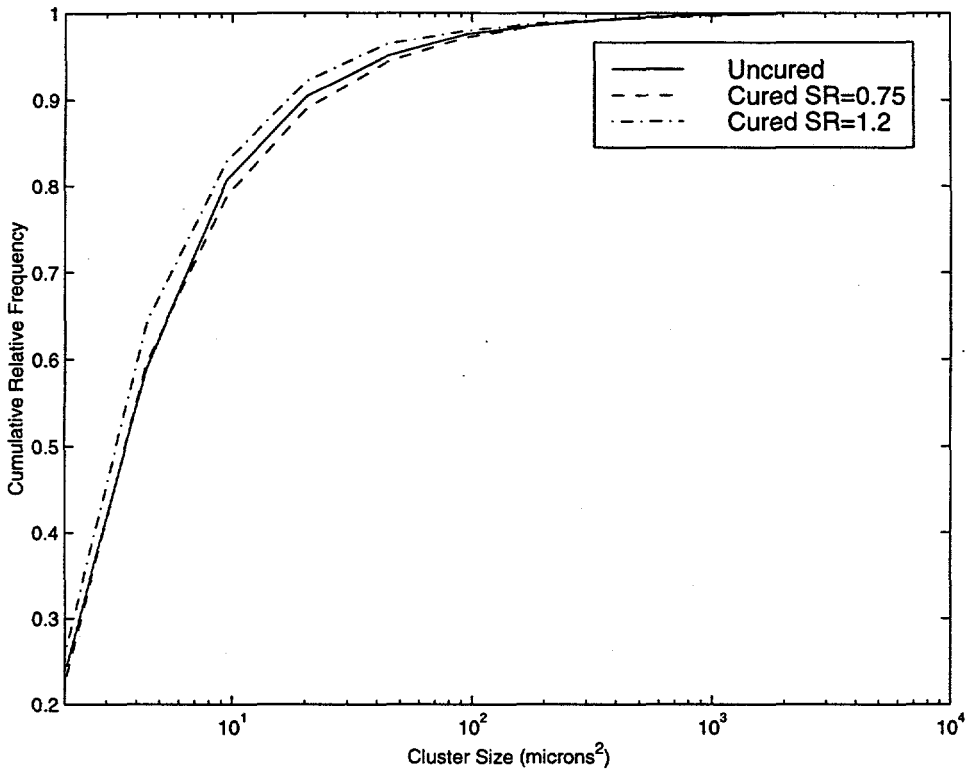

Figure 6-4 Cluster sizes of Black Thunder deposits at position 1 (low heat rate)

due to a low contrast level in the backscattered image. The lower contrast level tended to separate particles that would have been connected at a higher contrast level. The cause of this problem is believed to be a poor quality carbon coat of the sample (necessary to prevent image distortion). Because of this problem it is not possible to make a definitive statement on the influence of the oxygen content on deposit sintering based on these data. However, manual inspection of the images themselves yielded a qualitative perception of greater sintering in the sample cured under reducing conditions than observed for the uncured sample.

Composition data were also measured for these same high heat rate deposits and are provided in Fig. 6-6. The results indicate increased mixing as evidenced by an increase in the amount of Ca-Al-Silicate, a mixed phase, in both of the cured samples. This increase is balanced by a decrease in the number of Kaolinite points (an unmixed phase), also indicative of increased mixing.

Mixing is further supported by use of NPCA (see Section 3) to examine the unclassifiable fraction of these samples. The results of this analysis are shown in Table 6-2. The data in this figure are plotted as the percent of total unclassifiable points. This means that the amounts for a given sample sum to the total percent of unclassifiable points. In this way, deposits with highly varying amounts of unclassifiable points can be compared on the same plot.

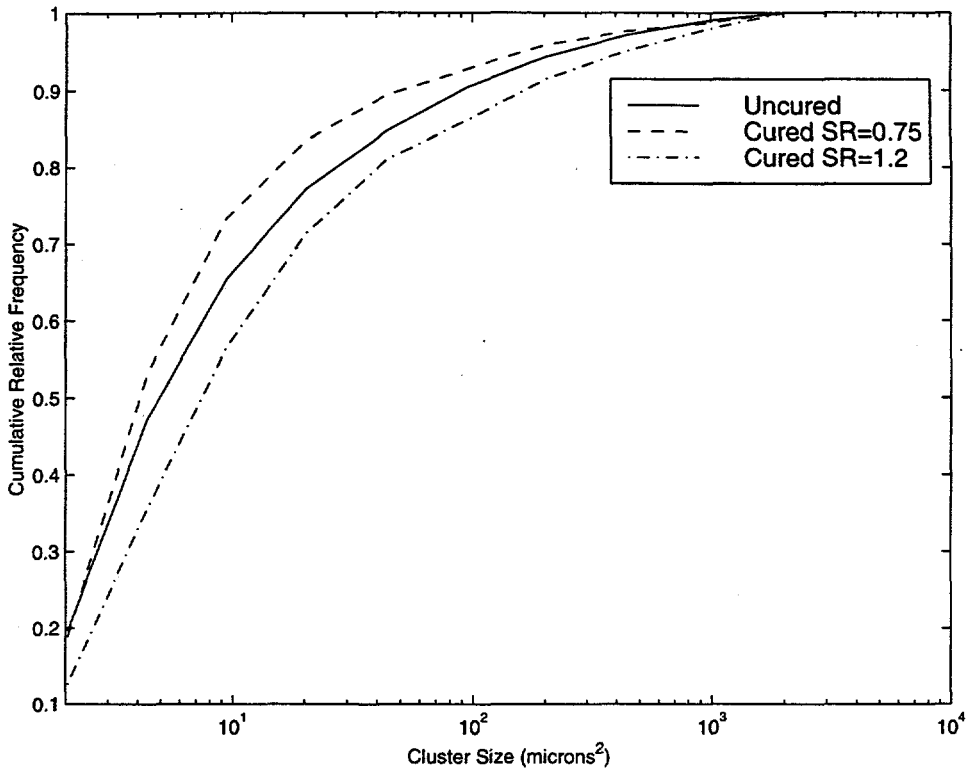

Figure 6-5 Cluster sizes of Black Thunder deposits at position 1 (high heat rate)

The total percent of unclassified points for the high temperature samples are similar; therefore, differences between peak heights in the nearest phase distribution diagram can be traced to actual trends in the samples. The most dramatic trend seen in Table 6-2 for these samples is in the near phase 24 points. The composition of points in this group corresponds to that of the organically-bound inorganic constituents in the coal. After curing there is a dramatic decrease in the number of points in this classification. Associated with this decrease is an increase in the number of mixed aluminosilicates. Specifically, there is an increase in the amount of material found near phases 35, 45, and 50. As mentioned previously, there is also an increase in the number of points classified as Ca-Al-Silicate in the cured samples collected at the high heat rate. These shifts in the phase composition indicate that the organically-associated material has mixed with ash formed from discrete minerals (quartz and clays) to form an increased number of amorphous, sintered clusters.

The effect of mixing on the composition distribution of the high temperature deposits can be clearly shown with use of ternary diagrams. Figures 6-7, 6-8, and 6-9 are ternary diagrams for the uncured, cured under reducing conditions, and cured under oxidizing conditions samples, respectively. Since magnesium and calcium tend to occur together as organically-bound elements in Black Thunder, they are plotted together in these figures. The composition of the uncured sample is similar to that of the ash (see Section 4). The large peaks on the (Ca+Mg) - Al axis correspond to the organically-bound

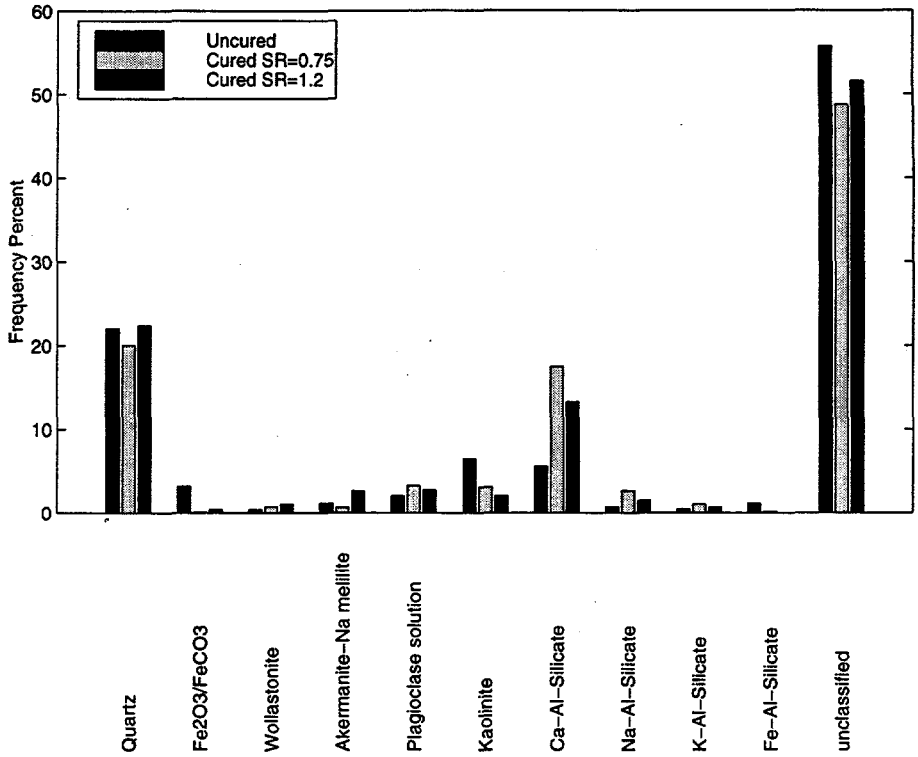

Figure 6-6 Composition data for Black Thunder deposits at position 1 (high heat rate)

elements (near phase 24). Upon curing, this material mixes with the quartz and clay species resulting in the peaks in the center of Figures 6-8 and 6-9. A close examination of the ternary diagrams for the two cured samples reveals that the oxidizing sample may be more mixed than the sample cured under reducing conditions. In any case, the difference in level of mixing of the two samples is relatively minor, and it is safe to conclude from these results that the presence of reducing conditions did not promote or enhance sintering in these deposits.

The cluster size distributions for the samples collected at sampling position 2 are shown in Figure 6-10. Curing had little effect on the cluster size distribution. These clusters are larger than those collected at position 1 with a low heat rate; this was expected because of the higher temperatures present at position 2. However, the clusters were not as large as those observed at position 1 under the high heat rate.

The cluster size distributions for the samples collected at sampling position 3 are shown in Figure 6-11. Note that neither of these samples were cured. The sample collected under staged conditions shows a larger cluster size distribution than the sample collected under conventional conditions. The increased sintering observed under staged conditions was probably due to the higher temperatures present at the deposit collection point under those conditions.

Table 6-2 NPCA results for unclassified fraction

Near Phase	% of Unclassified	Na	Mg	Al	Si	P	S	Ca	Fe
1 u	1.8	1.5	0.5	3.0	80.4	0.8	0.1	8.6	3.9
1 r	1.3	1.0	1.2	2.4	79.0	0.3	0.1	10.5	3.0
1 c	1.6	2.0	0.5	5.6	81.0	0.0	0.0	7.6	1.4
3 u	1.0	0.8	5.7	5.2	1.7	0.2	0.0	20.6	64.6
3 r	0.2	0.7	3.1	8.0	6.7	0.0	0.0	3.7	77.3
3 c	0.4	1.9	5.8	7.2	4.3	0.0	0.0	5.5	75.0
12 u	0.5	0.2	6.0	6.5	33.2	0.0	0.0	49.6	2.6
12 r	2.2	0.1	8.0	5.7	34.2	0.6	0.0	47.2	3.5
12 c	0.9	0.1	7.6	6.8	32.8	0.9	0.0	47.5	2.8
23 u	2.0	0.2	13.8	27.6	0.5	0.9	0.0	45.3	10.0
23 r	0.9	0.0	9.7	27.2	0.0	1.6	0.0	45.0	14.4
23 c	0.2	0.0	15.5	27.5	1.2	0.0	0.0	43.7	10.0
24 u	19.0	0.1	13.6	20.2	1.0	1.3	0.0	52.8	8.8
24 r	3.9	0.0	11.2	24.5	0.9	1.5	0.0	45.3	15.1
24 c	3.0	0.0	11.6	28.3	1.7	3.5	0.0	43.8	9.7
35 u	3.6	1.2	5.2	4.7	52.6	0.3	0.0	25.5	8.9
35 r	5.6	0.6	5.5	5.6	51.3	0.2	0.0	29.6	5.9
35 c	5.5	1.1	8.1	6.1	50.0	0.1	0.0	27.5	5.6
45 u	5.9	0.9	7.6	11.6	34.3	0.4	0.0	33.5	9.2
45 r	10.3	0.2	8.2	11.8	36.2	0.3	0.0	32.2	8.0
45c	13.0	0.6	8.0	12.9	36.0	0.8	0.0	31.5	7.9
50 u	13.7	0.7	13.4	18.7	18.0	0.8	0.0	37.5	8.0
50 r	16.0	0.3	10.0	22.5	22.5	1.4	0.0	34.0	6.6
50 c	18.6	1.0	9.4	19.5	29.1	1.2	0.0	30.8	6.8
52 u	2.7	3.4	1.7	9.7	67.9	0.6	0.0	9.1	3.8
52 r	3.9	2.6	1.8	8.9	66.1	0.3	0.0	11.9	4.8
52 c	4.4	3.1	1.7	9.6	68.4	0.1	0.0	10.8	2.7
53 u	1.5	1.4	4.7	21.2	18.9	0.6	0.0	17.3	33.5
53 r	1.2	1.7	8.8	21.2	23.3	0.0	0.0	10.5	25.3
53 c	0.9	0.9	9.9	20.7	16.2	0.3	0.0	14.4	36.5

u - uncured, r - cured under reducing conditions, c - cured under oxidizing conditions

6.1.2 Sulfation

As mentioned above, the effect of staged combustion on sulfate formation was examined for the Black Thunder coal. Sulfates play a key role in the development of strength for certain types of deposits formed from this coal.

As an elemental analysis showed sulfur in the deposits, the deposit was carefully analyzed to gain insight into how the sulfur was found in the deposit. It was discovered that the sulfur was always found in combination with calcium, presumably as a calcium sulfate. Furthermore, the sulfur was found almost exclusively in a particular kind of particle. This type of particle has an open network structure as shown in Figure 6-12, which is a backscattered electron image of a portion of the uncured deposit formed at the high heat rate from position 1. Such particles are believed to have formed from the in-situ burnout of char particles in the deposit. The composition of these network-like structures was primarily calcium, aluminum, and magnesium, similar to the composition of the organically-

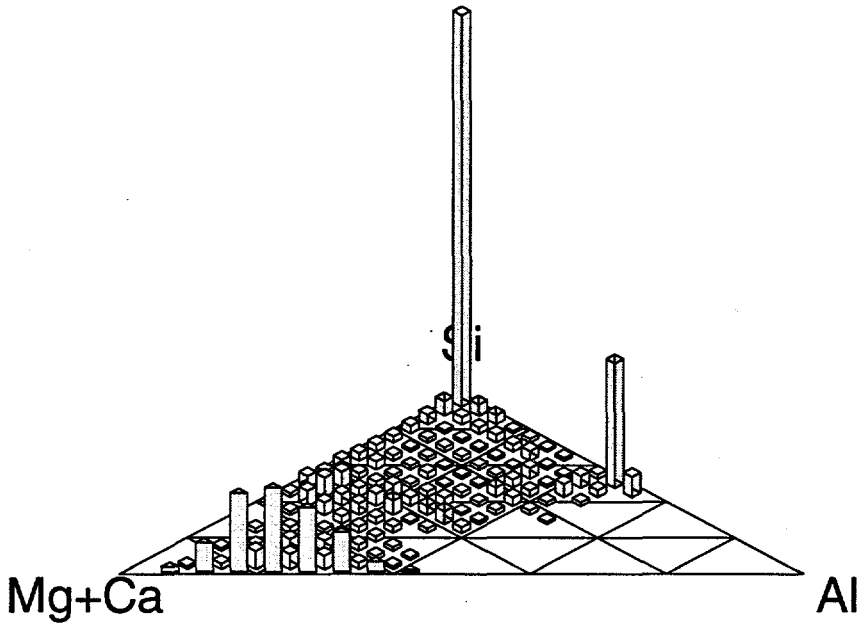

Figure 6-7 Black Thunder uncured deposit at position 1 (high heat rate)

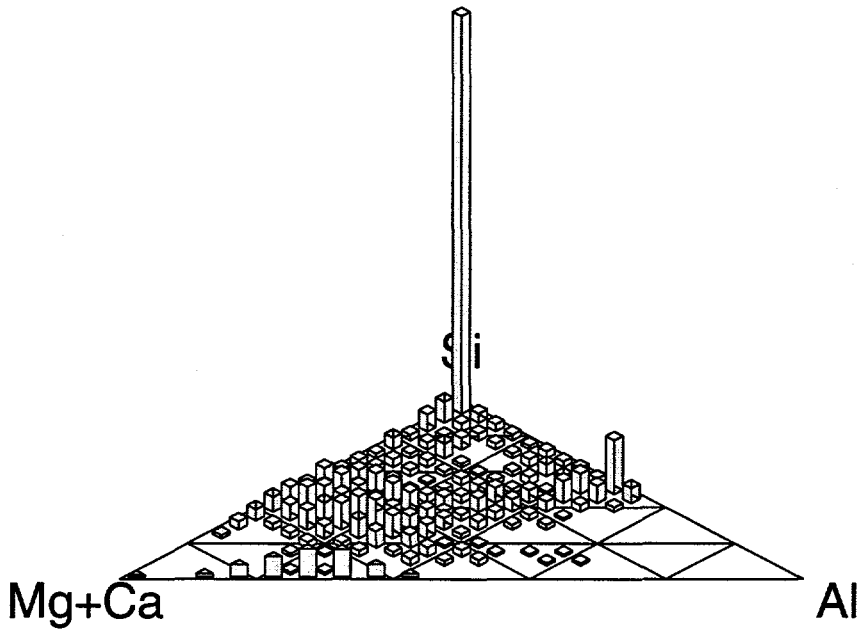

Figure 6-8 Black Thunder deposit at position 1: reducing cure (high heat rate)

bound inorganic constituents. The circles on the image correspond to sulfur-rich points analyzed in the SEM. As can be seen, the sulfur-rich points are all located on the open network-like structures.

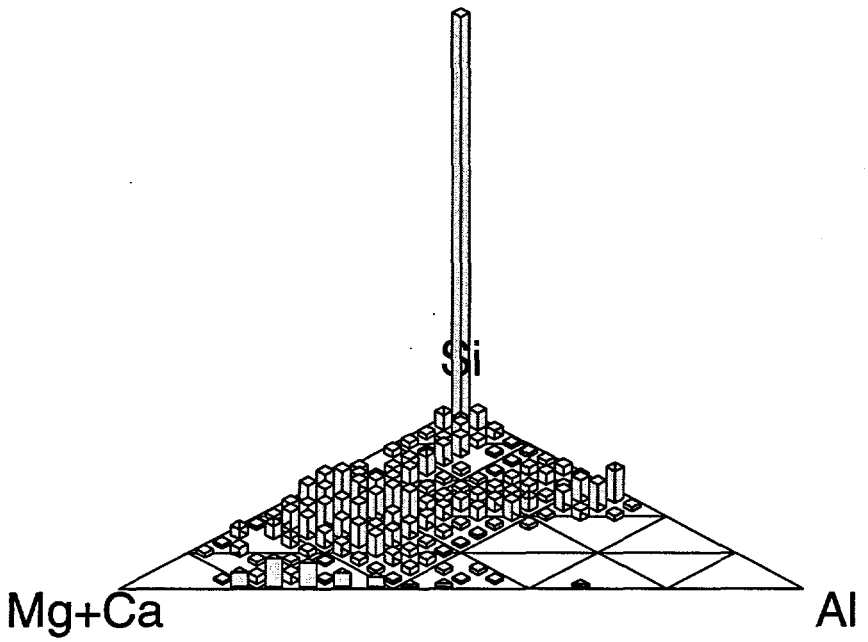

Figure 6-9 Black Thunder deposit at position 1: oxidizing cure (high heat rate)

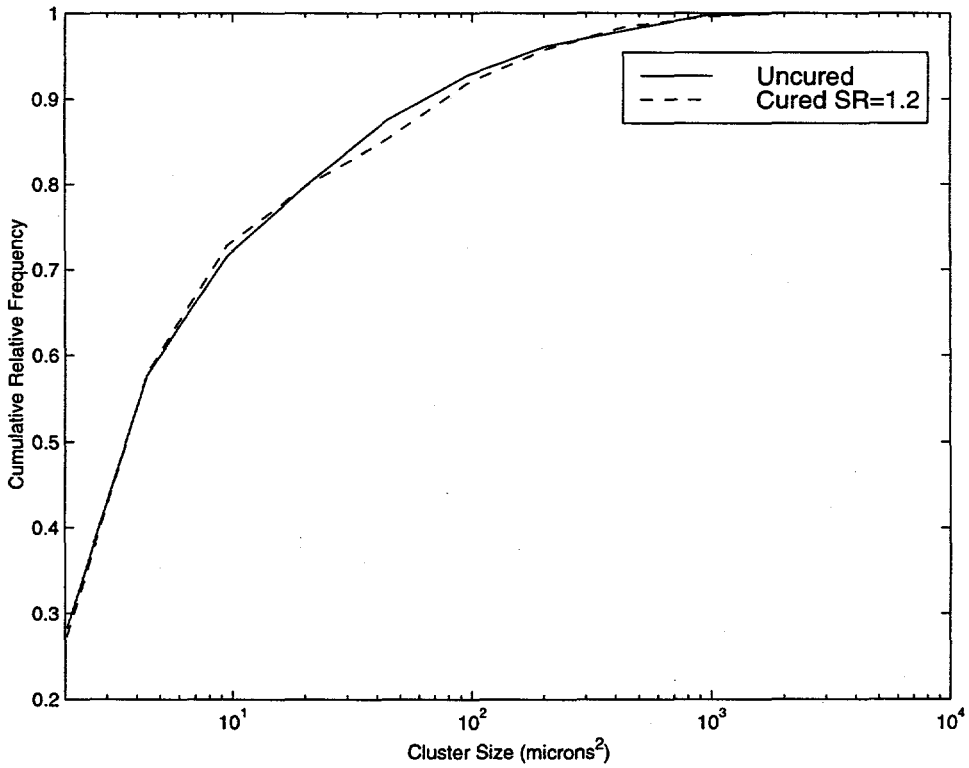

Figure 6-10 Cluster sizes of Black Thunder deposits at position 2 (low heat rate)

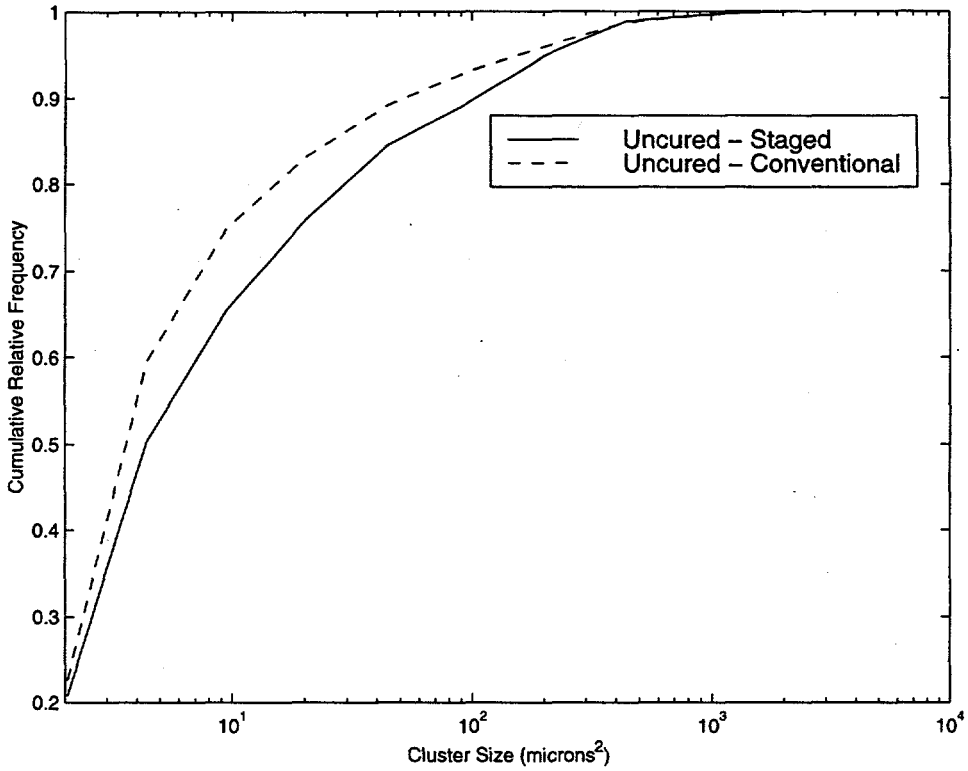

Figure 6-11 Cluster sizes of Black Thunder deposits at position 3 (high heat rate)

Analysis of the sulfur content in the deposit showed that the sulfur concentration varied throughout the thickness of the deposit. The sulfur distributions for the high heat rate samples are shown in Figure 6-13 where the distance from the tube surface has been normalized by the height of the deposits. The dominant feature of this figure is the peak in the sulfur concentration of the uncured high heat rate sample near the center of the deposit. In contrast, both of the cured samples showed very little sulfur.

The peak in the sulfur distribution for the uncured sample can be explained as follows. The sulfur levels were low near the tube due to a very low rate of sulfation caused by low temperatures in that region. Temperature, sulfation rate, and the extent of sulfation all increased with increasing distance away from the tube. The increase in the sulfur content, however, was short-lived as temperatures in the deposit became too high for the sulfate species to remain stable. In other words, the extent of sulfation dropped because the sulfate species were chemically unstable at the higher temperatures. According to Benson, the peak temperature for sulfate stability is approximately 1030°C (Benson, et al., 1993).

Examination of Figure 6-13 shows that the cured samples contained almost no sulfur. Therefore, the sulfur observed in the uncured sample must have returned to the gas phase during curing. Apparently, the lack of sulfur in the gas stream during curing changed the distribution of stable species, making the sulfate less stable. This observation

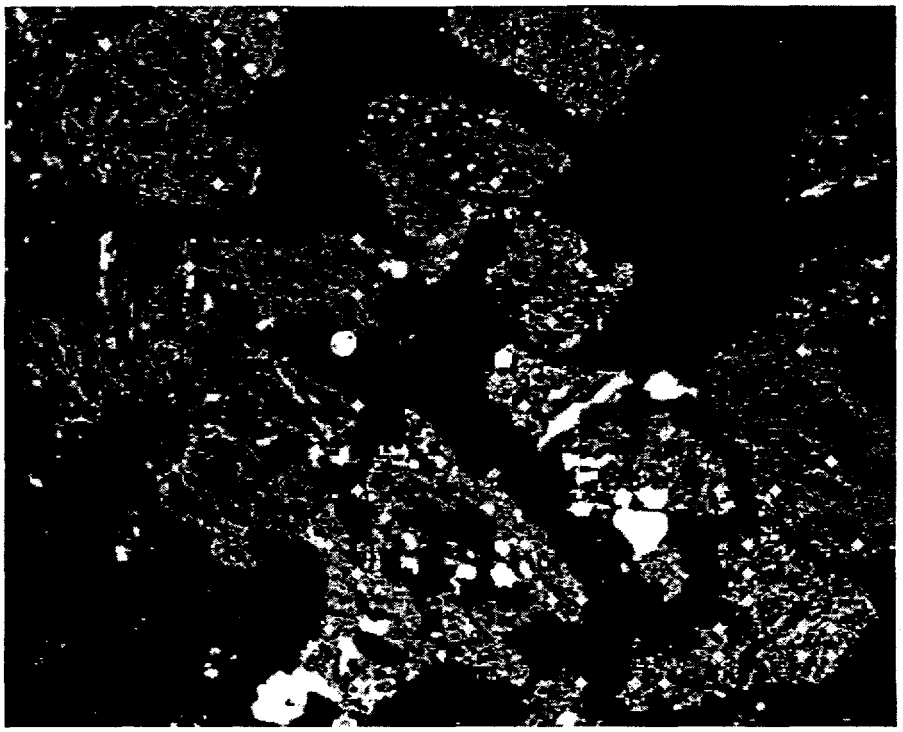

Figure 6-12 Backscattered electron image showing open network particle structure

implies that the extent of sulfate formation was a function of the amount of sulfur in the gas and, at least for this system, that the sulfation was reversible as evidenced by the loss of sulfur during the natural gas curing.

The above discussion on sulfation has potentially important practical implications. Deposits formed during staged combustion are more likely to have a larger fraction of incompletely combusted particles. These particles will burn out in-situ to form a high-surface-area structures which are prone to sulfation. Although the temperature slagging deposits may to too high for sulfate based deposits to be problematic, carbon carryover into the convective pass may influence the formation of sulfate-based deposits.

6.2 PITTSBURGH #8 SAMPLES

Two Pittsburgh #8 samples were collected as part of this study. These samples were collected at a heat rate of 40,500 BTU/hr. One sample was collected under oxidizing conditions (SR=1.1), the other under reducing conditions (SR=0.85). Both samples were collected at the first sampling position. The analysis of these samples included an examination of the cluster size and chemical composition.

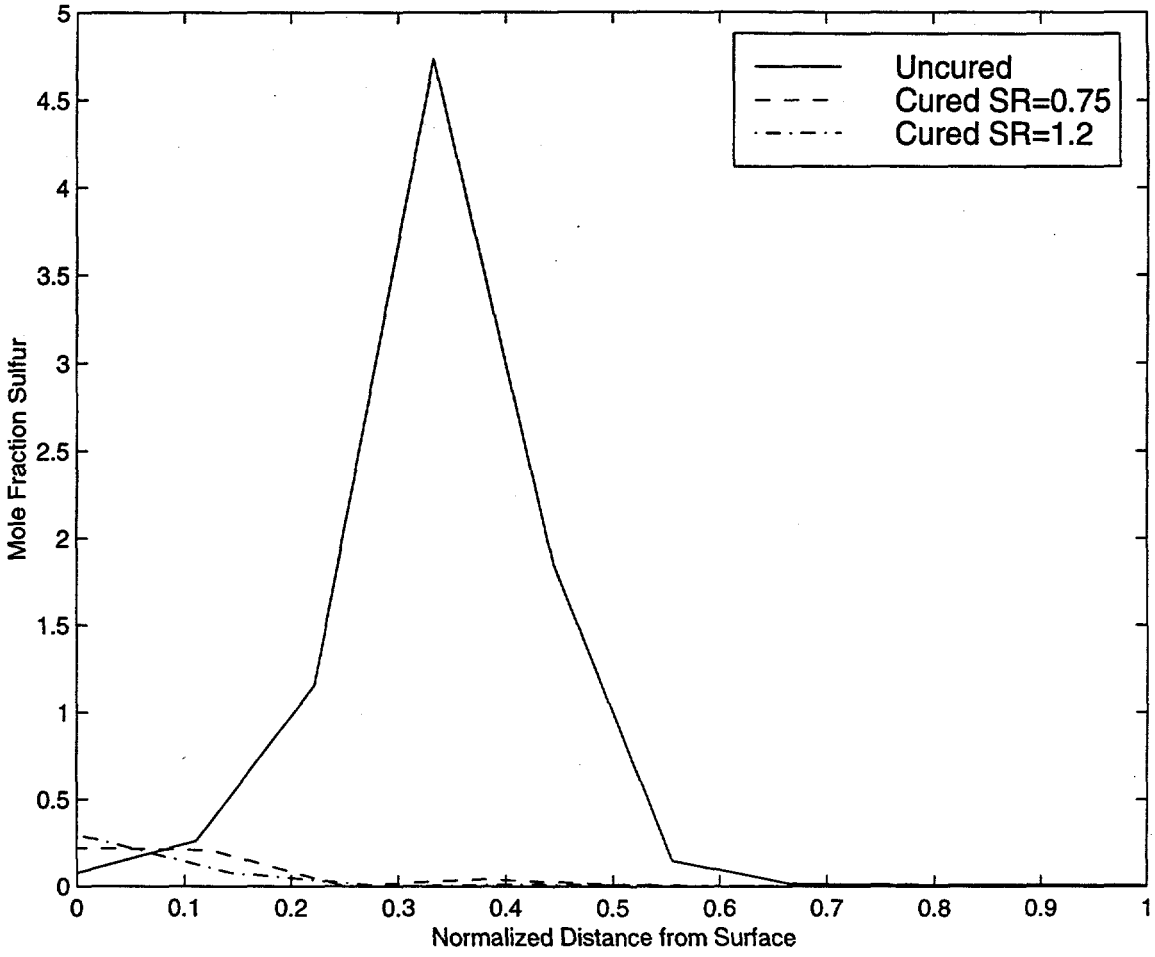

Figure 6-13 Sulfur distribution in Black Thunder deposits at position 1 (high heat rate)

The cluster size distributions for the deposits collected under oxidizing and reducing conditions are shown in Figure 6-14. The size distribution was plotted on the same scale as the Black Thunder results. However, the step in the distribution at the large end of the curves indicates that there is a significant number of particles larger than 1000 μm^2. Therefore, these samples were much more sintered than the Black Thunder deposits. Examination of this figure also shows that the two Pittsburgh #8 samples had similar cluster size distributions. Therefore, the fuel-rich region present under staged combustion did not appear to affect the deposit morphology or composition at a stoichiometric ratio of 0.85. However, it is still possible that a deeper level of staging may have an affect.

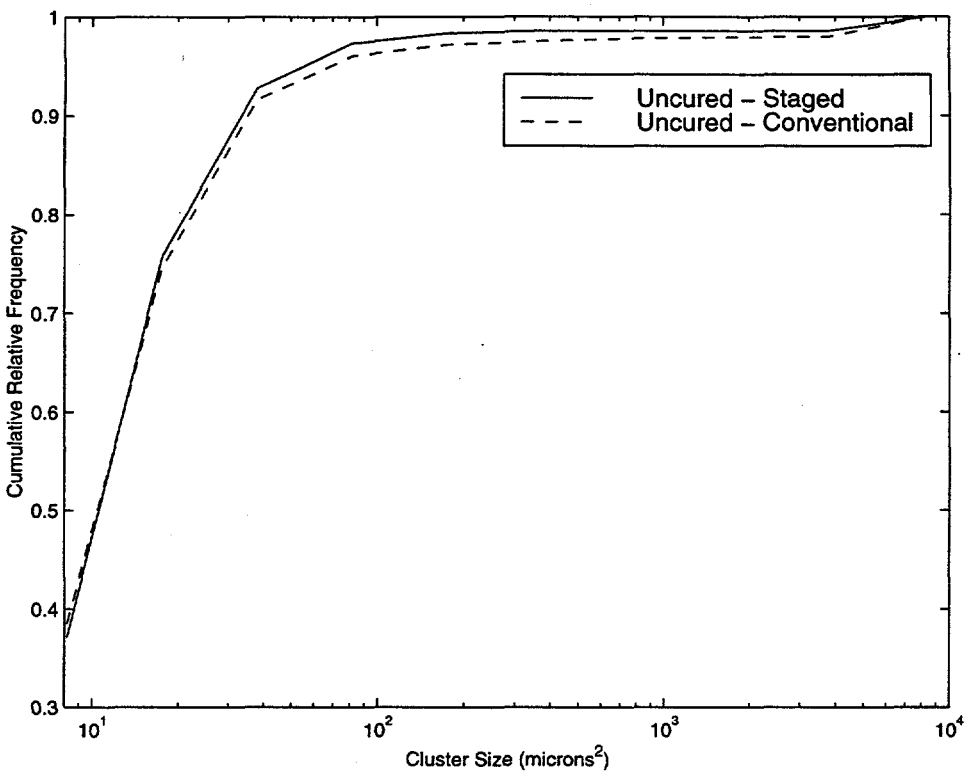

Figure 6-14 Cluster sizes of Pittsburgh #8 deposits

The ternary diagrams for the samples collected under oxidizing and reducing conditions are shown in Figures 6-15 and 6-16, respectively. It can be seen from these figures that there has been extensive mixing of the iron with the clay species, consistent with a high amount of sintering. However, no difference in mixing is seen between the two samples supporting the observation made above from the cluster size distributions.

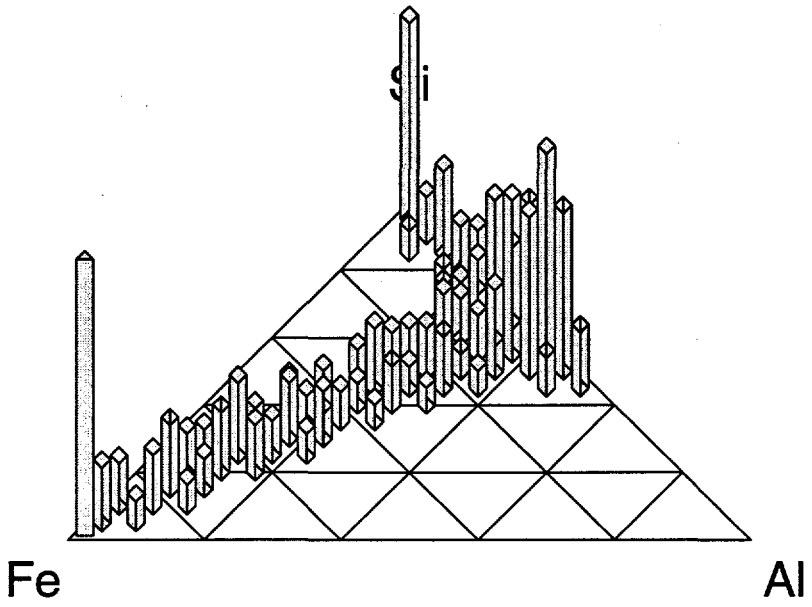

Figure 6-15 Composition data for Pittsburgh #8 deposit under convention conditions

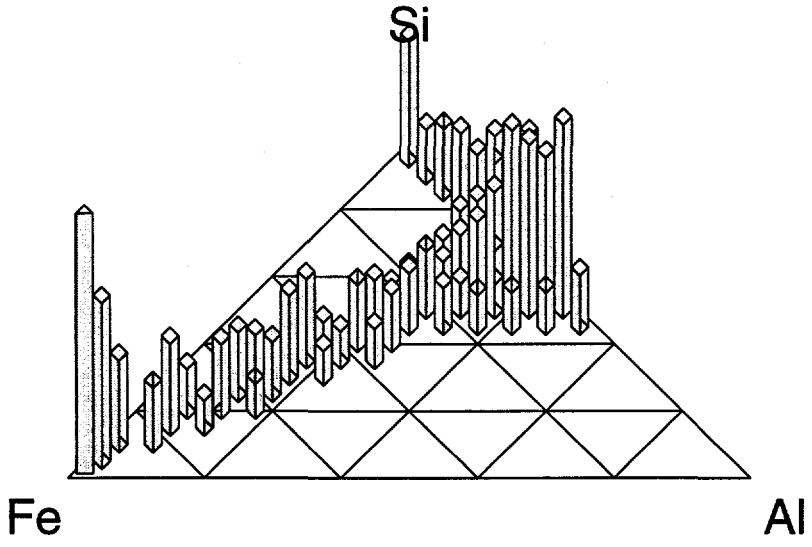

Figure 6-16 Composition data for Pittsburgh #8 deposit under staged conditions

SECTION 7

SUMMARY AND CONCLUSIONS

7.1 SUMMARY

The effect of staged combustion on the formation of fly ash and deposits was investigated experimentally using a pilot-scale combustor burning pulverized coal. Two coals were used in order to study ash formed from both organically-bound elements and mineral matter. Tests were performed under both conventional and staged combustion in order to compare the size and composition distributions of the resulting ash and deposits.

The size and composition of ash particles were determined using computer-controlled scanning electron microscopy (CCSEM). Black Thunder ash was found to contain significant (>60%) fractions of amorphous particles whose compositions could not be classified by the standard CCSEM phase identification routine. The nearest phase classification (NPC) algorithm was designed to classify such particles so that the compositions of samples obtained under conventional and staged combustion operating conditions could be compared. In addition, a char/ash association program for determining the liberation of ash particles associated with Pittsburgh #8 char particles was written and used to investigate differences in the behavior of included and excluded pyrite particles during staged combustion. A number of software tools for analyzing and presenting CCSEM results were also developed.

Deposit samples were also collected and analyzed by SEMPC as part of this study. To accomplish this, one of the combustor stages (1 ft. long) was modified to provide access for a deposition probe. Samples were collected under both staged and conventional combustion conditions. In addition, samples collected under the same conditions were cured for several hours under either reducing or oxidizing conditions to investigate the influence of the gas environment on deposit composition and morphology.

7.2 CONCLUSIONS

The following conclusions were made concerning the ash formation from the Black Thunder coal:

1) The effect of staged combustion on Black Thunder coal was to cause ash particles to coalesce to a greater extent than they do under conventional condi-

tions. This is believed to be due to slowing of char oxidation leading to reduced fragmentation.

2) The effect mentioned in (1) is not large. The large effects seen in previous studies occurred because ash and char particles experienced low oxygen concentrations for extended periods of time. When additional oxygen is introduced following a short time under reducing conditions, effects due to the reducing conditions are minimized.

3) Following (1) and (2), staged combustion of Black Thunder coal is not expected to alter significantly the size or composition of the fly ash in large-scale systems.

4) Staged combustion did not affect the bulk elemental composition of the Black Thunder ash by selective vaporization. However, a shift in the composition of small ash particles, consistent with less fragmentation of char particles under staged combustion, was observed.

In summary, staged combustion did influence ash formation from this coal. However, the impact was small enough that it is not expected to be important in practice. It should be noted, however, that the observed effect was more significant for particle sizes less than 10 microns; particles in this size range have been implicated in the formation of downstream sulfate-based deposits.

Study of ash formation from the Pittsburgh #8 coal yielded the following conclusions:

1) Staged combustion temporarily impedes the oxidation of pyrite particles. This effect is particularly evident for included pyrite (as opposed to excluded pyrite which is not associated with the organic matrix).

2) Following the introduction of staged air into the combustor, the remaining pyrite particles rapidly oxidize.

3) Staged combustion does not alter the bulk composition of the ash.

4) The extent of coalescence does not appear to be significantly affected by the initial reducing conditions associated with staged combustion.

From the deposition studies with the Black Thunder coal it was concluded that

1) The oxygen concentration in the gas did not appear to have a significant effect on deposit sintering.

2) The influence of temperature on deposit sintering was significant. Hence, changes in the radiative heat flux and/or gas temperatures present under low-NOx firing conditions are expected to have a substantial influence on deposition behavior.

3) Incompletely combusted particles which adhere to the wall will burn out in-situ to form a high-surface-area structure which is prone to sulfation. Therefore, carbon carryover into the convective pass may influence the formation of sulfate-based deposits.

Finally, the Pittsburgh #8 deposition studies showed no influence of staged combustion (S.R.=0.85) on deposit composition/ morphology for uncured deposits.

SECTION 8

REFERENCES

Adair, N. L. PhD Dissertation, Brigham Young University (1998).

Beeley, T., J. Crelling, J. Gibbins, R. Hurt, M. Lunden, C. Man, J. Williamson and N. Yang, "Transient High-Temperature Thermal Deactivation of Monomaceral-Rich Coal Chars," *Twenty-Sixth Symposium (International) on Combustion*; The Combustion Institute, , 3103-3110 (1996).

Benson, S. A., T. A. Erickson, J. P. Hurley, C. J. Zygarlicke and S. J. Selle "Field Testing Sherburne County Unit 1," Energy and Environmental Research Center, Combustion and Environmental Systems Research Institute, University of North Dakota, (1991).

Benson, S. A., M. L. Jones and J. N. Harb, *Ash Formation and Deposition,* In Coal Science and Technology 20: Fundamentals of Coal Combustion for Clean and Efficient Use, L. D. Smoot, Ed., Elsevier, New York , pp 299-373 (1993).

Bool, L. E., J. J. Helble, N. Shah, A. Shah, G. P. Huffman, F. E. Huggins, K. R. P. M. Rao, A. Sarofim, T. Zeng, R. Reschke, D. Gallien and T. Peterson "Fundamental Study of Ash Formation and Deposition: Effect of Reducing Stoichiometry," United States Department of Energy, Pittsburgh Energy Technology Center, Final Report for Contract DE-AC22-93PC92190 (1995).

Bool, L. E. I., and J.J. Helble, "Iron Oxidation State and Its Effect on Ash Particle Stickiness," *Engineering Foundation*, Waterville, New Hampshire, (1995).

Bryers, R. W., *Journal of Engineering for Power* , **101**, 506-515 (1979).

Casuccio, G. S., P. B. Janocko, R. J. Lee, J. F. Kelly, S. L. Dattner and J. S. Mgebroff, *Journal of the Air Pollution Control Association* , **33**, 937-943 (1983).

Couch, G., *Understanding Slagging and Fouling in PF Combustion*, IEA Coal Research, London, (1994).

Cunningham, A. T. S., W.H. Gibb, A.R. Jones, F. Wigley, and J. Williamson, "Inorganic Transformations and Ash Deposition During Combustion," *Enginering Foundation Conference on Inorganic Transformations and Ash Deposition During Combustion*, Palm Coast, Florida, USA, 271-284 (1991).

Dam-Johansen, K. and K. Oestergaard, *Chemical Engineering Science* , **46**, 827-837 (1991).

Erikson, T., 1994. Personal communication to Galen Richards

Galbreath, K., C. Zygarlicke, G. Casuccio, T. Moore, P. Gottlieb, N. Agron-Olshina, G. Huffman, A. Shah, N. Yang, J. Vleeskens and G. Hamburg, *Fuel* , **75**, 424-430 (1996).

Gan, H., S. P. Nandi and P. L. Walker, Jr., *Fuel* , **51**, 272-277 (1972).

Ghosh, S. K., *Mining Engineering* , 159-162 (1985).

Gopalakrishnan, R. and M. S. Seehra, *Energy & Fuels* , **4**, 226-230 (1990).

Gryglewicz, G. a. S. J., *Fuel* , **71**, 1225-1229 (1992).

Gupta, R. P., L. Yan, E. M. Kennedy and T. F. Wall, "System Accuracy for CCSEM Analysis of Minerals in Coal," *Engineering Foundation Conference on the Impact of Mineral Impurities in Solid Fuel Combustion*; The Enginering Foundation, Kona, HI, (1997).

Helble, J. J., S.G. Kang, and S. Srinivasachar, "The Effects of Combustion Stoichiometry on Ash Formation," *The Impact of Ash Deposition on Coal Fired Plants*; Taylor and Francis, Solihull, England, 583-597 (1993).

Hjalmarsson, A.-K. "NO_x Control Technologies for Coal Combustion," IEA Coal Research, IEACR/24 (1990).

Hunt, A., D. L. Johnson, I. Thornton and J. M. Watt, *The Science of the Total Environment* **138**, 183-206 (1993).

Jones, C., In *Power*; pp 54-60 (1997).

Jones, M. L., D. P. Kalmanovitch, E. N. Steadman, C. J. Zygarlicke and S. A. Benson, *Aplication of SEM Techniques to the Characterization of Coal and Coal Ash Products,* In Advances in Coal Spectroscopy, H. L. C. Meuzelaar, Ed., Plenum Press, New York , pp 1-27 (1992).

Kalmanovitch, D., 1991. Personal Communication to John Harb regarding phase identification criteria

Kim, D. S., P. K. Hopke, G. S. Casuccio, R. J. Lee, S. E. Miller, G. M. Sverdrup and R. W. Garber, *Atmospheric Environment*, **23**, 81-84 (1989).

Kim, D. S., P. K. Hopke, D. L. Massart, L. Kaufman and G. S. Casuccio, *The Science of the Total Environment*, **59**, 141-155 (1987).

Laitinen, R. "LIEKKI Combustion Research Program," Aabo Akademi, AAA-LIEKKI-L93-1 (1993).

Lloyd, W. G., John T. Riley, Shiyong Zhou, Mark A. Risen, and Richard L. Tibbitts, *Energy and Fuels*, **7**, 490-494 (1993).

Massart, D. L. and L. Kaufman, *The Interpretation of Analytical Chemical Data by the Use of Cluster Analysis*, Wiley, New York, 237 (1983).

Muzio, L., Personal Communication, 1996.

Pierrot, R. M., *Chemical and Determinative Tables of Mineralogy (without the silicates)*, Masson Publishing USA, New York, (1979).

Quann, R. J. and A. F. Sarofim, *Fuel*, **65**, 40-46 (1986).

Raask, E., *Mineral Impurities in Coal Combustion: Behavior, Problems, and Remedial Measures*, Hemisphere, Washington, 484 (1985).

Richards, G. H. Ph.D. Thesis, Brigham Young University (1994).

Richards, G. H., Personal Communication, 1996.

Robl, T. L., J. C. Hower, U. M. Graham, J. S. Groppo, R. F. Rathbone, D. N. Taulbee and S. S. Medina, "The Impact of Conversion to Low-NOx Burners on Ash Characteristics," *1995 International Joint Power Conference*; The American Society of Mechanical Engineers, Minneapolis, MN, 469-475 (1995).

Simpson, D. R. and R. M. Bond, "The Behavior of Pyrite and its Reaction Products During Combustion," *Engineering Foundation Confrence on Mineral Matter and Ash Deposition from Coal*; United Engineering Trustees, Inc., Santa Barbra, California, 237-247 (1988).

Skorupska, N. M. and A. M. Carpenter, *Computer-controlled Scanning Electron Microscopy of Minerals in Coal*, IEA Coal Research, London, (1993).

Skorupska, N. M. and G. Couch, "Coal Characterisation for Predicting Ash Deposition: An International Perspective," *Engineering Foundation Conference on the Impact of Ash Deposition on Coal Fired Plants*; Taylor and Francis, Solihull, England, 137-150 (1993).